

Fabrication of Glass Ceramic Fibres for High Temperature Applications

by

Zurina Shamsudin

A thesis submitted for the degree of Doctor of Philosophy

June 2013



The
University
Of
Sheffield.

Department of Mechanical Engineering

Supervisor : Prof. Alma Hodzic

Abstract

MgO-Al₂O₃-SiO₂ (MAS) and LiO₂-Al₂O₃-SiO₂ (LAS) glass ceramic systems is a material which is reported to have very good mechanical properties and thermal stability. These properties are suitable not only for replacing the conventional materials but also embark new fields which can satisfy the technical demands especially in aerospace applications. However, this work is primarily focusing on the fabrication of glass ceramic matrix composites. Since these glass ceramics are reported to have good thermo-mechanical properties, the study embarked upon the fundamentals of processing of MAS and LAS glass ceramic fibres, in order to open a new avenue for advanced glass fibre composites in high temperature applications.

The present work aims to develop fundamental information for fabrication of MAS and LAS glass ceramic fibres and development of the glass ceramic fibre reinforced polymer (GCFRP) composite. The thesis gradually evolves in the direction of this goal by developing suitable bulk glass ceramics, glass ceramic fibres and glass ceramic fibre reinforced polymer composites.

In the first part, the bulk MAS and LAS glass ceramics were prepared using melting and casting process. This was followed by controlled heat treatments at different temperatures. The crystallisation behavior of both glass ceramics showed that the temperature increase enhanced the rigidity of the glass structure, thereby superior and reliable properties such as density, nanohardness and reduced Young's modulus were successfully derived in the MAS and LAS system prepared at different annealing and subsequent heat-treatment regimes. The thermo-mechanical properties were correlated to the crystalline phases present in the system. SEM analysis showed that there was a significant variation in morphology of the crystalline phases with the changes in the heat treatment temperatures.

In the second part, the mechanical properties of magnesium aluminium silicate (MAS) and lithium aluminium silicate (LAS) single fibres were investigated. The fibres were prepared using different methods namely melt drawing (MAS) and continuous drawing (LAS) respectively. The glass ceramic fibres were subjected to the optimised thermal treatments and the physical appearance observed indicated an absence of distortion before being tested using single fibre test (SFT). Relations between the properties of glass ceramic fibres and heat treatment conditions were

clearly demonstrated by changes in density and Young's modulus. The latter was obtained with an acoustic approach which was successfully used in both systems. The glass and glass ceramic fibre selected were tested using the SFT and showed that different methods in fibre manufacturing process and different gauge lengths in the single fibre tests generate significantly different values in the mechanical properties of glass and glass ceramic fibres. The fibre strength distributions were strongly correlated with the diameter values of the tested fibres, and variation of the Weibull parameters depended on the gauge lengths. Moreover, scanning electron microscopy (SEM) examination of the fracture surfaces revealed the presence of fracture-inducing flaws located at the surface or in the interior of the fibre.

Finally, an analysis of the fibrous glass ceramic MAS and LAS system was further developed towards the application in advanced composite materials. The manufacturing of single ply unidirectional glass ceramic fibre reinforced polymer composites was cautiously prepared at the fibre volume fraction of 30% by hand lay up technique due to the limited and fragile nature of the fibres. Both glass ceramic fibre composites were tested using dynamic mechanical thermal analysis (DMTA). The results showed distinctive differences in the storage modulus, E' and $\tan \delta$ between composites reinforced with MAS and LAS fibres. This indicates that the epoxy resin was strongly influenced by the presence of fibres of an appreciable fibres alignment. In addition, the quality of the laminate depended on the fibre volume fraction and void content. The investigation of surface fracture through fractography indicated a correlation between the properties of composites with the crystallinity of their structures. SEM photomicrographs displayed visibly good interfaces for all uncoated glass ceramic fibre systems in which MAS and LAS glass ceramic fibres were well bonded with the epoxy, compared to LAS and MAS uncoated glass fibre composites which revealed a weaker interface due to poor interfacial adhesion. Finally, their excellent dynamic thermo-mechanical properties conclude the scientific development carried out in this thesis, with the prospect of the continuing work into development of high-temperature applications in the aerospace industry.

List of Publications

The following publications are based on the work within this thesis:

1. Z. Shamsudin, A. Hodzic, R. J. Hand, P. S. Bailey, S. A. Hayes, C. Soutis, I. P. Bond. *Thermo-physical investigation of MgO-Al₂O₃-SiO₂ glass ceramic*. Proceeding of the 14th European Conference on Composite Materials, Budapest Hungary, June 2010.
2. Shamsudin Z, Hodzic A, Soutis C, Hand R J, Hayes S A, Bond I P. *Characterisation of thermo-mechanical properties of MgO-Al₂O₃-SiO₂ glass ceramic with different heat treatment temperatures*. Journal of Materials Science, 2011, 46(17): 5822-5829.
3. Z. Shamsudin, A. Hodzic, C. Soutis, R. J. Hand, I. P. Bond, G.P. McCombe. *The investigation of properties of glass ceramic fiber composite*. Proceeding of the 16th International Conference on Composite Structures, Porto Portugal, June 2011.
4. Z. Shamsudin, A. Hodzic, C. Soutis, R.J.Hand, I.P Bond, P.J.Howard, I.Szkoda *Tensile strength and fracture morphology studies in glass ceramic fibres*. Proceeding of the 15th European Conference on Composite Materials, Venice, June 2012.
5. Shamsudin Z, Hodzic A, Soutis C, Hand R J, Bond I P. Howard, P. J., Szkoda, I. *Investigation of the mechanical properties and fracture morphology of glass ceramic fiber*. Submitted to Journal of Composite Science and Technology.

The following presentations were delivered as a result of the work within this thesis:

1. Z. Shamsudin, A. Hodzic, R. J. Hand, P. S. Bailey, S. A. Hayes, C. Soutis, I. P. Bond. *Thermo-physical investigation of MgO-Al₂O₃-SiO₂ glass ceramic*. 14th European Conference on Composite Materials, Budapest Hungary, June 2010.
2. Z. Shamsudin, A. Hodzic, C. Soutis, R. J. Hand, I. P. Bond, G.P. McCombe. *The investigation of properties of glass ceramic fiber composite*. 16th International Conference on Composite Structures, Porto Portugal, June 2011.
3. Z. Shamsudin, A.Hodzic, C. Soutis, R.J.Hand, S.A.Hayes, I.P.Bond. *Investigation of thermo-mechanical properties of glass ceramic and fibres*. 11th Conference of Deformation and Fracture of Composites, 12-15 April 2011, Cambridge, United Kingdom.
4. Z. Shamsudin, A. Hodzic, C. Soutis, R.J.Hand, I.P Bond, P.J.Howard, I.Szkoda *Tensile strength and fracture morphology studies in glass ceramic fibres*. 15th European Conference on Composite Materials, Venice, June 2012.

Acknowledgements

Praises to the Allah and peace be upon the beloved final Prophet Muhammad. I am so thankful to Allah for giving me guidance in life and strength that keeps me withstanding, and for the hope that preserves my belief that this journey would be possible.

First and foremost, I would like to express my gratitude to my supervisor, Professor Alma Hodzic, for her inexhaustible encouragement, direction, regular intellectual discussions throughout the duration of this project and invaluable help throughout my stay in Sheffield since December 2008. I would also like to thank to my co-supervisor, Professor Constantinos Soutis, for his constant support and invaluable advice. I would like to extend my appreciation to all members of the Composite Systems Innovation Centre (CSIC) at The University of Sheffield for their help and support in my work. In particular, I would like to express my gratitude to Prof Russell J Hand, Dr S Hayes, Galal, Akin, Mulyadi, Carlos, Aidah, Pauziah, Alon, Seri Rahayu, Rafidah Hasan and to all my Malaysian as well as international friends in CISC and The University of Sheffield, our interactions and shared life in the UK will certainly be an unforgettable experience.

Secondly, I gratefully acknowledge both the Ministry of Higher Education Malaysia and Universiti Teknikal Melaka Malaysia for the PhD scholarship, which made this research possible.

I would also to record my special appreciation to the Departments of Mechanical Engineering and Department of Materials Science and Engineering for providing the facilities to carry out this project. I wish to thank all the staff for their help and support especially M Jackson, D Haylock, I Watt, B Lane, D Bussey, P Staton, N Reeves and R I Kangley. I would also like to thank C Hill from the Department of Biomedical Science and D P Jackson from the Chemistry Department for their help with performing scanning electron microscopy and glass treatment, respectively. I gratefully acknowledge Dr Paul Howard and Dr Iwona Szkoda from Alstom Ltd., for the supply of commercial glass ceramic, for providing the facilities support for this work. I would also like to acknowledge the ACCIS, University of Bristol for the providing access to their fibre tower facility.

Last, but not least, I would like to thank all my family members, especially my beloved husband who is also my best friend, Nor Azri Jaafar. I am truly indebted for his sacrifices, understanding and for patiently sharing my ups and downs during the period of my study. To my beautiful daughters, Ayu Mierza Zahra and Ayu Mierza Hana, we have shared a wonderful time together, despite the various constraints that we faced throughout our stay in Sheffield, also unforgettable my mum Hajah Hamidah Desa, my dad Haji Shamsudin and my parents-in-law, Hajah Hamidah, Haji Jaafar, my former lecturers, Prof Che Husna Azhari and Prof Andanastuti Muchtar, who has always supported me and prayed for my success in life and hereafter. I gratefully thank to Allah for reasons too numerous to mention.

Contents

Abstract	ii
List of publications	iii
Acknowledgements	v
List of figures	xi
List of tables	xv
Nomenclature	xvi
Abbreviations	xviii
1 Introduction	1
1.1 Motivation	1
1.2 Problem statement	3
1.3 Research objectives & scope	4
1.4 Outline of the thesis	5
2 Literature review	
2.1 Summary	7
2.2 Introduction to glass ceramic	7
2.2.1 Glass ceramic MAS ($\text{MgO-Al}_2\text{O}_3\text{-SiO}_2$) system	8
2.2.2 Glass ceramic LAS ($\text{LiO}_2\text{-Al}_2\text{O}_3\text{-SiO}_2$) system	10
2.2.3 Properties of glass ceramics	13
2.3 The formation of glass ceramic	16
2.3.1 Nucleation and crystallisation	16
2.3.2 Nucleating agents	20
2.4 The studies of glass ceramics fibre	22
2.5 Strength of glass fibre	26
2.5.1 An overview of fibre strength analysis	26
2.5.2 Weibull distribution	28
2.6 Glass ceramic fibre reinforced composites	30
2.6.1 An overview of glass ceramic composite	30
2.6.2 Properties characterisation	32
2.6.2.1 Dynamic mechanical thermal analysis (DMTA)	32
2.6.2.2 Thermogravimetric analysis (TGA)	33
2.6.2.3 Scanning electron microscopy (SEM)	34
2.7 Concluding remarks	37
3 Fabrication of glass and glass ceramic fibre	
3.1 Summary	39
3.2 Preparation of glasses	41
3.2.1 $\text{MgO-Al}_2\text{O}_3\text{-SiO}_2$ (MAS) glass	41
3.2.2 $\text{LiO}_2\text{-Al}_2\text{O}_3\text{-SiO}_2$ (LAS) glass	43
3.3 Heat treatment route of bulk glass	44
3.3.1 Nucleation and crystallisation	44
3.4 Fabrication of MAS and LAS glass ceramic fibre	47
3.4.1 Melt drawing	47
3.4.1.1 Molten glass	47
3.4.1.2 Drawing procedure	47

3.4.2	Continuous drawing	48
3.4.2.1	Preparation of glass rod	48
3.4.2.2	Drawing procedure	50
3.4.3	Heat treatment route of glass fibre	52
3.5	Fabrication of glass ceramic fibre reinforced polymer composite	53
3.5.1	Materials	53
3.5.1.1	Epoxy resin	53
3.5.1.2	Fibres	54
3.5.2	Preparation of composites	54
3.5.2.1	Epoxy resin	54
3.5.2.2	Preparation of fibres	56
3.5.2.3	Resin impregnation	57
3.5.2.4	Curing process	57
3.6	Concluding remarks	58
4	Experimental	
4.1	Summary	59
4.2	Characterisation of bulk glass system	60
4.2.1	Differential thermal analysis (DTA)	60
4.2.2	X-ray diffraction	61
4.2.3	Density measurement	62
4.2.4	Nanoindentation	63
4.2.4.1	Test specimens and test procedures	65
4.2.4.2	Data analysis	
4.2.5	Scanning electron microscopy (SEM)	
4.3	Characterisation of glass and glass ceramic fibre	65
4.3.1	XRD fibre specimen	65
4.3.2	Mechanical property measurement	66
4.3.2.1	Single fibre test	68
4.3.2.2	Data analysis	69
4.3.2.3	Weibull distribution	
4.3.3	Measurement of fibre diameter	69
4.3.4	Acoustic measurement	71
4.3.4.1	Test specimens and test procedures	71
4.3.4.2	Data analysis	73
4.3.5	Fractography	73
4.4	Characterisation of glass and glass ceramic fibre reinforced composite	74

4.4.1	Dynamic mechanical thermal analysis (DMTA)	74
4.4.2	Measurement of volume fraction	76
4.4.3	Microvoid observation	78
4.4.4	Density measurement	79
4.4.5	Fracture surface observation	79
4.5	Concluding remarks	80

5 Results and Discussion

5.1	Summary	81
5.2	Characterisation of bulk glass	81
5.2.1	MgO-Al ₂ O ₃ -SiO ₂ (MAS) glass	82
5.2.1.1	Differential thermal analysis	82
5.2.1.2	X-ray diffraction	86
5.2.1.3	Physical and mechanical properties	88
5.2.1.4	Scanning electron microscopy	93
5.2.2	LiO ₂ -Al ₂ O ₃ -SiO ₂ (LAS) glass	96
5.2.2.1	Differential thermal analysis	96
5.2.2.2	X-ray diffraction	98
5.2.2.3	Physical and mechanical properties	99
5.2.2.4	Scanning electron microscopy	102
5.3	Fabrication of glass fibre	105
5.3.1	Feasibility of melt drawing process	105
5.3.2	Feasibility of continuous drawing process	107
5.3.3	Characteristic of drawn glass fibre	109
5.4	Fabrication of glass ceramic fibre	111
5.4.1	Heat treatment trials	111
5.4.2	Characterisation of glass ceramic fibre	114
5.4.2.1	Density	114
5.4.2.2	X-ray diffraction	115
5.5	Properties of glass fibre	117
5.5.1	Measurement of the fibre diameter	117
5.5.2	Tensile strengths	120
5.5.2.1	Fibre strength	120
5.5.2.2	Weibull distribution	123
5.5.3	Acoustic measurement	127
5.5.4	Fractography	128
5.6	Glass ceramic reinforced polymer composite	131
5.6.1	Dynamic mechanical thermal analysis (DMTA)	131
5.6.2	Density and microvoid observation	134
5.6.3	Fibre volume fraction measurements	139
5.6.4	Failure Analysis	142
5.7	Concluding remarks	147

6 Conclusion	149
7 Recommendation for future work	152
References	154

List of Figures

Figure 2.1	Phase diagram of the MAS glass ceramic system.	9
Figure 2.2	Glass ceramic forming regions in MgO-Al ₂ O ₃ -SiO ₂ system.	10
Figure 2.3	Phase diagram of LAS glass ceramic system.	12
Figure 2.4	Idealised heat treatment schedule for a glass ceramic	16
Figure 2.5	Schematic of a) nucleation and b) crystallisation in glass ceramic	17
Figure 2.6	Scanning electron microscopy shows ‘spheres in matrix’ morphology.	19
Figure 2.7	Micrograph of spinodal decomposition with an interconnected morphology.	20
Figure 2.8	Micrograph of a) drawn fibre of circular shape and b) after heat treatment.	25
Figure 2.9	Diagram of variation in strength with flaw size for several different glasses and common glass objects.	27
Figure 2.10	Schematic of decomposition reaction.	34
Figure 2.11	Characteristics of the fibre/matrix interphase in a composite material.	35
Figure 3.1	Flow diagram for the processing of glass ceramic MAS and LAS systems.	40
Figure 3.2	Manual preparation of MAS glass.	42
Figure 3.3	Schematic of preparation of MAS glass ceramic.	45
Figure 3.4	Images of up-drawing process of MAS glass fibre.	48
Figure 3.5	Images of fabrication of LAS glass rods.	49
Figure 3.6	Sequence of a fibre drawing process of LAS glass using fibre tower.	51
Figure 3.7	Glass fibres in the electric furnace.	53
Figure 3.8	Illustration of preparation of resin epoxy.	55
Figure 3.9	Reinforcing LAS glass ceramic fibres.	56
Figure 3.10	Aluminium test frame.	57
Figure 4.1	Seimens D500 X-ray diffractometer.	60
Figure 4.2	Schematic of a) nanoindentation instrument b) positioned sample and c) sample preparation.	62
Figure 4.3	A schematic representation of load versus indenter displacement data from the nanoindentation technique. The quantities shown are: the peak indentation load, P_{max} , the indenter displacement at peak load, h_{max} , the final depth of the contact impression after unloading, h_f , the initial unloading stiffness, S .	63

Figure 4.4	Glass ceramic fibres mounted for X-ray diffraction analysis.	66
Figure 4.5	Photographs of the single fiber test a) test specimen, b) tensile test method and c) cut area.	67
Figure 4.6	Typical load-extension curve for a selected single LAS glass ceramic fibre tensile test.	68
Figure 4.7	Sample preparation of fibre diameter measurement and observation surface fracture for SEM.	70
Figure 4.8	(a)The EPOCH 500 series Olympus Ultrasonic Flaw detector, (b) coupling medium and (c) transducer	72
Figure 4.9	A schematic illustration of the acoustic device.	72
Figure 4.10	Schematic illustrations of a) Perkin Elmer Instruments, DMA8000 3, b) samples and c) three point bending mode.	75
Figure 4.11	Schematic illustrations of a) specimen dimensions for b) three point bending mode.	75
Figure 4.12	Schematic illustrations of a)TGA and b) heating programme.	77
Figure 4.13	Schematic illustrations of a) optical microscope, b) specimen and c) micrograph of cross section of sample.	78
Figure 5.1	DTA traces of the parent MAS glass from a) Alstom and b)Department of Materials Science and Engineering	83
Figure 5.2	Effect of heat treatment on the colour of MgO-Al ₂ O ₃ -SiO ₂ glass.	85
Figure 5.3	XRD patterns of heat treated glass of MgO-Al ₂ O ₃ -SiO ₂ samples, annealed at 700°C (sample A) and 570°C (sample B) prior to the heat treatment. T - magnesium aluminum titanate; M - magnesium aluminate; S - magnesium silicate; A-aluminum titanate; Q-quartz.	86
Figure 5.4	Densities of the treated MAS samples at various heat treatment temperatures.	89
Figure 5.5	Load-displacement curves for MAS glass annealed at 700 °C (sample A) and further subjected to different heat-treatment temperatures (leading to formation of crystalline phases). The MAS sample annealed at 570 °C and LAS glass showed a similar behavior.	90
Figure 5.6	Reduced modulus values of MAS systems with various heat treatment regimes.	92
Figure 5.7	Hardness results of MAS systems with various heat treatment regimes.	92
Figure 5.8	SEM micrographs of the crystallised MgO-Al ₂ O ₃ -SiO ₂ at a) 900°C, b) 950°C and c) 1140°C (Sample A).	94
Figure 5.9	SEM micrographs of the crystallised MgO-Al ₂ O ₃ -SiO ₂ at a) 900°C, b) 950°C and c) 1140°C (Sample B).	95
Figure 5.10	DTA traces of the parent LAS glass.	96
Figure 5.11	XRD patterns for glass ceramic in LAS system.	98
Figure 5.12	Densities of the LAS samples at various heat treatment temperatures (LAS 1: Annealed at 500°C for 15mins; LAS 2: 550°C nucleated for	99

	100h; LAS 3: Nucleated at 550°C for 100h, crystallised at 750 °C for 2h; LAS 4: Nucleated at 550°C for 100h, crystallised at 950°C for 2h; LAS 5: Nucleated at 600°C for 2h, crystallised at 750°C for 2h).	
Figure 5.13	Hardness of LAS system at various heat treatment regimes (LAS 1: Annealed at 500°C for 15mins; LAS 2: 550°C nucleated for 100 hours; LAS 3: Nucleated at 550°C for 100 hours, crystallised at 750 °C for 2 hours; LAS 4: Nucleated at 550°C for 100 hours, crystallised at 950°C for 2 hours; LAS 5: Nucleated at 600°C for 2 hours, crystallised at 750°C for 2 hours)	101
Figure 5.14	Reduced modulus results of LAS systems for various heat treatment regimes (LAS 1: Annealed at 500°C for 15mins; LAS 2: 550°C nucleated for 100 hours; LAS 3: Nucleated at 550°C for 100 hours, crystallised at 750 °C for 2hours; LAS 4: Nucleated at 550°C for 100 hours, crystallised at 950°C for 2 hours; LAS 5: Nucleated at 600°C for 2 hours, crystallised at 750°C for 2 hours).	101
Figure 5.15	SEM micrograph of LAS systems at various heat treatment regimes.	104
Figure 5.16	Photographs of the glass rod before and after continuous drawing trials a) before drawing, b) 840°C, c) 950°C d) 1000°C.	106
Figure 5.17	Dilatometer curve showing the onset of softening temperature.	107
Figure 5.18	Photographs of the a) glass rod before drawing and b) fibre glass after drawn.	108
Figure 5.19	SEM micrograph of MAS glass fibre surface after drawing.	110
Figure 5.20	Droplet crystallisation on the surface of MAS glass fibre during trials.	110
Figure 5.21	Bent LAS glass fibres with a mean diameter of 50µm.	111
Figure 5.22	Photographs of the MAS glass fibres after the heat treatment a) after annealing temperature, b) at 900 °C and c) at 1140 °C for different diameters.	113
Figure 5.23	Photographs of the LAS glass fibres after the heat treatment at 750°C.	113
Figure 5.24	XRD diffraction patterns of LAS glass fibre treated at 750°C.	115
Figure 5.25	XRD diffraction patterns of MAS glass fibre a) treated at 900°C and b) treated at 1140°C.	116
Figure 5.26	Diameter variations detected by SEM and micrometer for a) MAS and b) LAS with a 60mm gauge length.	118
Figure 5.27	a) External aspect of the fibres at room temperature as they appear circular in cross section b) Longitudinal view of the LAS fibre.	119
Figure 5.28	Percentage of distribution for the equivalent diameter of MAS fibres with a gauge length of 60mm.	120
Figure 5.29	Average fibre strengths of a) LAS system and b) MAS system.	122
Figure 5.30	Weibull plots for tensile strength of a) LAS 50µm system, b) LAS 70µm system and b) MAS system at gauge length of 30mm.	125
Figure 5.31	Weibull plots for tensile strength of a) LAS 50µm system, b) LAS 70µm system and c) MAS system at gauge length 60mm.	126
Figure 5.32	Fracture morphology of MAS a) glass fibre and b) glass ceramic	129

	fibre.	
Figure 5.33	Fracture morphology of LAS a) brittle fracture morphology of the fibre at room temperature of glass fibre and b) glass ceramic fibre.	130
Figure 5.34	Storage modulus (E') for Epikote 828, LAS glass fibre, LAS glass ceramic composite, MAS glass fibre and MAS glass ceramic fibre between a temperature range of 0 to 180°C.	133
Figure 5.35	Temperature dependency of $\tan \delta$ at 10Hz for all range composites.	134
Figure 5.36	Morphology of MAS a-b) glass and c-d) glass ceramic composite system observed with optical microscopy.	137
Figure 5.37	Morphology of LAS a-b) glass and c-d) glass ceramic composite system observed with optical microscopy.	138
Figure 5.38	Typical TGA results illustrating percentage of weight loss versus temperature of Epikote 828 resin and the composite specimens.	140
Figure 5.39	Typical TGA results illustrating rate of weight loss versus Epikote 828 resin and the composite specimens.	141
Figure 5.40	Fracture surface of Epikote 828.	143
Figure 5.41	Fracture surface of a-c) MAS glass fibre and d-f) MAS glass ceramic fibre composite after bending.	145
Figure 5.42	Fracture surface of a-c) LAS glass fibre composite and d-f) LAS glass ceramic composite after bending.	146

List of Tables

Table 2.1	Examples of composition and crystallisation temperatures in the MAS glass ceramic system.	11
Table 2.2:	Properties of MAS glass ceramic compared to standard glasses used in composites reported in selected references.	14
Table 2.3	Properties of LAS glass ceramic with the addition of nucleating agents.	15
Table 3.1	Glass composition of MAS system.	42
Table 3.2	Schedule of annealing temperatures of glass ceramics.	43
Table 3.3	Heat treatment schedule of MAS glass systems.	46
Table 3.4	Heat treatment schedule of LAS glass systems.	46
Table 3.5	Heat treatment schedule of MAS and LAS glass fibres.	52
Table 3.6	Mechanical properties of the resin.	54
Table 5.1	Effect of heat treatment on colour of MgO-Al ₂ O ₃ -SiO ₂ glass.	85
Table 5.2	Reduced Young's modulus and hardness results of the selected MAS glasses from the nanoindentation tests.	91
Table 5.3	Effect of heat treatment on colour of LiO ₂ -Al ₂ O ₃ -SiO ₂ glass.	97
Table 5.4	Reduced Young's modulus and hardness results of the selected LAS glasses from nanoindentation test.	100
Table 5.5	Process parameters for drawing of LAS glass ceramic.	109
Table 5.6	The density of the glass fibre.	114
Table 5.7	Weibull characteristic of LAS glass fibre.	124
Table 5.8	Weibull characteristic of MAS glass fibre.	124
Table 5.9	Young's moduli of both glass systems measured using acoustic approach.	127
Table 5.10	Average density of Epikote 828 and composites.	135
Table 5.11	Volume fibre fraction and volume void fraction in MAS glass fibre composite (MASG), MAS glass ceramic fibre composite (MASGC), LAS glass fibre composite (LASG), LAS glass ceramic fibre composite and E-glass fibre composite.	142

Nomenclature

A	Fibre cross-section area
A_f	Cross-section area of fibre
$A(h_c)$	Tip contact area in nanoindentation
D	Fibre diameter
D_{mic}	Fibre diameter measured by micrometer
D_{sem}	Fibre diameter measured by SEM
d	Thickness of sample
E	Young's modulus
E'	Storage modulus
E''	Loss modulus
E_i	Young's modulus indenter tip
E_r	Reduced modulus
E_s	Reduced modulus indented material
F_{max}	Force at the failure
H	Hardness
h_c	Contact depth in nanoindentation
h_f	Final contact depth in nanoindentation
h_{max}	Maximum displacement
l_0	Fibre in gauge length
Δl	Elongation fibre length
m	Mass
m	Shape parameter or Weibull modulus
N	Number of sample
P_f	Probability of failure
P_{max}	Maximum load in nanoindentation
S	Stiffness in nanoindentation
T	Temperature
t	Time-of-flight
T_a	Annealing temperature
T_c	Crystallisation temperature

T_d	Softening temperature
T_g	Glass transition temperature
T_m	Melting temperature
T_n	Nucleation temperature
T_o	Onset of peak crystallisation temperature
V	Volume
V_f	Fibre volume fraction
W_1	Initial weight
W_2	Final weight
W_f	Fibre weight fraction
σ_0	Scale parameter at fibre length
σ_f	Fibre tensile stress at a length
σ	Fracture stress
w	Specimen width
α	Coefficient of thermal expansion
δ	Delta
β	Beta
ε	Tensile strain
λ	Wavelength
n	Planes of atoms
θ	Incident angle
δ	Tolerance in gauge length
γ	Fracture surface energy
c	Length of critical flaw
λ	Fibre wavelength
ν_i	Poisson's ratio indenter tip
ν_s	Poisson's ratio indented material
ρ	Density
ν_l	Longitudinal velocity
ν_s	Poisson's ratio indented material

Abbreviations

ASTM	American Society for Testing and Materials
BAS	Barium aluminasilicate
BDMA	Benzyl dimethylamine
CAS	Calcium-aluminium-silicate
CTE	Coefficient of thermal expansion
DGEBA	Diglycidylether of bisphenol A
DMTA	Dynamic mechanical thermal analysis
DTA	Differential thermal analysis
GCFRP	Glass ceramic fibre reinforced polymer
ICCD	International centre for diffraction data
JCPDF	Joint committee on powder diffraction standard
LAS	Lithium-aluminium-silicate
LASG	LAS glass
LASGC	LAS glass ceramic
MAS	Magnesium-aluminium-silicate
MASG	MAS glass
MASGC	MAS glass ceramic
NMA	Nadic methylene anhydride
OM	Optical microscopy
PTFE	Polytetrafluoroethylene (Teflon)
SAS	Strontium aluminasilicate
SEM	Scanning electron microscopy
SFT	Single fibre test
SOFC	Solid oxide fuel cell
TGA	Thermogravimetry analysis
UD	Unidirectional
XRD	X-ray diffraction
ZAS	Zinc-aluminium-silicate

Chapter 1

Introduction

1.1 Motivation

Glass ceramic technologies have developed rapidly in the past few decades due to their excellent mechanical properties and thermal stability of glass ceramic materials. These properties are attractive for replacing conventional materials and can also satisfy the technical demands for new applications, such as radomes and coatings. Recent studies have been dedicated to the fabrication of glass ceramic matrix composites [1-4]. However, limited research has been reported about the potential use of glass ceramic MAS ($\text{MgO-Al}_2\text{O}_3\text{-SiO}_2$) and LAS ($\text{LiO}_2\text{-Al}_2\text{O}_3\text{-SiO}_2$) fibres, mainly as reinforcements for composite materials. Use of these fibres remains largely unexplored since the standard and specialty composites are manufactured using different reinforcement, typically E-glass.

Very little work has been done concerning the fabrication of fibres from glass ceramics in terms of the analytical assessment of high melting temperatures, crystallisation times and manufacturing methods. Thus there is a gap of knowledge regarding the forming processes and implementation of glass ceramic fibres in composite applications. These factors have made it difficult for glass ceramics to develop in parallel with other advanced materials. The potential usage of the glass ceramic materials as fibre reinforcement could be achieved by tailoring properties using controlled heat treatment [5]. Development of fibres began in 1964 [6] and has since been continued by other researchers [7-10]. Ashbee's

study [7] of the green $\text{SiO}_2\text{-Li}_2\text{O-ZnO}$ glass ceramics system using an extrusion method provided a foundation for additional research using different glass ceramic systems [11-13]. The strength and stiffness of the fibres must be within an acceptable range in order to introduce a glass ceramic fibre reinforced composite. Generally, fibres must be stronger and stiffer than the matrix in order to be primary stress carriers and must be capable of resisting the propagation of cracks under steady or cyclic loads. Production of a glass ceramic fibre composite, having both high strength and high toughness, is critically dependent on the fabrication of the fibre. It is therefore of crucial importance to optimise fabrication properties in order to extend the use of glass ceramics for such applications. It has been reported [14] that the thermomechanical properties of glass ceramic fibres are varied during fabrication. The process for the preparation of glass ceramics include the selection of its composition and the nucleating agent that influences the prevalence of crystalline phases as well as the melting and annealing temperatures. These are important parameters in achieving the desired microstructure and material properties [15]. Consequently, the fundamental parameters that control the performance of the fibre are often related to the development of the microstructure in glass ceramics. Controlled heat treatments that dictate the final properties of the fibre reflect these factors.

Glass ceramics have been crystallised using a range of nucleating agents which yielded high Young's moduli and low thermal expansion coefficients [16-20]. This desirable combination of properties arises from the formation of several phases. High modulus of elasticity is desirable when the glass is used in the form of fibre reinforcement. These materials are hard to prepare due to the high melting and forming temperatures, wide a range of crystallisation behaviours and complex processes of phase separation during cooling and compositional changes. Hence, these materials may be considered as potential replacements for conventional reinforcing glass fibres in composite applications. Although the investigation of the general properties of glass ceramic fibres has been explored in various research fields, research on glass ceramic fibres for reinforced composites is still in its early stages.

1.2 Problem statement

Composite design aims to strike a balance of stiffness, strength and toughness by way of fibre reinforcement. E-glass fibres have been widely used due to their advantageous properties. However, this material has limited application for use where high modulus is required at high service temperatures. In general comparison of mechanical properties between the glass and glass ceramics, especially their moduli, glass ceramic possesses higher modulus than E-glass in bulk forms (138GPa for MAS [167] compared with 76GPa for E-glass fibres [49], and 88GPa for S-glass [49]) and can withstand significantly higher temperatures. In a standard process, glass ceramics are formed through controlled crystallisation. Desired properties are produced based on the various crystalline phases within the glass ceramic. The glass system called as non-crystalline produced without any controlled crystallisation.

Generally, the inclusion of glass ceramic fibres is expected to show a significant improvement in Young's modulus for composite materials based on the research on the production of glass ceramic MAS system done by Wange et al. [16] and Shao et al. [17]. Previously, a number of researchers used glass ceramic MAS systems in their studies as the matrix for composites combined with other materials such as SiC fibres and whiskers [3-4, 119]. Fabrication and manufacturing optimisation of LAS system has been studied [11, 22-23] however it has not been commercially developed for composite applications.

Manufacture and analysis of fibres from glass ceramic MAS and LAS systems is essential for the optimisation of the mechanical properties of their composites. The main challenge lies in the process of drawing these fibres which involves very high melting temperatures (>1600°C). This is followed by controlled heat treatment to convert the original glass composition to glass ceramic MAS and LAS.

1.3 Research objectives & scope

The present work aims to develop fundamental processing conditions for MAS glass ceramic fibres. The main objectives of this research are:

- i) To study the effect of heat treatment on the thermomechanical bulk properties of MAS and LAS glass ceramics.
- ii) To develop a detailed schedule for the heat treatment based on thermomechanical properties obtained in the bulk material.
- iii) To fabricate glass fibres using different methods of fiberisation and to select the optimal heat treatment schedule to convert glass fibres to glass ceramic fibres.
- iv) To evaluate and compare the mechanical properties of the glass ceramic fibres with those of the glass fibres.
- v) To analyse the dynamic stiffness of composites over a range of temperatures produced from the selected glass ceramics fibres.

In this study, fibrous glass ceramic will be prepared from MAS and LAS systems and combined with a thermoset epoxy resin. The glass ceramic fibre composites (GCFC) will be investigated using standard mechanical tests for composite materials. Glass ceramics will be prepared by first melting MAS and LAS glasses under controlled conditions, and then annealing and crystallisation, also under controlled conditions. The properties of these materials will then be characterised in the bulk form using differential thermal analysis (DTA), X-ray diffraction (XRD), density measurement and nanoindentation before proceeding with the fibre drawing process. Several heat treatments will be trialled in order to produce glass- ceramic fibres. The properties of the fibres will be tested according to standard testing requirements and failure analysis will be conducted using scanning electron microscopy (SEM). Fabrication of the composites will be undertaken by wet lay-up and the performance will be evaluated by dynamic mechanical thermal analysis (DMTA), fibre volume fraction (weight measured using TGA) and density (Archimedes' technique). Observation of the microstructure and surface morphology will be performed using optical microscopy (OM) and scanning electron microscopy (SEM).

1.4 Outline of the thesis

This thesis is divided into 6 chapters, including an introductory chapter. A brief description of each chapter is presented here.

CHAPTER 2 presents relevant literature with a focus on glass ceramic materials as reinforcing fibres. The fabrication techniques were also reviewed with special reference to glass ceramic fibres. The most recent work related to the use of glass ceramics in high temperature applications is presented here.

CHAPTER 3 presents the details of the fabrication works used, encompasses preparation of glass ceramic in bulk, glass and glass ceramic fibre. The methods used to fabricate glass ceramic fibres reinforced polymer composites is also presented here.

CHAPTER 4 presents the details of the experimental techniques used, including characterisation of glass ceramic in bulk and glass fibre as well as thermal and physical measurements. The measurements of mechanical properties of glass and glass ceramic fibre were performed using a single fibre test. The measurements of mechanical properties glass ceramic fibres reinforced polymer composites are also presented here.

CHAPTER 5 presents the results and discussion for characterisation of the material properties of bulk glasses, glass ceramic fibres and glass ceramic fibre reinforced composites. This chapter also includes results obtained from a study of the relation between methods of fabrication and the mechanical properties of glass ceramics.

CHAPTER 6 presents conclusions deduced from this study.

CHAPTER 7 presents suggestions for future research in this area utilising the findings obtained from this work.

Chapter 2

Literature Review

2.1 Summary

The literature survey in this chapter presents an overview of the processing of glass ceramics. The relationships between the properties of glass ceramics and their constitutions are also covered, with particular focus on glass ceramics of MgO-Al₂O₃-SiO₂ (MAS) and LiO₂-Al₂O₃-SiO₂ (LAS) systems. The Weibull concept is introduced. This chapter also provides a comprehensive review on the history of glass ceramic fibres with the emphasis on the relationships between thermomechanical properties, phases and microstructure. Also included is an overview of the application of glass ceramics as matrices in composites and the underlying need for this work. Finally, there is a review of characterisation methodologies that encompasses dynamic mechanical analysis, thermogravimetric analysis and scanning electron microscopy.

2.2 Introduction to glass ceramics

Glass ceramics have been defined as polycrystalline materials [24] that have been prepared by the controlled heat treatment of suitable glass compositions. Glass ceramics were first investigated by Stookey at Corning Glass in the 1940s [25]. Many systems of glass ceramics such as Li₂O-Al₂O₃-SiO₂ (LAS), ZnO-Al₂O₃-SiO₂ (ZAS), CaO-Al₂O₃-SiO₂ (CAS) and MgO-Al₂O₃-SiO₂ (MAS) have been

extensively studied due to their excellent properties which have been deemed suitable for advanced applications.

Owing to their brittleness, glass ceramics are limited to applications in which the mechanical stresses, particularly tensile stresses, are nonexistent or sufficiently low. Therefore a better combination of high strength, hardness and stiffness is an essential requirement for the development of competitive composite materials. Among the recent developments to be considered in this study are magnesium aluminosilicate (MAS) and lithium aluminosilicate (LAS) glass ceramics. In this study MAS and LAS glass ceramic systems will be used to evaluate the feasibility of utilising glass ceramic fibres in polymer composites.

2.2.1 Glass ceramic MAS (MgO-Al₂O₃-SiO₂) system

Glass ceramics with a very low coefficient of thermal expansion (CTE), good mechanical properties and high chemical durability can be obtained by tailoring compositions in MAS glass ceramic systems [16, 26-28]. It has been reported that systems containing cordierite as a major phase possess a high modulus of elasticity. Thus, MAS glass ceramics have been widely used in applications that strictly require high resistance to thermal shock accompanied with high Young's modulus.

Figure 2.1 shows a phase diagram of the MAS glass ceramic system [29]. The main phase of the glass ceramic investigated in the MAS system has been based on cordierite (2MgO-2Al₂O₃-5SiO₂). Other crystalline phases, including clino-enstatite (MgO-SiO₂), cristobalite (SiO₂), forsterite (2MgO-SiO₂), mullite (3Al₂O₃-2SiO₂) and spinel (MgO-Al₂O₃) were also produced in minor proportions in some materials [Strand, 1986] and which depend on the percentage of MgO or Al₂O₃ during the preparation of those glass ceramics.

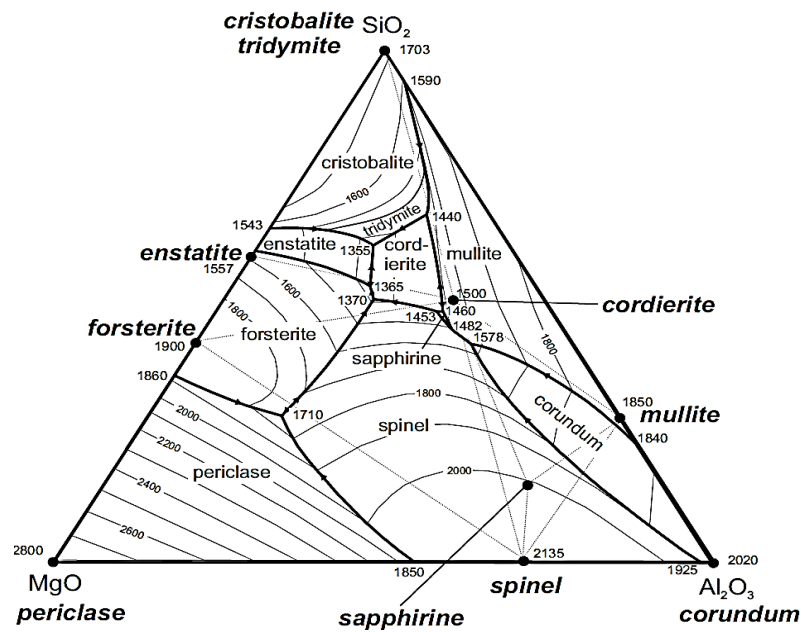


Figure 2.1: Phase diagram of the MAS glass ceramic system [29].

In general, devitrification of this system begins with the precipitation of metastable β -quartz followed by two main phases, for example indalite and cordierite [31]. The precipitation phases depend on the cooling regime and the initial composition of the raw materials employed. Rawson [32] clarified that the presence of MgO influences the liquidus temperature which has also been supported by Amista et. al [33] by reporting that a high content of MgO lowers the temperature of crystallisation. Moreover, crystal growth was markedly affected by small changes in composition and as a consequence the mechanical properties of the material were also affected [25]. However, it was not completely clear from the results which phases were formed in the system due to the sensitivity of the temperature of heat treatment and dwelling time. The ratio of the raw materials is subject to certain limitations as reported by McMillan [24] in Figure 2.2. A cordierite composition can occur anywhere in the shaded area. It may be further debased by the addition of fluxes to aid melting, and nucleating agents to aid crystallisation. Nucleation temperatures were reported within a range of 850°C-900°C and subsequently the glass ceramic systems were heated to temperatures of up to 1250°C to allow the development of desired crystal phases. Table 2.1 summarises the composition and crystallised phases in the MAS glass ceramic system.

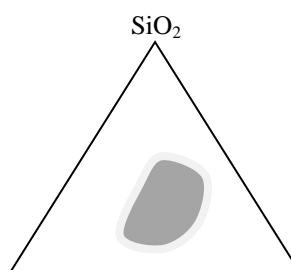


Figure 2.2: Glass ceramic forming regions in MgO-Al₂O₃-SiO₂ system [24].

2.2.2 Glass ceramic LAS (LiO₂-Al₂O₃-SiO₂) system

LiO₂-Al₂O₃-SiO₂ glass ceramic (LAS) is a glass ceramic with several desirable mechanical properties. High visible transparency [34-35] and extremely low thermal expansion coefficient [21] makes LAS a versatile material. The surface roughness of this group has also been studied by Kim and co-workers [36] as the surface quality offered by this system may permit its use as a substrate in electronic devices [37]. In contrast to MAS system, this type of glass ceramic was introduced in the early 1960s in a number of studies involving crystallisation and microstructural evolution [38-39].

Table 2.1: Examples of composition and crystallisation temperatures in the MAS glass ceramic system.

Heat Treatment Temperature °C (h)	Composition wt (%)			Nucleating agent wt (%)	Crystallised phases	References
	SiO ₂	MgO	Al ₂ O ₃			
1275 (20)	51.2	13	35.8	TiO ₂ (9.8)	Cordierite, Rutile, Mullite	[31]
1200 (3)	51.4	8.8	28.9	TiO ₂ (10.9)	Cordierite, Aluminum titanate	[16]
1150 (1)	52.4	14.7	20.3	TiO ₂ (9), Li ₂ O (1.8), Na ₂ O (1.8)	Cordierite, Rutile	[28]
1200 (1)	64.8	9.3	18.5	TiO ₂ (7.4)	μ-Cordierite, α-Cordierite	[40]
1000 (2)	NM	NM	NM	TiO ₂ (NM)	Cordierite Mg ₂ Al ₄ Si ₅ O ₁₈ (MAS)	[41]
1200 (2)	20-40	10-20	15-35	TiO ₂ (5-10)	Cordierite, Cristabolite, Aluminum titanate,	[17]

*NM = Not Mentioned

Numerous studies [34, 42-43, 19-20] have been conducted to determine the crystalline phases formed during nucleation and crystallisation stages. Most of the studies concluded that LAS system had an attractive composition as an alternative material for application where a low CTE was required. The solid solution of β-quartz (Li₂O-Al₂O₃-2SiO₂) is the cause of very low (or zero) thermal expansion in this system. The transformation of this phase to a spodumene phase occurs between the temperatures of 900°C-1000°C [44]. Both of these phases are extensively used and studied among the phases that have been found to be controlled by this

characteristic. For this reason, LAS system is usually employed as a glass ceramic matrix in composite applications [18, 45-46].

Figure 2.3 shows a phase diagram of LAS glass ceramic system [44]. The main glass ceramic phase investigated in the LAS system has been based on β -quartz ($\text{Li}_2\text{O}-\text{Al}_2\text{O}_3-2\text{SiO}_2$) or β -eucryptite ($\text{LiSi}-\text{AlO}_4$) including β -spodumene ($\text{Li}_2\text{O}-\text{Al}_2\text{O}_3-4\text{SiO}_2$). The precipitation of these phases is found to depend on the nature of the nucleating agents and the heat treatment temperature used [25]. These phases were produced in glass ceramics by controlling the crystallisation of parent glasses. This is subject to the estimated ratio of the composition within the range of 55-70 wt% SiO_2 , 15-27 wt% Al_2O_3 and 1-5 wt% Li_2O by incorporating suitable nucleating agents [44].

Since this has shown improvement of the properties [11, 22-23], a few studies have introduced LAS as materials for the fabrication of glass ceramic fibres. This has contributed to greater knowledge for the fabrication of glass ceramic fibre reinforced polymers (GCFRP).

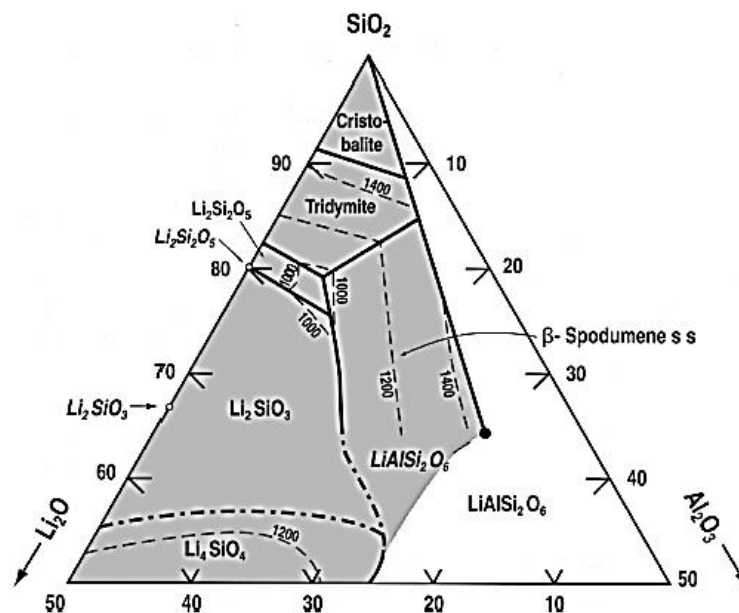


Figure 2.3: Phase diagram of LAS glass ceramic system [44].

2.2.3 Properties of glass ceramics

Arun [47] reported that the mechanical properties of glass-crystal composites are generally very poor in comparison with glass ceramics. Generally, the crystal size is considerably smaller in the glass ceramics. Glass ceramics as a class therefore consist of relatively strong materials; in general the strength of a polycrystalline ceramic increases as the crystal size is reduced [32]. This is because of a very uniform particle size distribution and near-zero porosity. Besides being stronger, it also possesses higher fracture toughness relative to the parent glass primarily because of the deflection of fracture fronts around the crystalline particles. These crystals control the flaws and slow down the rate of crack propagation [48] which can relate to the Griffith (1920) equation [24];

$$\sigma = \sqrt{\frac{2E\gamma}{\pi c}} \quad [2.1]$$

where E is the elastic modulus, γ is the fracture surface energy, and c is the length of the critical flaw. The coefficient of thermal expansion can be as low as zero because the properties controlled by adjusting the composition have superior abrasion resistance to normal glasses.

The strength of the MgO-Al₂O₃-SiO₂ glass ceramic depends on whether cordierite can develop as the major crystal phase. Cordierite glass ceramics can possess strengths of up to ~250MPa and the clino-enstatite materials have shown even higher strengths up to 350MPa. The strength of E-glass and S-glass were reported around 3.5GPa and 4.6GPa, respectively [14]. Glass ceramic with a very low thermal expansion coefficient can be made by choosing the composition of the MgO-Al₂O₃-SiO₂ system [32] with cordierite as the major crystalline phase present in the MAS system. Although a number of studies have specifically examined the relationship between nucleation and crystallisation in the MAS glass ceramic system, a literature survey revealed that little investigation of mechanical properties, especially on the Young's modulus and strength, has been reported to date.

Studies by Wange et al. [16] and Shao et al. [17] using combinations of the composition $\text{MgO-Al}_2\text{O}_3\text{-SiO}_2$ nucleated with TiO_2 showed very interesting mechanical properties (Table 2.2) compared with commercial glass fibre.

Table 2.2: Properties of MAS glass ceramic compared to standard glasses used in composites reported in selected references.

Materials	Young's Modulus (GPa)	Hardness (GPa)	Reference
E-glass (electrical fibre)	72.4-76	5.2	[49]
S-glass (high strength fibre)	84-88	5.7	[49]
MAS glass ceramic (bulk form)	139	9.5	[16]
	137	8.5	[17]

Wange et al. [16] reported that at 1080°C low quartz was found to be the dominant phase, before transforming to cordierite at 1200°C , resulting in a high modulus of 139GPa, and 9.5GPa for hardness. On the other hand, Shao et al. [17] observed the maximum elastic modulus of 137GPa accompanied by a microhardness of 8.5GPa and a density of 2.924g/cm^3 when the glass was heated at 1100°C . Cordierite and low quartz phases were identified for achieving high strength glass ceramic. Moduli were measured using the pulse-echo method with an ultrasonic tester.

However, LAS with a main crystalline phase of β -spodumene has a low CTE, a low strength of approximately 100-140MPa [24-25] and a high crystallisation temperature. The low CTE is likely to result in circumferential tensile stresses in the residual glass phase around the crystals. Similar findings have also been reported for strength with different nucleating agents [50]. Serbena and co-workers [19] used nanoindentation and pulse-echo method to measure the Young' modulus of sintered LAS glass ceramic. The result showed that the modulus measured by nanoindentation (74.7 GPa) is slightly equivalent with that measured by the pulse-echo instrument (81.5 GPa).

A nanoindentation technique will be used in this present study to determine the mechanical properties in bulk systems due to the brittleness of the materials [51-53] with Young's modulus of glass fibre measured by the ultrasonic technique. This is also seen as one of the alternatives to minimise the amount of damage on surface fibres during handling in measurement [54]. The results of the Young's modulus of glass fibre are expected to slightly increase or to approximate that of the bulk system [55]. This is related to the linear contraction within the glass which causes compaction and density increase after subsequent heat treatment [56]. Therefore, the acoustic method is used as a selection tool for accurate measurement. An error often appears from scattered attenuation of elastic waves due to internal defects such as cracks or porosity [57, 47] which are related to the object's geometry or material composition of the sample. Furthermore, the glass ceramics are known as less porosity or zero porosity materials, as this material is produced by a glass route without involving pressing or sintering.

Table 2.3: Properties of LAS glass ceramic with the addition of nucleating agents [25]

Nucleating Agent	Main crystalline phases	Bending strength (MPa)	Thermal Expansion $\alpha \times 10^7$	Density (g/cm⁻³)
TiO ₂	Spodumen, eucryptite, high temperature quartz (ss)	100-130	0-10	2.48-2.57
P ₂ O ₅	Li ₂ O.2SiO ₂	Up to 400	100	-

As mentioned earlier, heat treatment processes associated with the changes in properties include density [55]. Goswami et al [159] studied MAS system and concluded that the density of the glass ceramic depends on the controlled heat treatment. As a consequence, the heat treatment develops densification of the glass [56]. Other factors also induce the degree of formation of different phases which depends on the glass composition, as reported by Zdaniewski [40] and Shao et al. [17].

2.3 The formation of glass ceramic

The first stage in the formation of glass ceramics is producing a glass from a selected composition and subsequently crystallising the glass by controlled heat treatments. This heat treatment comprises two steps; crystal nucleation and crystal growth as shown in Figure 2.4 and Figure 2.5.

2.3.1 Nucleation and crystallisation

Generally, nucleation promotes formation of nuclei in a glass [24]. Nuclei are uniformly dispersed throughout the bulk of the parent glass through the process of crystallisation [30]. The conversion starts when melted elements are cooled at a constant temperature, where the lattices are less ordered and may be considered amorphous. Nucleating agents further initiate nucleation of crystals when the glasses are further thermally treated. The nucleation occurs when the glass is heated to the nucleation temperature for a period of time before reaching the crystal growth temperature. Bulk crystallisation depends on the density of nuclei which can be obtained either through homogenous or heterogeneous nucleation.

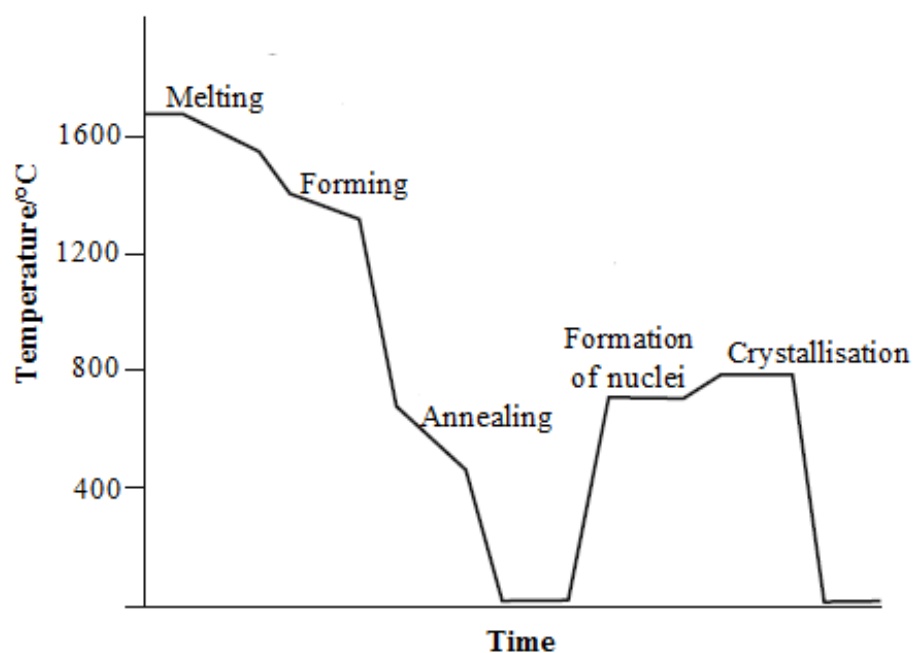


Figure 2.4: Idealised heat treatment schedule for a glass ceramic [24].

Homogenous nucleation occurs with no preferential sites for nucleus formation. However, Strand [30] reported that such cases were rarely found, because in a real phase it is possible to incorporate defects, e.g. foreign surfaces, grain edges and impurities which occur during the experiment. In contrast, heterogeneous nucleation involves formation of the nuclei of new phases on the surface of an already existing phase boundary, which is more generally observed. Bulk nucleation could occur at random times and locations as well as surfaces [47]. However, Strand [30] acknowledged that most glasses showed only surface nucleation because of the low density of nuclei formed on the surface and the generation of crystal growth from the surface towards to the centre due to the addition of nucleating agents. The methodologies of preceding studies [41, 58-60] have reported the temperatures, base compositions, additions of another components and amorphous phase separations that have been used to achieve fine glass ceramic crystal phases. These parameters can be used to pre-determine the processing conditions for MAS and LAS glass ceramic fibres.

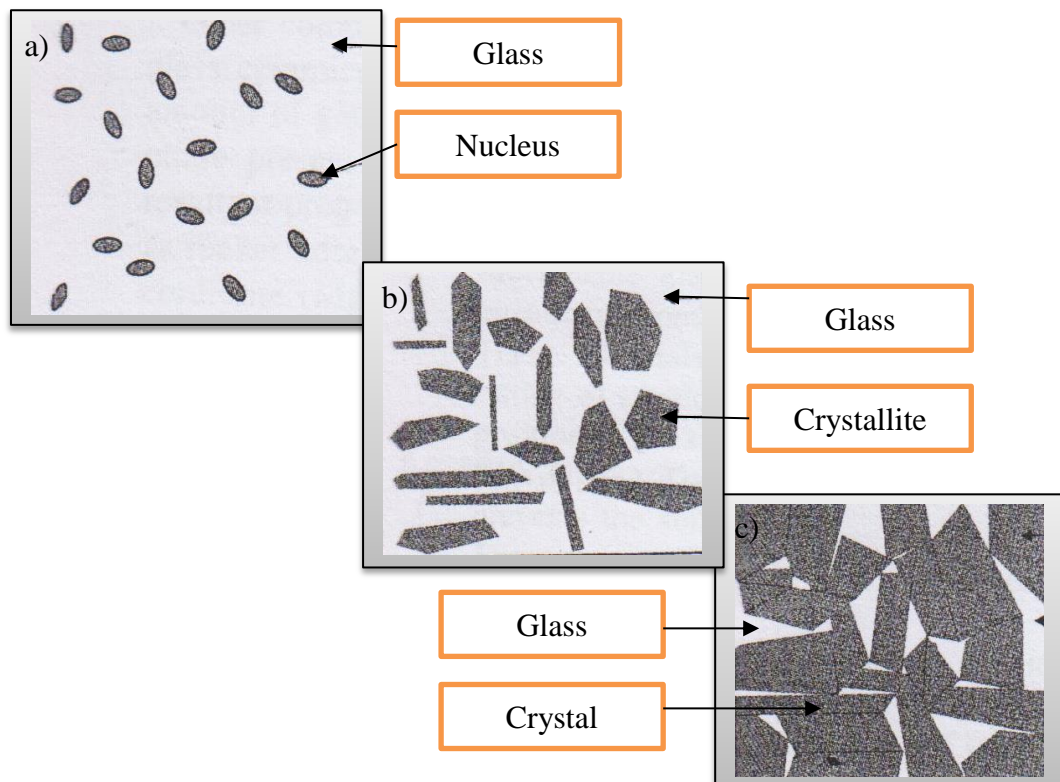


Figure 2.5: Schematic of a) nucleation and b), c) crystallisation in glass ceramic [61].

It is clear that the process involved in the heat treatment of polycrystalline solids is much more intricate than that of amorphous materials. The process for heat treatment is also dependent on the phase separation of the glass ceramic system [62]. This phase separation occurs in two mechanisms:

- 1) Precipitation of the crystal (nucleation and growth);
- 2) During changes in composition between two phases until the immiscibility boundary has been reached, which is called 'spinodal decomposition'.

Different morphologies develop as the result of these mechanisms of phase separation. Figure 2.6 shows an example of the morphology of phase separation due to nucleation and crystallisation. The microstructure of the nucleated sample has similarities with that of the crystallised sample. The phase separation occurs since crystals grow individually, nuclei remain isolated and the second phase formation appears to be liquidus. This second phase will appear as isolated spheres of one equilibrium composition due to the surface energy being minimized and dispersed randomly throughout the matrix of the other equilibrium composition. A low local connectivity of spheres may appear since the nucleation and second phase occur randomly within the melt. This only happens when two neighboring spheres overlap.

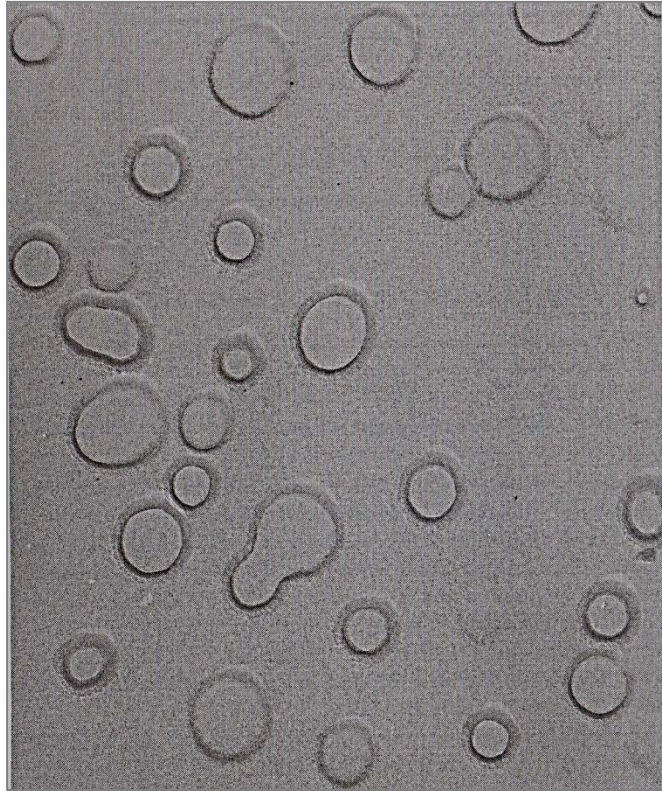


Figure 2.6: Scanning electron microscopy shows ‘spheres in matrix’ morphology [62].

In contrast to that, the spinodal decomposition represents a second phase with a high degree of connectivity and regularly distribution, as illustrated in Figure 2.7. This morphology was referred to as the interconnected region. Therefore, the results obtained from the selected temperatures and dwelling time make the corresponding heat treatment useful for making qualitative descriptions.



Figure 2.7: Micrograph of spinodal decomposition with an interconnected morphology [62].

2.3.2 Nucleating agents

Various nucleation agents have been applied in glass ceramic systems. Titanium dioxide, TiO_2 is predominantly used in glass ceramic $\text{MgO-Al}_2\text{O}_3\text{-SiO}_2$ systems and in other systems as well. This nucleating agent is soluble in molten glasses. However, during cooling or subsequently reheating, large numbers of sub-micron particles are precipitated and utilised in the development of major crystal phases. The preferred nucleating agents for cordierite based glass ceramics are TiO_2 or combinations of TiO_2 and ZrO_2 [30]. According to Zdaniewski [40] TiO_2 causes glass formation during glass separation and leads to the crystallisation of cordierite. Phases in glass ceramic MAS system nucleated with TiO_2 are summarised in Table 2.1. McMillan [24] reported an efficient and fast nucleating process with TiO_2 used as a mixture with a total mass between 3-5wt%. TiO_2 was reasonably soluble in silicate melts since 20% or more of this oxide can be dissolved and markedly lower the viscosity of the glass melts [63]. Shyu and Wu [63] reported that the addition of

TiO₂ improved the nucleation and crystal growth, in agreement with the work of Mingsheng et al. [64] which reported that phase separation and crystal seed increased with the increasing content of TiO₂. Moreover, Gür and Ozturk [65] showed that an additional 2wt% of TiO₂ initially altered the elastic properties of the parent glass. Furthermore, Wange et al. [16] added 10.9wt% and facilitated an increase in Young's modulus up to 137GPa. Many researchers have obtained good mechanical properties by adding TiO₂ to the glass [16-17, 28, 31, 40]. Shao et al. [17] used TiO₂ as a nucleating agent in MAS glass-ceramic and treated it to 1100°C for 2 hours, producing a maximum elastic modulus of 137GPa accompanied by a microhardness of 8.5GPa.

A study by Guo and Yang [66] concluded that the presence of fluorine promotes β -spodumene without transformation from β -quartz at lower crystallisation temperatures. A study by Khater and Idris [67] reported that a low content of TiO₂ greatly affects both the crystalline phase composition and the uniform fine-grained microstructure. Development of β -spodumene has been seen at the earliest stage of crystallisation and has lowered the crystallisation temperature. In contrast, the addition of small quantities of ZrO₂ retarded the formation of β -spodumene but still produced a very fine-grained microstructure. Moreover, crystal growth was markedly affected by small changes in composition and as a consequence the mechanical properties of the material were also affected [68].

Therefore, the choice of nucleating agents can have a marked influence upon the crystal phases present in the final glass-ceramics. One possible explanation for the high strength of MAS glass-ceramic is the role played by the nucleation agent in the development of crystal phases during heat-treatment.

2.4 The studies of glass ceramics fibre

Reinforcements are constituents in composite materials that are embedded into the matrix in order to enhance or reinforce its mechanical properties. In most cases, the reinforcement is harder, stronger and stiffer than the matrix, although there are some exceptions [69]. Despite serving as a purely structural member as they impart high strength and stiffness in the matrix it may also be used to change physical properties such as wear resistance, electrical resistance, friction coefficient, or thermal conductivity [37]. However, the effectiveness of the reinforcement is dependent on the geometry of the reinforcing phase; or in other words, as mentioned by Mathews and Rawling [69], the mechanical properties of composites are a function of the shape and dimensions of the reinforcement.

High modulus of elasticity is desired in component design where glass ceramic fibres are used for reinforcing polymers. Despite these good properties, they are hard to prepare due to the high melting and forming temperatures, large crystallisation tendency and complex processing, phase separation on cooling and compositional changes.

Glass ceramic materials have attracted researchers due to their wide range of glass-forming compositions and properties [70-71]. Several studies have suggested that controlled heat treatment has an important role in modifying the properties of various glass ceramic systems depending on the temperature regime, base composition, addition of other components, amorphous phase separation and the mechanisms of heat treatment [9-10, 25, 30, 72]. These factors affect preparation of the nuclei (nucleation stage) which should be sufficiently ordered in order to promote the crystal growth (crystallisation stage) in a stable manner. These parameters can determine which melts will form glasses on cooling and therefore also determine the processing conditions for a glass ceramic fibre.

A study by Booth and Rindone [6] comprised the crystallisation characteristics of untreated and AgNO_3 - treated fibres. Their findings indicated that the crystallisation behaviour was controlled either by a growth process or a nucleation

process, depending on whether the temperature was below or above peak crystallisation, respectively.

In 1976, Stringer and co-workers [73] prepared a glass ceramic fibre from an aluminosilicate system. This fibre had a microcrystalline interior and a relatively amorphous outer surface layer which was obtained by a coating of potassium nitrate and was heat treated at two heat treatment regimes. These were between the temperatures of 400°C to 420°C and 490°C to 525°C. The strength of the glass ceramic fibre was 38% higher at the higher temperature range than at the lower heat treatment. These results supported the finding that the additional surface coating on the glass ceramic fibre contributed to the value. The modulus was also slightly higher by 3.5%, due to the precipitation of phases that did not cause any considerable changes with the different temperatures employed.

One of the earliest works on glass ceramic fibres was conducted by Jones and McMillan [8] on a lithium disilicate system. They both agreed that the tensile strength of glass ceramic fibres decreases with the crystallisation time for any given temperature of crystallisation. This is due to the influence of the size of flaws. They proposed that the size of flaws increased due to the volume change which occurred during crystallisation where large residual stresses developed. However, the modulus inversely increased with the increase in crystallisation temperatures. This has been related to the development of the phases within the glass ceramic fibre.

The study of Yuan et al. [74] investigated the effect of crystallisation on the mechanical properties of a Li-Al-B-Ti-Zn-silicate system glass ceramic fibre. Their study indicated that tensile strength and alkali resistance were affected by phase separation, nucleation, crystallisation and microcracks. They suggested that the properties of the glass ceramic fibre could be optimised if the temperatures of phase separation, nucleation and crystallisation were closely controlled. Additionally, these parameters led to a finer size of crystallites. They also discovered that both properties could be increased by characterising the glass ceramic fibre at low temperatures (near to T_g) and covering the surface of the fibre with a suitable coupling agent during the heat treatment.

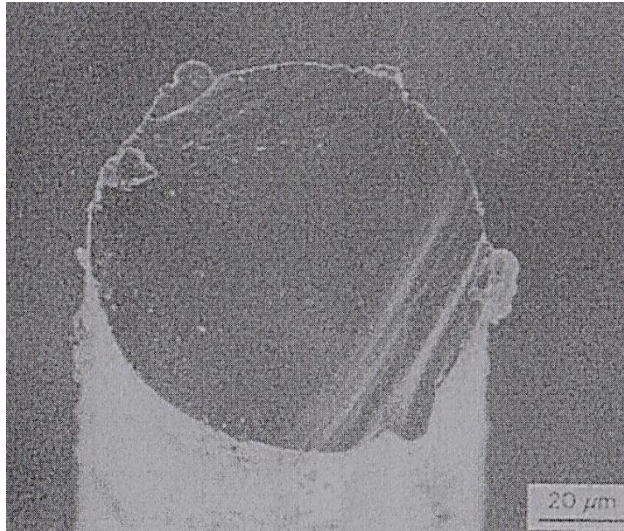
Raju [75] used pegmatite obtained from lepidolite mica and prepared the fibres by pulling them out from the melt using alumina rods before heat treating them at different temperatures and durations. The results from DTA, X-ray and SEM analyses were compared with as-cast glass of the same composition. The Vickers microhardness of these fibres was higher and they had fewer pores than the parent and as-cast glasses. It was summarised that initial phase separation had taken place during fibre drawing which led to crystal formation and did not cause any appreciable changes at high temperature in comparison to as-cast glass.

Ashbee [7] extruded oriented $\text{SiO}_2\text{-Li}_2\text{O-ZnO}$ glass ceramic fibres near to the crystallisation temperature before fibre drawing. The volume fraction of oriented crystals was observed to increase even after drawing process. Moreover, significant enhancement in Young's modulus was also observed. Onishi et al. [12] prepared a glass preform with different compositions of Bi-Pb-Sr-Ca-Cu-O glass ceramic and softened it before successfully drawing it into fibres with smooth surfaces and without observed porosity. In contrast, Sakamoto and Yamamoto [11] used crystallised $\text{LiO}_2\text{-Al}_2\text{O}_3\text{-SiO}_2$ (LAS) preforms in order to study the drawing formability. The LAS glass ceramic capillaries drawn from the crystallised preform showed a low thermal expansion coefficient and excellent mechanical properties. They expanded on their work [22-23] in order to produce silica glass ceramic single-mode optical fibres (GC-SMFs). An excellent high-temperature resistance ($\sim 500^\circ\text{C}$) has been achieved. Attention has been drawn to the use of glass ceramic fibres in superconducting applications.

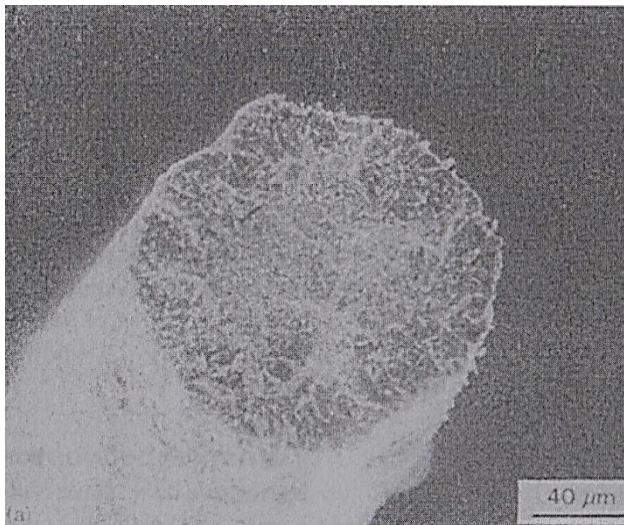
Hirose et al [76] and Komatsu et al. [77] used a $\text{Bi}_2\text{Sr}_2\text{CaCu}_2\text{O}_x$ system to develop and investigate the resistivity of Bi-based fibre glass using glass ceramics. Glass ceramic fibre has thus shown progress in superconductivity by controlling the microstructure, which depends on the annealing temperature.

Hu et al. [78] took a further step with $\text{Bi}_2\text{Sr}_2\text{CaCu}_2\text{O}_x$ system by studying the effect of Al_2O_3 on the fabrication of glass ceramic fibres. A glass preform was used to draw fibres above the crystallisation temperature. It was found that the fibres

successfully drawn over 100cm in length were consistent in diameter and circular shape (Figure 2.8(a)).



(a)



(b)

Figure 2.8: Micrograph of a) drawn fibre of circular shape and b) after heat treatment [78].

The Al_2O_3 played a role in controlling the transition and crystallisation temperatures [79] but was not significantly applied to a glass working range.

However, issues involving shrinkage and distortion arose during the heat treatment process due to the addition of Al_2O_3 , as shown in Figure 2.8(b).

Tick [80] studied passive scattering losses on SMFs and developed [81-82] high transparency glass ceramic fibres. This work suggested that the distortion of glass ceramic fibres might be due to heat treatment. They suggested that appropriate heat treatment ranges need to be determined experimentally. They also proposed that the ceramming process should be limited to less than one hour in order to avoid the possibility of distortion. These suggestions agree with Samson et al. [82] and Liu et al. [83] whose studies found that the strength and ease of handling of glass ceramic fibres is highly dependent on the details of the particular heat treatment schedule used.

Although the various parameters for heat treatment are well understood and have been studied by several researchers as mentioned above, the factors affecting strength in glass ceramic fibres remain unclear. Thus far, some of the details of the relationship between properties and structure remain to be determined. With estimated thermo-mechanical data, it is now possible to identify some of the factors that lead to the development of glass ceramic fibres for high temperature applications.

2.5 Strength of glass fibre

2.5.1 An overview of fibre strength analysis

It has been reported earlier that microscopic flaws critically affected mechanical properties, especially fibre strength [24, 84]. Strength measurements tend to have a relatively large scatter in data due to several factors [85] including the quality of raw materials, surface and heat treatment, thermal history, handling procedures, fabrication and test methods [55,86-88]. Kurkjian [89] presented a diagram representing the relationship between the strength of a glass and its flaws. The presence of these flaws were categorised as being pre-existing or introduced by the application of the material (Figure 2.9).

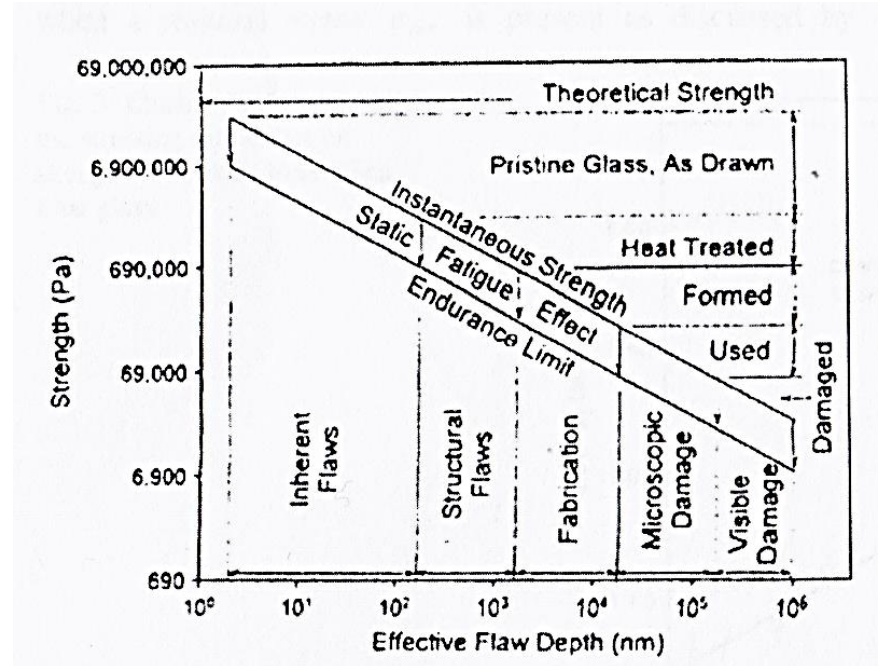


Figure 2.9: Diagram of variation in strength with flaw size for several different glasses and common glass objects [89].

Scatter in the strength values may be explained by the existence of a distribution of flaws of various lengths of the fibre [90-91]. The earliest study by Griffith on strength was conducted in 1921 [92]. He assumed that the materials are homogenous, linearly elastic, and isotropic and that the applied stress is constant and the presence of narrow elliptical internal crack. The study suggested that the apparent strength of glass is more severely affected by the existence of surface flaws rather than internal flaws. As given by Equation 2.1 in **Section 2.2.3**, the presence of a fracture is due to the concentration of stress on a crack tip as an external load is imposed. Hence, propagation of cracks leads to fracture. Therefore, it may be assumed that strength is not an intrinsic material property of the glass.

In addition, it can be seen that pre-existing cracks are related to the size of samples, that is the fibre diameter [93]. This study on wool fibre suggested that the tensile behaviour of fibres is closely related to variations between and within fibre diameters. Zhang and Wang [94] reported that the results of the tensile strength were visibly affected by fibre flaws and geometrical irregularities which hence

required alteration of the Weibull model to produce a prediction gauge length effect with precision. In the present work, this Weibull model is not covered.

This literature study shows a possible difference in values between practical and theoretical strengths, where the practical strengths tend to be lower. Despite the numerous studies mentioned above, few studies have been undertaken on the strength of glass ceramic fibres.

2.5.2 Weibull distribution

Measured strength exhibits a statistical distribution, which may be explained by the existence of a distribution of flaws along the fibre length [92, 95]. Therefore a statistical method was used in which a set of single fibres at different gauge lengths were tested to measure their strength. The Weibull distribution most frequently used for predicting the probability of glass fracture due to a given stress [96].

The majority study of the fibre strength tested often shows a dependency on the gauge length tested as low as 20 μm [97] as compared to the fibre diameter. The tensile strength of fibres was observed to fall with the increasing gauge length as reported by [90, 98-99]. This trend has also been reported by other researchers [100-101] related to the increase in flaw population, which is directly related to the amount of damage sustained by the surface during handling. In addition, Naito et al. [102] suggested that flaws are likely to occur due to the presence of micropores. This hypothesis was supported by Anderson et al. [103] and was found to be responsible for much of the variation in fibre strength, which hence required alteration of the Weibull modulus.

A statistical analysis of the fibre strength was performed using the two-parameter Weibull probability [96]. This is based on ‘the weakest-link theory’ and assumes a random location of independent flaws causing mechanical failure. The probability of failure, P_f , is defined as:

$$P_f = 1 - \exp\left[-\left(\frac{l}{l_0}\right)\left(\frac{\sigma_f}{\sigma_0}\right)^m\right] \quad [2.2]$$

Where P_f is the probability of failure in a length l at the applied stress σ_f , which is the fibre stress at a length l_0 , σ_0 is a scale parameter and m is a shape parameter or Weibull modulus. This is the two-parameter Weibull distribution that was used in the analysis of the strength data. The two parameters (m and σ) were determined experimentally by loading a sample of the material until failure occurred.

The slope of the Weibull modulus is determined by first rewriting Eq [2.2] as:

$$\ln\left[\ln\left(\frac{1}{1-p_f}\right)\right] = m \ln(\sigma_f) + \ln(l) - m \ln \sigma_0 \quad [2.3]$$

Hence, if $\ln(\sigma)$ is plotted against the left-hand side of Eq. [2.3], the gradient from the line appears as the Weibull modulus, m and the characteristic strength, σ_f is obtained from the intercept. The stress at failure is measured and then the probability of failure (and Weibull parameters) can be determined from a dataset, N . The probability of failure, P_i for a series of N samples is based on ranking the failure strength of the fibres from the weakest to the strongest. This ranking was calculated by [104]:

$$P_i = \frac{i-0.5}{N} \quad [2.4]$$

where $i = 1, 2, 3 \dots N$, and P_i indicates the probability of failure corresponding to the i th strength value. These estimators have often been used by Zafeiropoulos and Baillie [105], Thamae et al.[106] and Feih et al.[107] where the definition of $(i-0.5/N)$ produced the least biased m value [108] and did not significantly change the parameters. A study by Faucher and Tyson [109] concluded that a minimum of 30 specimens are sufficient for a good characterisation of the strength of a brittle material in order to assure the reliability of the estimated Weibull parameters.

2.6 Glass ceramic fibre reinforced composites

2.6.1 An Overview of glass ceramic composites

As the term implies, glass ceramic composites have glass ceramic matrices reinforced with fibres. In recent years, glass ceramic is a common matrix material that has been intensively investigated [46, 110-113]. The increase in the popularity of glass ceramic materials is due to their unusual combination of properties [21]. An additional benefit of this material is the ease with which it can be produced at a relatively low process temperature using glass manufacturing routes. Properties that have made glass ceramic materials desirable as a matrix in comparison to other matrix materials include low coefficients of thermal expansion (CTE), high mechanical strength, high abrasion resistance and excellent thermal resistance [44]. Hence, it has received special attention for its use in many structural purposes such as in aerospace applications, such as randomes and solid oxide fuel cell (SOFC) sealants [24,114]. These materials have been particularly attractive in terms of absolute stiffness and strength.

The most common of the commercially successful glass ceramics is $\text{LiO}_2\text{-Al}_2\text{O}_3\text{-SiO}_2$ (LAS) with different additions of nucleating agents. A great number of studies [45-46, 115-116] have aimed towards the development of main crystalline phases which are solid solutions of β -quartz or β -eucryptite and β -spodumen in order to achieve desired properties, especially CTE with an almost zero value. This remarkable property makes LAS easily matched with bonding materials. The increased interest in the use of $\text{MgO-Al}_2\text{O}_3\text{-SiO}_2$ (MAS) system as matrices in composite materials has paved the way for increased research activities in the field for high temperature applications [3-4, 117-119]. Interest in this glass ceramic system continues because cordierite, the main crystalline phase, appears to impart excellent mechanical strength, low thermal expansion, stability at high temperature, good dielectric properties and transparency to radar waves [30].

Many research activities in recent years have focused on understanding of the mechanical behaviour of these glass ceramic materials as matrices but not as reinforcements. This is due to the nature of challenges in the fabrication of glass ceramic fibres which are often too fragile to easily apply in composites. The primary function of a reinforcing fibre is to increase the strength and stiffness of a matrix material so that the resulting part can satisfy the design requirements or replace an existing part with equivalent strength, stiffness and lower weight [120]. Literature regarding the development of glass ceramics as matrices suggests that there are potential applications in the structural sector where low density materials with high temperature capabilities are needed. Unfortunately not much work to date has been undertaken in glass ceramic fibre reinforced composites except those with metal matrices. Stringer and Jones [73] tested several samples fabricated with various pressing methods on glass ceramic fibre reinforced tin. The fibres produced from recrystallised lithia/silica glass were infiltrated with molten tin in a mould. Results revealed that the composites were stronger than the unreinforced metal by 50%. Since the work of Stringer and Jones, very limited the data has been made available for glass ceramic fibre reinforced polymer (GCFRP) in comparison to glass ceramic matrix composite. This thesis has been motivated to continue the study of GCFRP and thus compile information about the mechanical and structural performance of these composites. This has been done from the perspective of the storage modulus, as measured using dynamic mechanical thermal analysis (DMTA) and through observation of the glass ceramic fibre/matrix interphase. Although the study of glass ceramic fibre composites is limited, the literature related to the interphase of glass ceramic matrices is more abundant.

2.6.2 Property characterisation

A brief review of the methodologies used in this study for characterisation and analysis are provided in this section. The description of analytical equipment has also been mentioned.

2.6.2.1 *Dynamic mechanical thermal analysis (DTMA)*

As mentioned earlier, this approach proved necessary because of the limited dimensions of the GCFRP composites produced. Moreover, this method remains a favourable way to evaluate a composite's high temperature performance, interphase and provides a comparison of the moduli as a function of temperature [121-125]. Most of reported results in thermal analysis are taken from the measurement of T_g . This is performed by dynamic mechanical techniques, in which the modulus and damping are measured [126]. Dynamic mechanical analysis has the advantages of offering excellent sensitivity when studying glass transition phenomena and the ability to detect all secondary motion transitions at low temperatures which influence impact resistance of materials [127-128]. Moreover, the modulus curve can be used to interpret structural properties including molecular weight, degree of crosslinking and fibre/matrix interfacial bonding [129].

DMTA is a technique for measuring viscoelastic phenomena. DMTA results are expressed by three main parameters: (i) the storage modulus (E'), corresponding to the elastic storage modulus indicating the elastic storage of energy; (ii) the loss modulus (E''), a measure of the dissipation of energy and (iii) the loss tangent ($\tan \delta$), which is defined as (E'/E'') ratio, useful for determining the occurrence of molecular mobility transitions such as the glass transition temperature [127]. Kuzak and Shanmugam [129] studied the effects of postcuring on storage modulus and $\tan \delta$ using glass-reinforced phenolics. The specimens were tested using dynamic mechanical analysis. The results showed that the un-postcured reinforced sample had a slightly higher E' after the T_g . This is due to the fact that the material encompasses strong fibre/matrix interfacial bonding. However, $\tan \delta$ was lower due to the rigidity of the interface. Therefore, the glass transition temperature (T_g) has become an accepted criterion as a diagnostic aid. This criterion can be correlated to

the mechanical properties of a composite, the chemical structure of its matrix and to the performance of the material under selective environmental conditions [130]. As many end product properties are ‘ T_g -related’, the achievement of a single T_g in a compatible blend can contrast sharply with two or more T_g values in incompatible blends [126], which may also be applicable to composites. Moreover, the relationship between the modulus and temperature depend on their structure and processing conditions. These include the environmental absorption of water, which may cause degradation of mechanical properties, including swelling, formation of internal stresses and possible lowering of the glass transition temperature [69,131].

2.6.2.2 Thermogravimetric analysis (TGA)

Thermogravimetric analysis (TGA) with a sensitive balance is used for measuring the weight changes of the substances as a function of temperature or time. It may be used to determine the decomposition temperature, as shown in Figure 2.10 [48]. The differences in weight denoted with ΔW [initial weight, W_1 – final weight, W_2] are used in quantitative calculations. Yee and Stephens [132] developed this method to measure the fibre volume fraction, which agreed with results obtained by conventional methods. Moreover, this method used comparatively less time and a lower mass of materials. Moon et al. [133] measured the fibre content in composites with results that were in good agreement with standard digestion and ignition loss methods. This method has been documented in ASTM Standard E1131 [134] and analysed using ASTM D3171-99 [135], as described in **CHAPTER 4**.

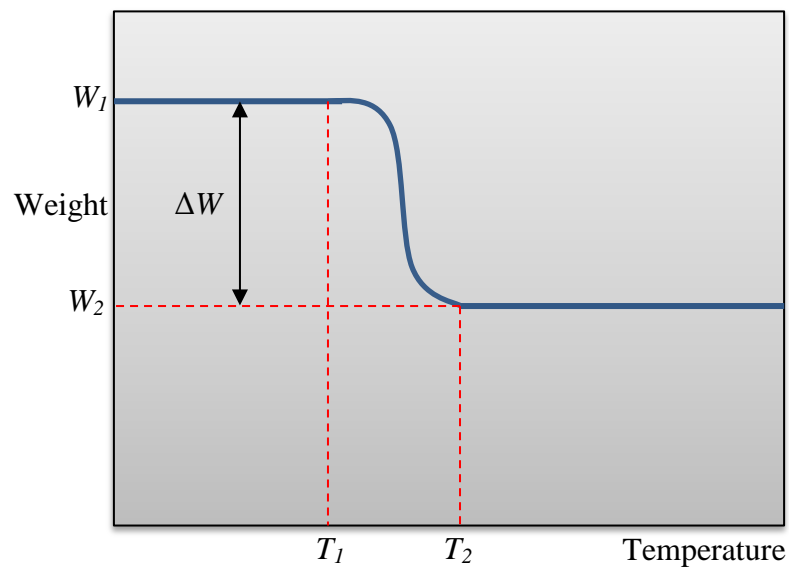


Figure 2.10: Schematic of decomposition reaction [48].

2.6.2.3 Scanning electron microscopy (SEM)

Scanning electron microscopy was used in this study to observe fractured samples. These observations focused on the fibre/matrix interface and related to the properties of the composite. The interface between the matrix and reinforcement have an intense effect on the composites materials [115, 136-137, 1986; 138-140]. This can be illustrated by Figure 2.11 which shows a schematic diagram of the fibre-matrix interface and all of its components within a circular region called the interphase [141]. Herrera-Franco and Drzal [141] summarised that the interphase consists of a three-dimensional area of contact between the interface of the matrix and the reinforcement system and incorporates a finite thickness on both sides of the interface.

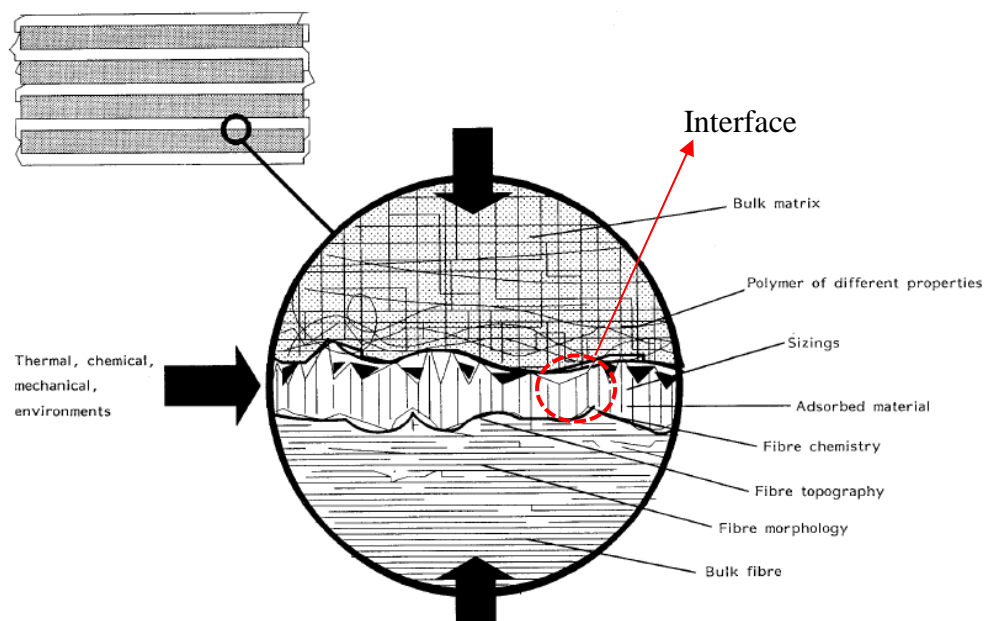


Figure 2.11: Characteristics of the fibre/matrix interphase in a composite material [141].

This interphase included a sizing layer. Almost all glass fibres are sized in order to avoid surface damage, which also functions as a bonding agent between the fibre and matrix. However, some researchers [142-143] have reported that untreated glass fibres adhere well to epoxy. This may be due to the acidic nature of glass surfaces [144]. Glass fibres are normally sized with silanes in order to prevent surface damage which is expected during fibre handling [145-146] and sizing can prevent considerable absorption of moisture from the environment [147].

The interphase plays an important role in determining the static and dynamic properties of composite materials, [148] which are influenced by several factors during manufacturing [149] including the presence of voids and impurities, unreacted polymer components, chemical reactions at the interface and variation in the morphology of the matrix close to the surface of the reinforcement [150]. Low interfacial adhesion results in a weak interface, which may cause fibres to debond from the matrix. This may generate voids, which can grow into cracks and precipitate failure.

Bansal [110] reported limited improvement in the properties of unidirectional (UD) composites from glass ceramic reinforced with uncoated SiC fibres produced by chemical vapour deposition. Fibre volume fractions of 24% were obtained. The fibre/matrix bonding was tested using fibre push-out, the results of which correlated well with SEM fractography. SEM observation of fracture surfaces of uncoated SiC composite samples showed good interfacial adhesion between the SiC fibres and the glass ceramic matrix. This was sufficiently strong to prevent the fibres from being pushed out. Compatibility showed a presence of chemical reaction after composite processing between the two materials. An oxidation by the carbon fibre contributed stronger bonding at the interface. The ultimate strength of the unidirectional SiC fibre/SAS (strontium aluminosilicate) composite measured by three-point flexure was directly influenced by the strength of the adhesion.

Ye et al. [111] embedded short carbon fibres in barium aluminosilicate glass ceramic (BAS) and BSAS, as well as BAS doped with strontium aluminosilicate (SAS). These composites were prepared by hot pressing before measurement of fracture toughness and flexural strength. The results showed that the mechanical properties increased with reinforcement by a fibre volume fraction of 30% in a BAS glass ceramic composite. TEM (transmission electron microscopy) revealed good bonding at the fibre/matrix interface region with BAS and BSAS. Moreover, the use of SAS as a doping agent was supported by the findings of reduced mismatch between the coefficients of thermal expansion. In addition, Vicen et al. [113] found that fibre coatings inhibit interfacial degradation under most of the temperature conditions used.

2.7 Concluding remarks

The following conclusions can be drawn from this review:

- Glass ceramics are versatile materials that have been widely utilised for advanced applications due to their excellent mechanical and thermal properties. However, these properties are strongly influenced by the composition and development of phases which are dependent on heat treatment. Recent studies that have dealt with the fabrication of the glass ceramics have encountered challenges in increasing the strength of these materials due to their brittle nature and the presence of surface flaws. Subsequent improvements in control of heat treatment and handling during fabrication of glass ceramic fibres may simultaneously reduce the severity of surface flaws and increase the fibre strength.
- Recently, glass ceramics have been extensively investigated as matrices in composites for their low thermal expansion and high mechanical properties. It has been shown that the use of glass ceramic as matrix systems for the fabrication of fibre reinforced composites has been well accepted in high performance applications. It is more focused on the carbon fibre due to the mismatch in thermal expansion. Based on the literature development of glass ceramic as matrices, it is seen that there is a potential application in introducing glass ceramic fibre in composite. Owing to very limited information available for glass ceramic fibre reinforced polymer (GCFRP), it has been shown that the fabrication of glass ceramic fibre composites has been a challenge.

This thesis will focus first on the development of glass ceramic fibre in MAS and LAS systems. The thermal and mechanical properties of the bulk glass ceramic system will be evaluated based selection of the parameters heat treatment. The optimum heat treatment will be selected to fabricate the glass ceramic fibre and will be tested. The investigation of glass ceramic fibre reinforced composites is extremely limited. The aim of this thesis is therefore to study the feasibility of the

fabrication of glass ceramic fibre reinforced composites. In addition, the relationship between the fibre/matrix interface and the parameters that influence the material properties will be presented.

Chapter 3

Fabrication of glass and glass ceramic fibre

3.1 Summary

This section outlines the research methodology used during fabrication work. All the experimental procedures are detailed in **CHAPTER 4**. It comprises three main parts, as shown in Figure 3.1. Topics covered in this chapter include: preparation and characterisation of bulk samples, fabrication of glass and glass ceramic fibres and preparation of glass ceramic fibre reinforced polymer composites. This study considers glass systems consisting of MgO-Al₂O₃-SiO₂ (MAS) and LiO₂-Al₂O₃-SiO₂ (LAS).

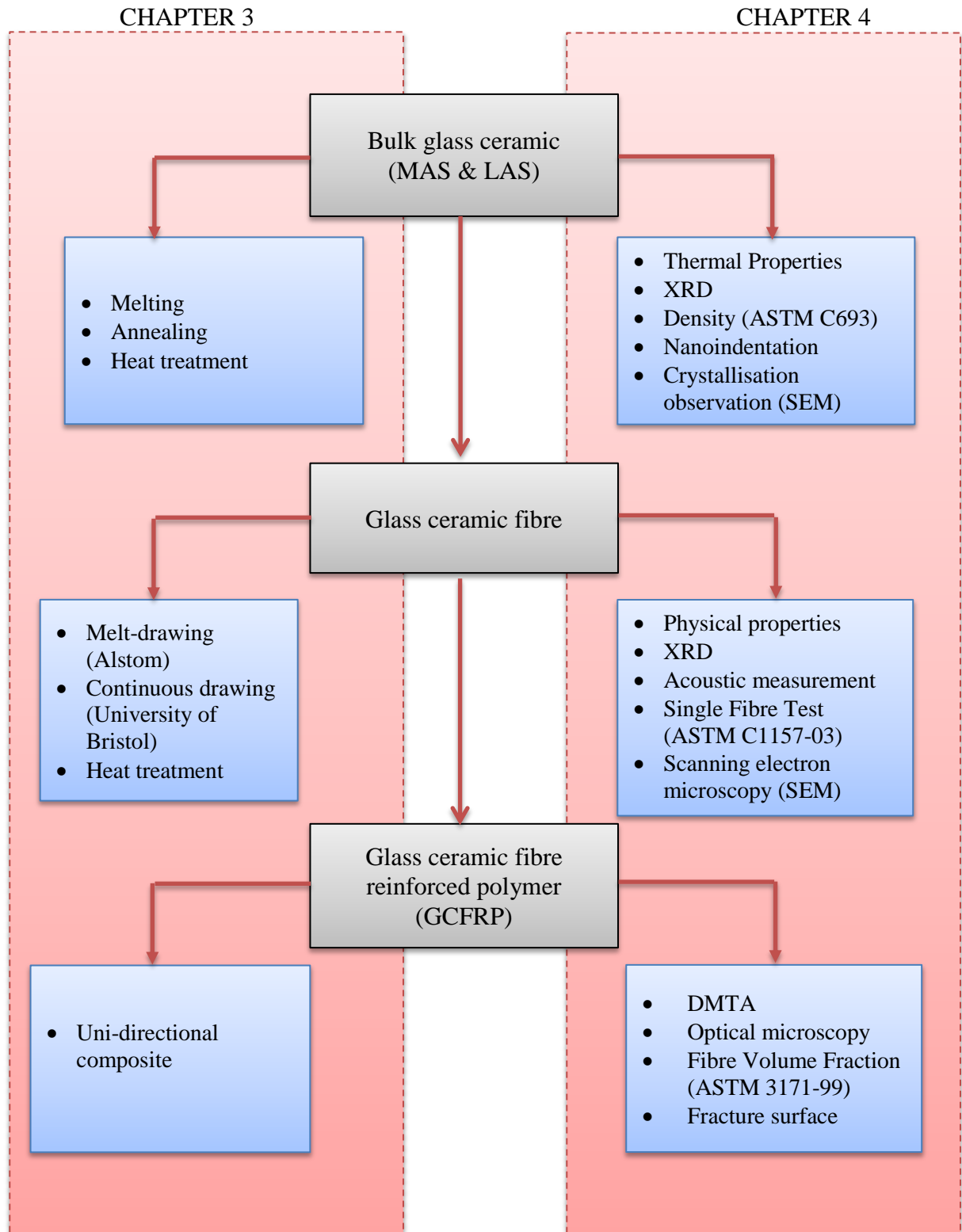


Figure 3.1: Flow diagram for the processing of glass ceramic MAS and LAS systems.

3.2 Preparation of glasses

3.2.1 MgO-Al₂O₃-SiO₂ (MAS) glass

The composition of the MAS glass ceramic investigated in this work is shown in Table 3.1. The batch of the MAS system was prepared using reagent-grade chemicals supplied by Fisher Scientific, except for SiO₂ (Loch Aline Silica) where high quality silica glass-making sand was used. Throughout the study, this composition was chosen from the literature [16]. This composition has been selected for its suitability in forming glass ceramic fibres for particular applications. Previous investigations have reported that is characterised by excellent Young's modulus in bulk form. Despite the good depth of study into this material, there are some outstanding areas of interest related to the preparation of glass melt and heat treatment processes that are considered by this study.

Batches of MAS were weighed using a balance with an accuracy of ± 0.01 g to produce a 700 gram melt, and placed separately onto brown sugar paper. The batches were then mixed through manual rolling with a spatula for 5 minutes prior to storage in polyethylene bags before followed up with the melting stage (Figure 3.29(a-d)). The bag was manually shaken for 1 minute before the mixed batches being placed in alumina crucibles. They were then calcined overnight at $1000^{\circ}\text{C} \pm 2^{\circ}\text{C}$ with a heating rate of $5^{\circ}\text{C}/\text{min}$ in an electric furnace before the melting process. The purpose of calcination was to avoid thermal shock and to ease the handling of low density powders, notably magnesium carbonate. During this process the volume of the batch was reduced, and settled on the bottom of crucibles. This allowed the batch to be easily handled and transferred to the gas furnace without encountered possibility of agitation and thus contamination of the powder.

Table 3.1: Glass composition of MAS system [16].

Oxide	Fraction (wt%)	Raw material	Supplier	Purity (%)
SiO ₂	51.4	SiO ₂	Tilcon	99
Al ₂ O ₃	28.9	Al(OH) ₃	Fisher Scientific	>98
MgO	8.8	MgCO ₃	Fisher Scientific	>98
TiO ₂	10.9	TiO ₂	Fisher Scientific	98

The melting process was carried out at $1600^{\circ}\text{C} \pm 2^{\circ}\text{C}$ for about 3 hours in a gas furnace for the purpose of refinement in the absence of stirring where it was expected that a clear homogenous melt would be obtained. An optical pyrometer was used to ensure similarity between the programmed input (1600°C) and melting temperatures. The glass melts were cast onto two preheated steel plates with dimension 30mm x 15mm x 15mm and then annealed in a muffle furnace to minimise thermal strains.

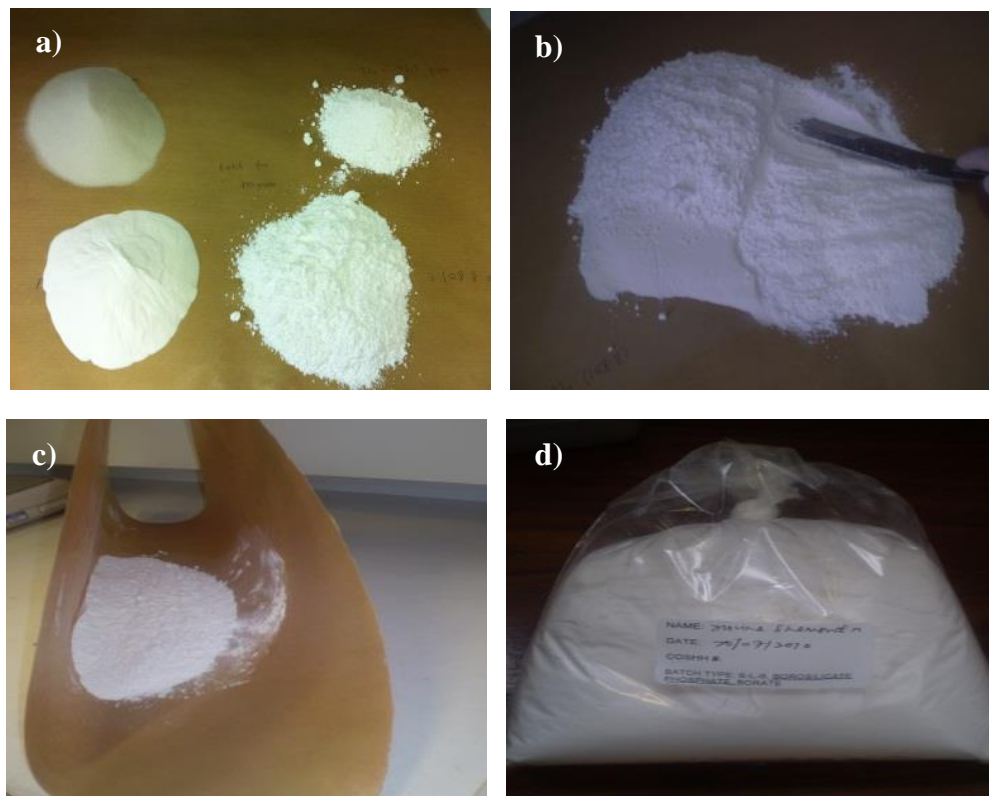


Figure 3.2: Manual preparation of MAS glass a) raw materials, b) mixing using spatula, c) rolling process and d) storage in polyethylene bag.

Annealing reduced the thermal stresses that formed during the cooling of the glass after melting, since the outer surface cooled at a faster rate than the inner surface. The glass melts were cast as blocks onto the preheated steel plates and were annealed as specified in Table 3.2 before being oven cooled to room temperature. As Wange et al. [16] reported, the crystallisation sequence during heat treatment is dependent on the prior annealing schedule. In this work, two different annealing schedules were studied here. The cast glass was annealed and then cooled at 1°C/min. The annealed glasses were observed through a strain viewer to detect the presence and location of stresses and any flaws or imperfections that may have caused premature failure. The glass bars were then cut into 15mm x 15mm x 5mm sections for use in the nucleation and crystallisation processes. As-prepared glass bars were ground using an agate mortar and sieved through a 450 mesh to obtain glass powder for thermal analysis.

Table 3.2: Schedule of annealing temperature of glass ceramics.

Sample	Annealing temperature (°C± 2°C)	Time (hour)
A	700	1
	600	1
B	570	2

3.2.2 LiO₂-Al₂O₃-SiO₂ (LAS) glass

The composition and thermal properties of the LAS glass ceramic are not reported due to a confidential agreement. LAS glass ceramic was chosen for the unusually low temperature at which it densifies temperature (<1600°C), which enables fabrication in a low viscosity glassy state with subsequent transformation into a more refractory crystalline state.

The preparation of the batch was done at the Research Technologist –Materials Laboratory, ALSTOM. The constituents were initially mixed and purified in the

presence of ethanol, after which the dried mixture was ground in a ball mill for one hour. Ethanol was used to entrap impurities and it evaporated without changing the composition. The mill was also allowed to run uninterrupted for 1 hour for a better mixing. The resulting glass powder was then sieved with alumina balls through a vibrating fine mesh screen. The prepared batch was then melted in a platinum crucible.

3.3 Heat treatment route of bulk glass

3.3.1 Nucleation and Crystallisation

In this study, two heat treatment steps were imposed on both glass systems. Figure 3.3 shows a schematic of a two-step heat treatment schedule to produce a glass ceramic. The first heat treatment step was a nucleation process that caused localised crystallisation. This was accomplished by holding the glass at a temperature between the glass transition point, T_g and the crystallisation point [24] to allow the formation of the required density of crystal nuclei. The second crystallisation heat treatment was carried out to promote the growth of nuclei in order to fully convert the substance to its glass ceramic phase. The selection of heat treatment temperatures for MAS and LAS system were based on DTA curves in Figure 5.1 and Figure 5.2, respectively.

The nucleation and the crystallisation of MAS and LAS glasses temperatures are shown in Table 3.3 and Table 3.4. The heat treatment of MAS glasses were carried out in Glass Laboratory, Department of Materials Science and Engineering, The University of Sheffield and LAS glasses in Research Technologist –Materials Laboratory ALSTOM, respectively. Samples with 5 mm thick cross-sections were cut from the parent MAS glasses and arranged in an electric furnace. The samples were heat treated to the nucleation temperature $720^{\circ}\text{C} \pm 2^{\circ}\text{C}$ for 3 hours at heating rate of $5^{\circ}\text{C}/\text{min}$ and subsequently cooled to room temperature at a rate of $1^{\circ}\text{C}/\text{min}$. Further heat treatments were carried out at different crystallisation temperatures between $800^{\circ}\text{C} \pm 2^{\circ}\text{C}$ and $1140^{\circ}\text{C} \pm 2^{\circ}\text{C}$ with a heating rate of $5^{\circ}\text{C}/\text{min}$ and cooling rate of $1^{\circ}\text{C}/\text{min}$. The glass ceramics

were then cooled to room temperature. Any visible changes onto samples were recorded.

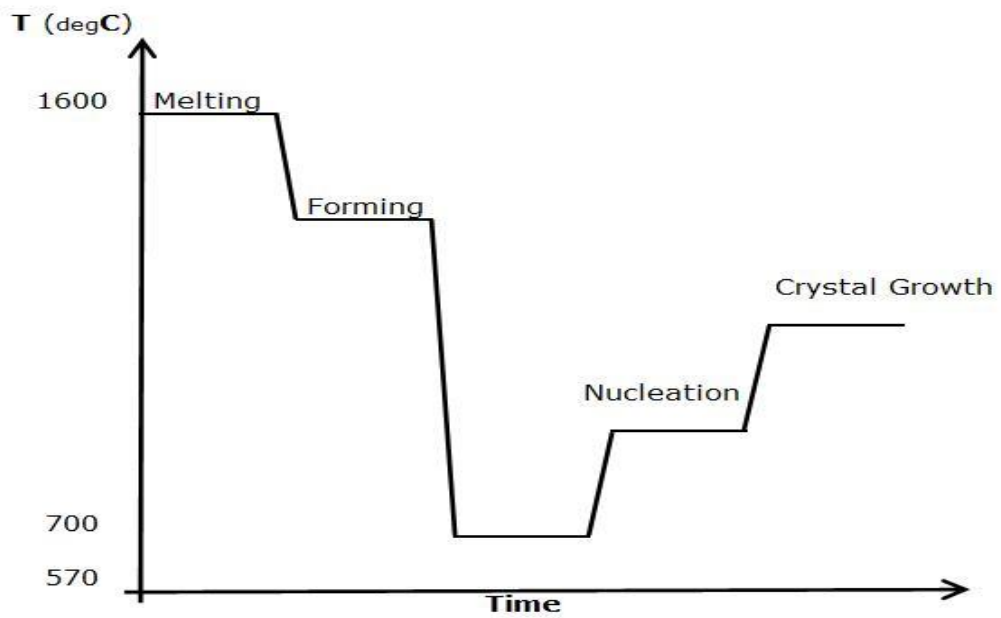
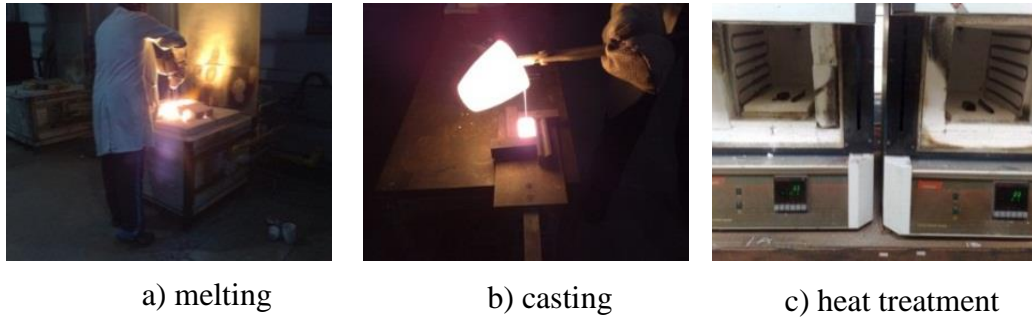


Figure 3.3: Schematic of preparation of MAS glass ceramic.

Table 3.3: Heat treatment schedule of MAS glass systems.

Heat treatment stage	Temperature (°C)	Heating/Cooling rates (°C/min)	Dwelling time (h)
Nucleation	720	Heating : 5 Cooling : 1	3
Crystallisation	800	Heating : 5 Cooling : 1	2
	850		2
	900		2
	950		2
	1000		2
	1140		2

Table 3.4: Heat treatment schedule of LAS glass systems.

Heat treatment stage	Temperature (°C)	Heating/Cooling rates (°C/min)	Dwelling time (h)
Nucleation	500	Heating : 5 Cooling : 1	100
Crystallisation	750	Heating : 5 Cooling : 1	2
	950		2
	$T_n : 600$ (2hr); $T_c : 750$ (2hr)		

3.4 Fabrication of MAS and LAS glass ceramic fibre

3.4.1 Melt drawing MAS fibre

3.4.1.1 Molten glass

1000 gram batches of MAS were weighed and calcined overnight in alumina crucibles at $1000^{\circ}\text{C} \pm 2^{\circ}\text{C}$ as described in **Section 3.2.1**. The melting process was carried out in the Materials Laboratory, ALSTOM. Calcined batches were then placed in platinum crucibles and melted at $1600^{\circ}\text{C} \pm 2^{\circ}\text{C}$ for 12 hours in an electric furnace (Carbolite 1800) to remove bubbles and ensure the formation of a clear homogenous bulk melt.

3.4.1.2 Drawing procedure

Figure 3.4 illustrates the melt drawing process. Figure 3.4a,b shows the molten glass was heating at melting temperature, $1600^{\circ}\text{C} \pm 2^{\circ}\text{C}$. The process started by transferring the platinum crucible from the main furnace and heating the platinum crucible in a controlled-atmosphere Carbolite furnace at a temperature of approximately $1240^{\circ}\text{C} \pm 2^{\circ}\text{C}$ (Figure 3.4c). A platinum wire with a diameter of 0.05mm was lowered into the platinum crucible and brought in contact with the melt as shown in Figure 3.4d. The MAS fibre was immediately up-drawn at a temperature of approximately $1240^{\circ}\text{C} \pm 2^{\circ}\text{C}$ at which point the melt viscosity was high enough to allow drawing of the glass fibres (Figure 3.4e). The diameter of the fibres was controlled by the speed at which the glass was manually pulled out. The overall speed was presumed the same, based on the same man power used. The overall height between the upper furnace and the pulley system was approximately 2 meters. Upon drawing the glass fibres were immediately cooled by the ambient temperature of the laboratory and cut at 15cm lengths using sharp scissors. Each of the single fibres was carefully placed in storage boxes filled with silica gel and arranged onto a piece of papers in separated layers in order to prevent fibre damage before further tests. No diameter measurement was done along the drawn length to avoid pre-existing defect.

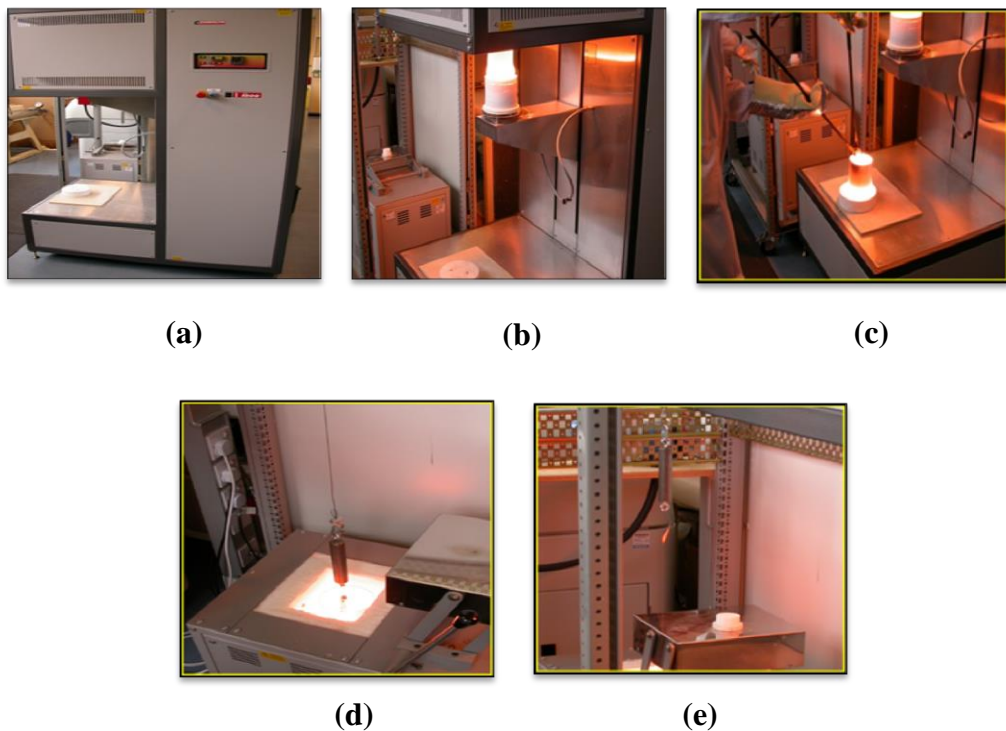


Figure 3.4: Images of up-drawing process of MAS glass fibre.

3.4.2 Continuous drawing of LAS fibre

3.4.2.1 Preparation of glass rod

The preparation of the glass melt was undertaken as described in **Section 3.2.2**. Strong rod glasses up to 1.5m in length with 5mm diameters were produced at the Materials Laboratory, ALSTOM. For rod glass making, a metal rod with an end cap diameter of 10mm was dipped into molten LAS glass processed with a similar method as the MAS fibre drawing described in **Section 3.4.1.2** (Figure 3.5(a,b)). Figure 3.5e shows the length of the rods, which was measured to be above 1.5 meters to enable the drawing process. These rods were used for continuous drawing with the fibre tower located at the Advanced Composites Centre for Innovation and Science (ACCIS) at the University of Bristol.

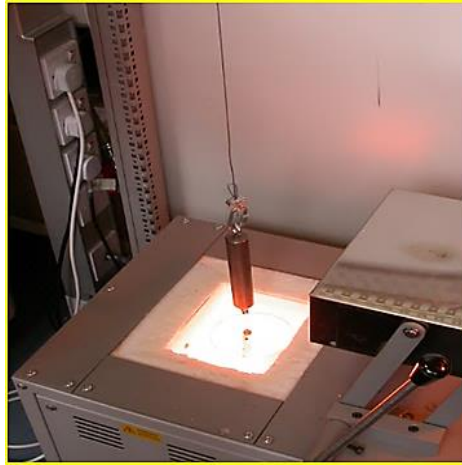
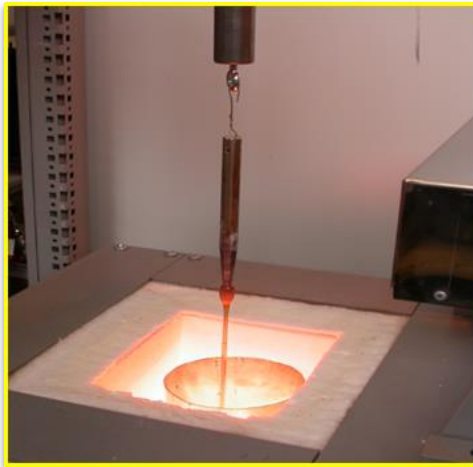
(a)**(b)****(c)**

Figure 3.5: Images of fabrication of LAS glass rods.

3.4.2.2 Drawing procedure

The drawing process produced glass fibres by reducing the diameter of a glass rod. LAS glass rods were cleaned with acetone prior to drawing, to remove any dirt and clamp adequately inside the gripper, as shown in Figure 3.6a. The furnace was used to heat the glass to its softening temperature to avoid degradation while drawing, and care was taken to prevent the glass rod from touching the heating coil of the furnace. A short orange flame was observed as the glass rod softened (Figure 3.6b), whereupon the lower end of the glass rod (gob) descended through the furnace by the force of gravity. The rod passed downward through the path of a laser operated monitor (Figure 3.6c)

that determined the diameter of the fibre. The emerging fibre was pulled manually to encourage its descent Figure 3.6d.

A Heathway controller monitored the reduction in diameter of the finely drawn fibre which was taken up by a rotating thread drum. Thus the thickness of the fibre was dependent upon the rate of drawing and the feed rate was adjusted to precisely control the fibre diameter. The furnace temperature was also constantly monitored and recorded. Drawing and winding continued until the glass rod was fully drawn (Figure 3.6e). The fibre glass was connected with drum during the drawing and assembled into frames (Figure 3.6f) which were carefully placed in a box filled with silica gel and arranged onto a piece of plastic film into separate layers in order to prevent fibre damage.

The fibres were heat treated in order to convert the microstructure from glass to glass ceramic. For this purpose, the temperature and dwell times followed the heat treatment schedule of the bulk system. Any visible changes on the fibres were documented. Some of the fibres appeared white as a result of crystallisation on the surface and/or inside the samples.

An experimental approach was implemented in order to find the optimum heat treatment temperature and dwell time, as suggested by Tick et al. [81]. This was imperative due to the sensitivity of the fine samples to heat distortion. Thus,

precise determination of temperature and dwell time was only obtained by visible changes to the physical glass fibre.

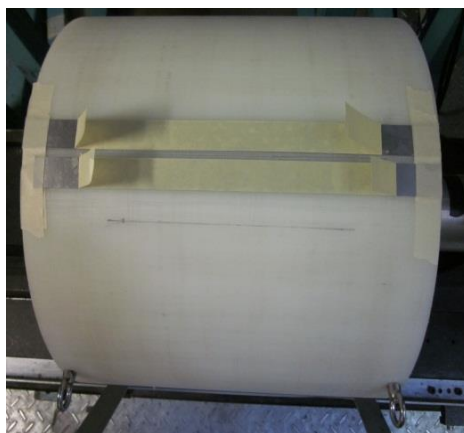
**(a)****(b)****(c)****(d)****(e)****(f)**

Figure 3.6: Sequence of a fibre drawing process of LAS glass using fibre tower.

3.4.3 Heat treatment route of glass fibre

Samples of annealed LAS glass fibres were gently cut into 15cm lengths and were individually placed on a ceramic plate with a separation of 5mm from one another before insertion into an electric furnace (Figure 3.7). MAS glass fibres were segregated into three groups according to their diameter sizes. The preliminary heat treatment was done according to the same procedure as that of LAS glass fibre.

The ideal temperature and dwell time for each glass system are presented in Table 3.5 based on visual observations of physical change (e.g colour, physical shape) which describes in **CHAPTER 5**. Both glass systems were then treated with heating and cooling rates of 5 °C/min and 1°C/min, respectively.

Table 3.5: Heat treatment schedule of MAS and LAS glass fibres.

Glass system	Annealing temperature, T_a (°C ± 2°C)	Nucleation temperature, T_n (°C ± 2°C)	Crystallisation temperature, T_c (°C ± 2°C)	Time (h)
MAS	570	720	900	T_a :0.25 T_n :1 T_c :1
LAS	500	550	720	T_a : 0.25 T_n :2 T_c :1



Figure 3.7: Glass fibres in the electric furnace.

3.5 Fabrication of glass and glass ceramic reinforced polymer composite

3.5.1 Materials

3.5.1.1 Epoxy resin

In this study, the polymer matrix used was an epoxy resin of Epikote 828, diglycidyl ether of bisphenol-A (DGEBA) obtained from Delta Resin Ltd, UK, cured with an anhydride hardener consisting of 1-methyl-5-norbornene-2,3-dicarboxylic anhydride (NMA) supplied by Robnor Resins, UK. This formulation was added with an accelerator consisting of benzyldimethylamine (BDMA), supplied by Robnor Resin, UK. The mechanical properties of the cured resin used in this preparation are summarised in Table 3.6. The density of the resin was 1.23 g/cm^3 . The preparation cure schedule of the resin is given in **Section 3.5.2.1**.

Table 3.6: Mechanical properties of the epoxy resin Epikote 828 [151].

Elastic modulus (GPa)	Shear Yield Stress (MPa)	Yield Stress (MPa)	Failure Strain (%)
3.3 ± 0.1	73.5 ± 0.6	127.2 ± 0.9	4.5 ± 0.2

3.5.1.2 Fibres

The reinforcing fibres were LAS glass, LAS glass ceramic, MAS glass and MAS glass ceramic. These MAS and LAS fibres were laboratory-prepared. In this study, the fibre diameter of the LAS system was approximately 50 μm , and approximately 70-80 μm for the MAS system. These fibres were measured using SEM as describe in **Section 4.3.3**. The densities of the glass were given in Table 5.6. All the densities were measured using balance equipment ($\pm 0.0001\text{g}$).

3.5.2 Preparation of composites

3.5.2.1 Epoxy resin

Preparation of the epoxy resin mixture is summarised in Figure 3.8. The composition of the epoxy-hardener-accelerator mixture followed earlier reports [151, 152]. The formulation of resin was prepared by heating and stirring the resin with 90% by weight of hardener at 80°C for 20 minutes until the hardener had fully dissolved. 1% by weight of accelerator was added and further stirred for 10 minutes. The resin mixture was fully stirred and further degassed in a vacuum oven at 80°C for 20 minutes to eliminate air bubbles. Then the bubble-free resin mixture was poured into a pre-heated silicone rubber mould and degassed again at 80°C for 20 minutes.

After degassing, a PTFE release film was placed on top of the mould and weighted with a glass plate to produce flat and near-net shape specimens before curing in a conventional oven. The curing schedule started with pre-curing at 80°C for 2 hours, curing at 120°C for 3 hours and post-curing at 150°C for 4 hours, with heating rates of 1°C/min before being allowed to cool down to 25°C at

1°C/min. Cured specimens were carefully trimmed, ground and polished to the required testing dimensions. Samples were stored in a vacuum oven at 25 °C and removed immediately before testing.

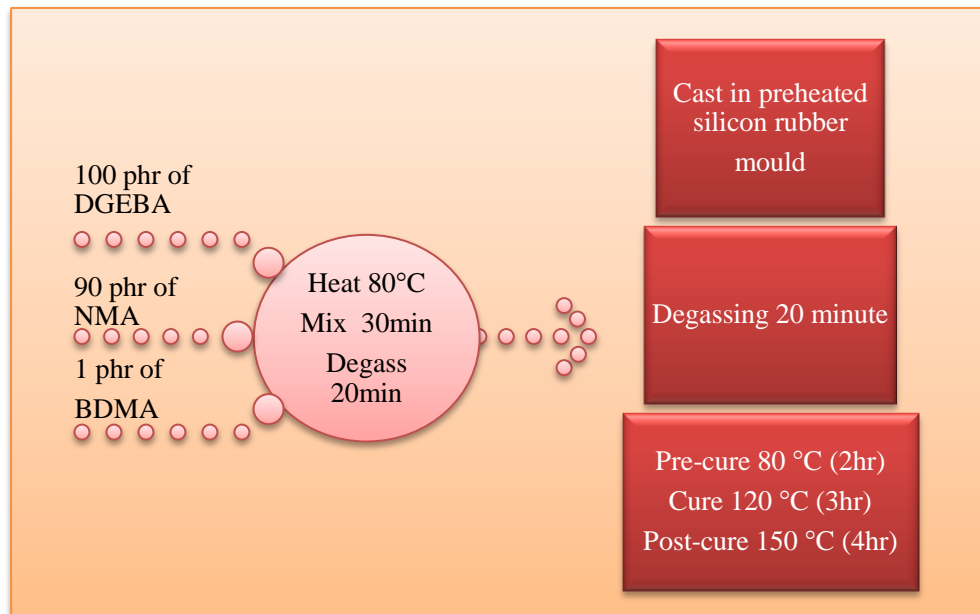


Figure 3.8: Illustration of preparation of resin epoxy.

3.5.2.2 Preparation of fibres

The next stage of the process was to produce unidirectional glass fibre reinforced polymer (GFRP) from loose fibres, as illustrated in Figure 3.9.

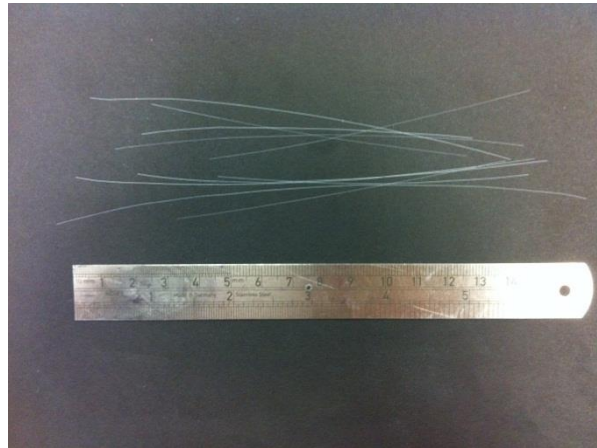


Figure 3.9: Reinforcing LAS glass ceramic fibres.

Due to the limited number of fibres and challenges in producing a composite from handling loose fibres, the fibre volume fraction was limited to 30%. The primary research objective in making the glass ceramic composite was to demonstrate the feasibility of using the fibres in the composite application. Fibres were weighed to a target of a 30% fibre volume fraction and manually arranged into an aluminium test frame with three slots cut to length, width, and depth dimensions of 75mm x 10mm x 1mm, as illustrated in Figure 3.10. Care was taken to preserve fibre alignment in these strips which were stored with silica gel before the impregnation process.

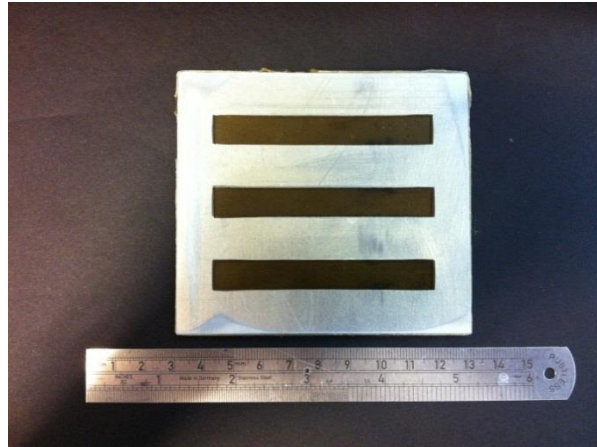


Figure 3.10: Aluminium test frame.

3.5.2.3 Resin impregnation

After preparing the resin as described in **Section 3.5.2.1**, the mixture was degassed in a vacuum oven at 80°C for 20 minutes and was gently poured into a wrapped tray with PTFE release film. The test frame was then placed in the tray, so that the whole fibres were immersed in the resin. The tray was returned to the vacuum oven for further degassing at 80°C for 20 minutes. Due to the brittleness of the fibres, care was taken to avoid placing pressure on the frame to avoid distortion and misalignment of the fibres. Degassing aided wetting by capillary action of the resin on the fibres. The tray was removed from the oven after 20 minutes and the fibres were fully immersed in the resin. The tray was returned back into the vacuum oven for a further 1 hour of degassing. Overall the mixed resin spent 90 minutes under vacuum at 80°C, by which time the viscosity had increased.

3.5.2.4 Curing process

The test frames were removed from the vacuum oven and placed between glass panels. The glass plate was placed between the test frames. A block steel plate was placed on top of the glass plate to give a weight in order to compress the test frame. The composite part was cured in a convection oven without any applied pressure. The cure schedule remained as same described in **Section 3.5.2.1**. Once the curing cycle had completed, frames were cut away to leave the composite strip.

3.6 Concluding remarks

This chapter describes the glass and glass ceramic fibres fabricated from two glass systems (MAS and LAS) and subjected to a series of trial heat treatments. The optimum heat treatment temperatures were selected based on their performance on physical observation and mechanical properties (**CHAPTER 4**). The one-ply laminate of glass ceramic fibre reinforced polymer composites were fabricated using a wet lay-up technique. The overall performances of these systems were evaluated through physical observation, thermal, nanoindentation, single fibre test (SFT), acoustic measurement, thermogravimetric analysis (TGA), dynamic mechanical analysis (DMTA), optical microscopy (OM) and scanning electron microscopy (SEM) techniques are presented in **CHAPTER 4**.

Chapter 4

Experimental

4.1 Summary

This section outlines the research methodology used in the experimental work, including all the experimental procedures. It comprises three main parts, as shown in Figure 3.1. Topics covered in this chapter include: characterisation of bulk samples, investigation of properties of glass and glass ceramic fibres and examination of glass ceramic fibre reinforced polymer composites. This study considers glass systems consisting of MgO-Al₂O₃-SiO₂ (MAS) and LiO₂-Al₂O₃-SiO₂ (LAS).

4.2 Characterisation of bulk glass system

4.2.1 Differential thermal analysis (DTA)

The glass transition temperature (T_g) and the crystallisation temperature (T_c) were determined using DTA on a Perkin Elemer Pyris ITGA-DTA7 unit in flowing air with a temperature range of 20-1200 °C at a constant heating rate of 10°/min. A glass powder weighing 50 mg was prepared in a platinum holder and another platinum holder containing alumina powder was used as a reference material. Data were recorded using computer-driven data acquisition system. The results were used as a guide for determining the heat-treatment temperatures required to induce crystallisation of the parent glasses.

4.2.2 X-Ray diffraction (XRD)

X-ray powder diffraction as shown in Figure 4.1 was used to identify amorphous and crystalline phases within the MAS and LAS systems that had undergone extensive crystallisation. Samples with 5 mm thick cross sections were ground flat upper alternately using 240, 600, and 1200 grit papers. The samples were polished prior to the scanning, which was carried out using a Siemens D500 X-ray diffractometer over a scan range of 20°-80° at a rate of 2° per min in 2 θ step sizes using Cu K α (1.54050 Å) radiation.



Figure 4.1: Seimens D500 X-ray diffractometer.

The identification process was calibrated using pure Si oxide with a precisely determined peak. Once scanning parameters were set, the intensity of diffracted X-rays was continuously recorded and interpreted at peak positions of 2θ . Phase identification was based on Bragg's Equation [48]:

$$n\lambda = 2d \sin \theta \quad [4.1]$$

It started with the wavelength (λ) of the incident X-ray penetrating the planes of atoms (n) in its structure (sample tested) at the incident angle θ at which gives the d-spacing that produce the constructive interference. The position of peaks was identified by the interplanar spacing using WinXPOW software. Experimental X-ray diffraction patterns were compared with standards compiled by the International Centre for Diffraction Data (ICDD).

4.2.3 Density measurement

The densities of both the bulky parent glass and the glass ceramics of MAS and LAS were determined using an Archimedes' technique with distilled water as the immersion medium. Three specimens were measured for each of the system. The densities were calculated according to the ASTM D693 [153], from the dry (m_1) and immersed (m_2) sample masses, the density of distilled water ($\rho_{\text{distilledwater}}$) and the volume of the samples, as calculated by the following relations:

$$V_{\text{sample}} = \frac{m_1 - m_2}{\rho_{\text{distilledwater}}} \quad [4.2]$$

$$\rho_{\text{sample}} = \frac{m_1}{V_{\text{sample}}} = \frac{m_1 \rho_{\text{distilledwater}}}{m_1 - m_2} \quad [4.3]$$

4.2.4 Nanoindentation

4.2.4.1 Test specimen and test procedure

Nanoindentation has been an increasingly popular technique for material characterisation, including depth sensing indentation that has been used to test the mechanical properties of materials at the nano-scale. In this study, nanoindentation was used to test local mechanical properties, including the hardness (H) and reduced elastic modulus (E_r) in the glass ceramic multiphase material.

Samples were cut with approximately 5mm cross-sectional sides and prepared using a standard metallographic technique and cold mounted in epoxy resin (Figure 4.2c). The specimens were manually ground and polished to reach a very low roughness grade on a series of diamond pastes of 6 μm , 3 μm , 1 μm and 0.25 μm . The final height of the coupons after polishing was approximately 6mm. The samples were cleaned with acetone prior to nanoindentation.

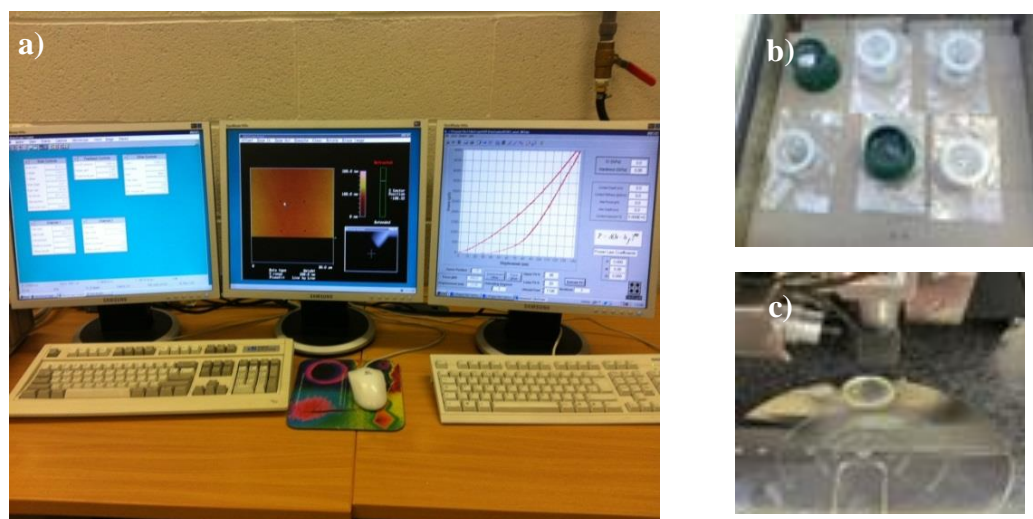


Figure 4.2: Schematic of a) nanoindentation instrument, b) sample preparation and c) positioned sample.

Measurements were performed using a Nanoindenter Triboscope Nanomechanical Testing System. Samples were mounted onto a Dimension 3100 (Veeco) as

shown in Figure 4.2b. A load of 5 mN was applied with a Berkovich diamond tip (Hysitron) to indent the samples in square arrays of 2 x 2 indentations regularly spaced at 20 μ m from each other. Each sample was indented four times at five different locations. It took 15 seconds to upload, hold and unload the tip for each indentation.

4.2.4.2 Data analysis

The reduced modulus, E_r , was extracted from the stiffness, S , of the initial part of the unloading curve.

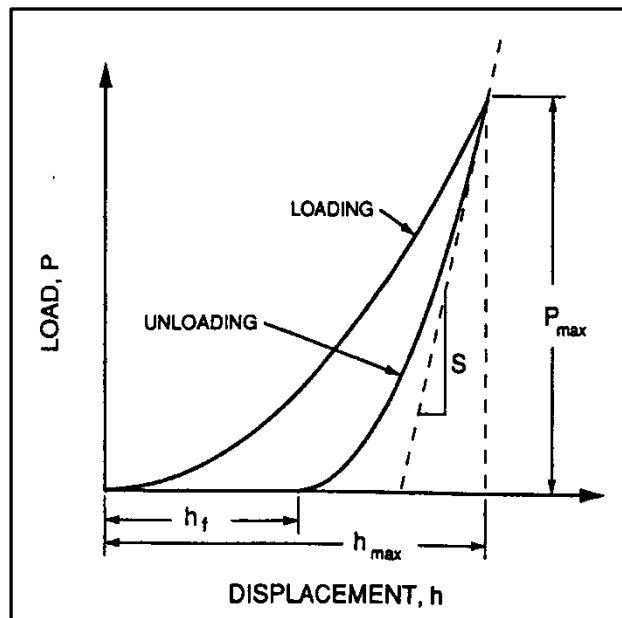


Figure 4.3: A schematic representation of load versus indenter displacement data from the nanoindentation technique. The quantities shown are: the peak indentation load, P_{max} , the indenter displacement at peak load, h_{max} , the final depth of the contact impression after unloading, h_f , the initial unloading stiffness, S [154].

Data analysis was carried out following the procedure proposed by Oliver and Pharr [154]. The hardness and reduced elastic modulus of materials are calculated from the following expression.

Hardness of material calculated from at h_c using the relationship:

$$H = \frac{P_{\max}}{24.5h_c^2} \quad [4.4]$$

where P_{\max} is the load and h_c is the contact depth of the indent and $24.5 h_c$ is the projected contact area of depth relationship for Vickers and Berkovich indenter derived from the geometry of the tip. The contact depth of the indentation has the same geometry as the geometry as the indenter tip. Therefore h_c is calculated from h_{\max} , indentation depth at the maximum load P_{\max} excluding the elastic displacement in the contact region and contact depth. The reduced Young's modulus was proportional to hardness, H as shown in the equation below :

$$E_r = \frac{\sqrt{\pi} S}{2\beta \sqrt{A}} \quad [4.5]$$

where A is the contact area, $\beta = 1.034$ for a triangular indenter and S stiffness from the initial gradient of the unloading curve. The modulus of the indented material was obtained from the following equation:

$$E_r = \left[\frac{1-\nu_i^2}{E_i} + \frac{1-\nu_s^2}{E_s} \right]^{-1} \quad [4.6]$$

Where E_i , ν_i are the Young's moduli and the Poisson's ratios of indenter tip (diamond). E_s , ν_s are equivalent properties of the indented material. For diamond $E_i = 1141$ GPa and $\nu_i = 0.07$. The reduced modulus obtained from the nanoindentation test are not directly comparable to E as there is also an elastic contribution from the indenter. The results of this study are presented in **CHAPTER 5**.

4.2.5 Scanning electron microscopy (SEM)

The morphologies of the crystalline phases developed by heat treatment of the glass samples were examined by scanning electron microscopy (SEM). For the determination of crystallisation; small slices of glass were set in epoxy resin blocks and manually ground using 400, 600, 800 and 1200 SiC grit and polished to a mirror finish using diamond pastes of 6 μ m down to 1 μ m grade. The glass ceramic samples were etched with a 2.5% HF solution for 30 s and were gold coated to increase the conductivity of the surfaces and prevent charge build-up by the electrons. The surfaces of etched samples were examined using a FEI Nova200 FEG-SEM scanning electron microscope with an operating voltage of 15kV. In this work, the Materials and Engineering Research Institute (MERI) of Sheffield Hallam University carried out the scanning electron microscopy.

4.3 Characterisation of glass and glass ceramic fibre

4.3.1 XRD fibre specimen

Both glass ceramic fibre systems were examined using XRD after heat treatment. The examination was done prior to the single fibre testing to ensure that the glass fibres were fully heat treated and not in an amorphous state.

XRD was performed using an X-ray STOE Stadi P Diffractometer (IP-PSD). Samples with small diameters were used to avoid errors arising from large X-ray diffraction. Sample preparation was critical to obtaining satisfactory results due to the requirement for perfect packing of the surface of the samples. Glass ceramic fibres were cut into lengths of approximately 10mm and vertically arranged in the diffractometer (Figure 4.4). The X-ray patterns obtained were matched to the ICDD files using the Stoe X-ray diffraction computer analysis software WinXPOW. Phase identification followed the same procedure as described in **Section 4.2.2.**

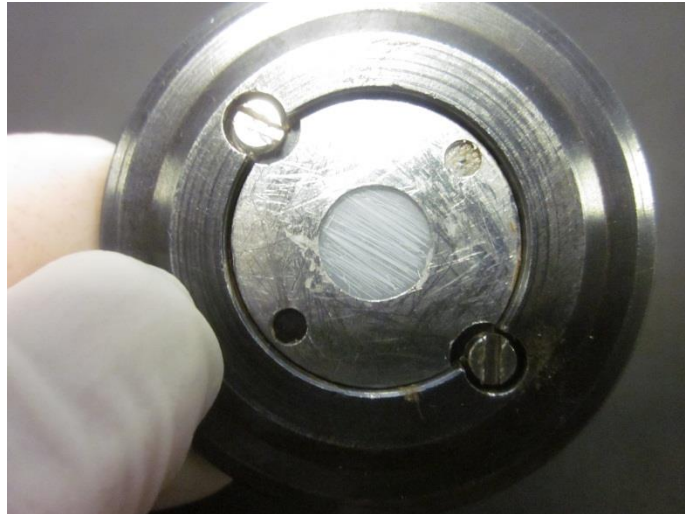


Figure 4.4: Glass ceramic fibres mounted for X-ray diffraction analysis.

4.3.2 Mechanical Property Measurements

4.3.2.1 Single fibre test

The aim of this research was to produce glass ceramic fibres which possess excellent mechanical properties. The mechanical properties were characterised by single fibre testing of annealed glass fibre and heat treated fibre glass ceramic. Single fibres were carefully stored with silica gel and arranged into separated layers in order to prevent fibre damage prior to sample preparation. Sample preparation followed ASTM C1157-03 [155]. Fibres were then mounted on a rectangular frame with cyanoacrylate adhesive (Loctite 404 Quick Set TM, Hartford, CT) used to fasten the fibre ends as illustrated in Figure 4.5a. The samples were stored under ambient conditions for at least 24 hours before testing.

Uniaxial tensile tests were performed using a Hounsfield H25K-S universal testing machine. In order to obtain the maximum single filament tensile strength, the single fibre must be aligned along the loading direction (Figure 4.5b). Therefore the grip should not be clamped on the glued part. Meanwhile, an absolute vertical line was used as a control to ensure the single filament in one direction with respect to the loading direction. The fibres were aligned to the vertical axis of tension within a tolerance of less than $\pm 2\%$ of the fibre gauge length, δ :

$$\delta \leq \frac{l_0}{50} \quad [4.7]$$

where l_0 is the fibre gauge length in unit metres. This was done to prevent any bending strains and/or stress concentrations occurring between fibre ends within tab.

The card frame was cut away prior to testing (Figure 4.5c). The test was conducted at a constant rate of displacement of 0.2mm/min to fulfil the condition of quasi-static tension. The load cell was rated to 10N. The gauge lengths of the tested fibres were 30mm and 60mm. All tensile tests were carried out at room temperature under ambient conditions. Thirty fibres were tested for each gauge length for each system of both untreated and treated glass fibres.

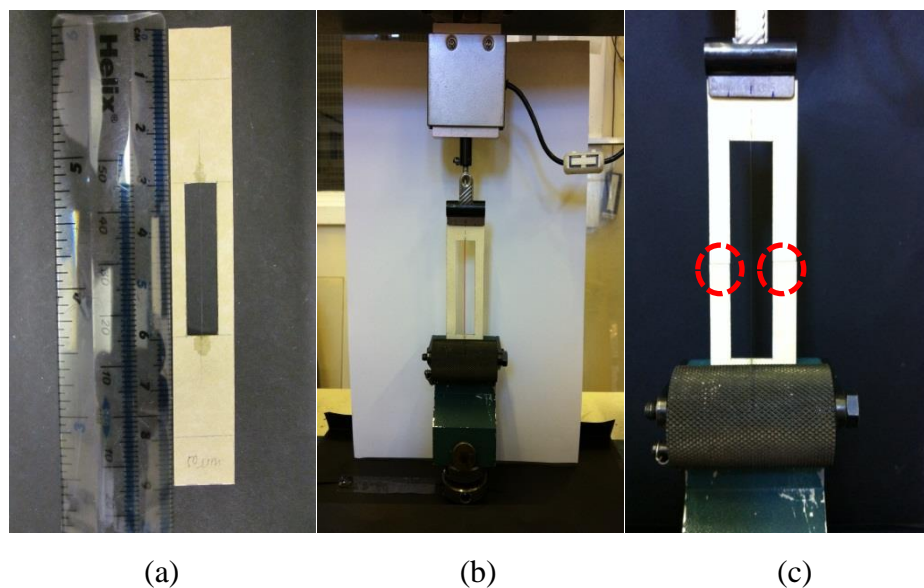


Figure 4.5: Photographs of the single fiber test a) test specimen, b) tensile test method and c) cut area.

Figure 4.6 illustrates the brittle failure of a fibre following Hooke's law, represented by measurements of displacement and applied load. The specimens were examined closely during the test to ensure that only the fibre which failed in tension was included in the results. Once the fibre failed, the load-extension plot was examined to ensure that the load on the fibre built up to a maximum, and then

dropped instantly to zero. If not, it was considered that fibre slippage occurred in the adhesive, and the test was discarded. The tested fibres were stored with silica gel for measurement of diameter and fractography.

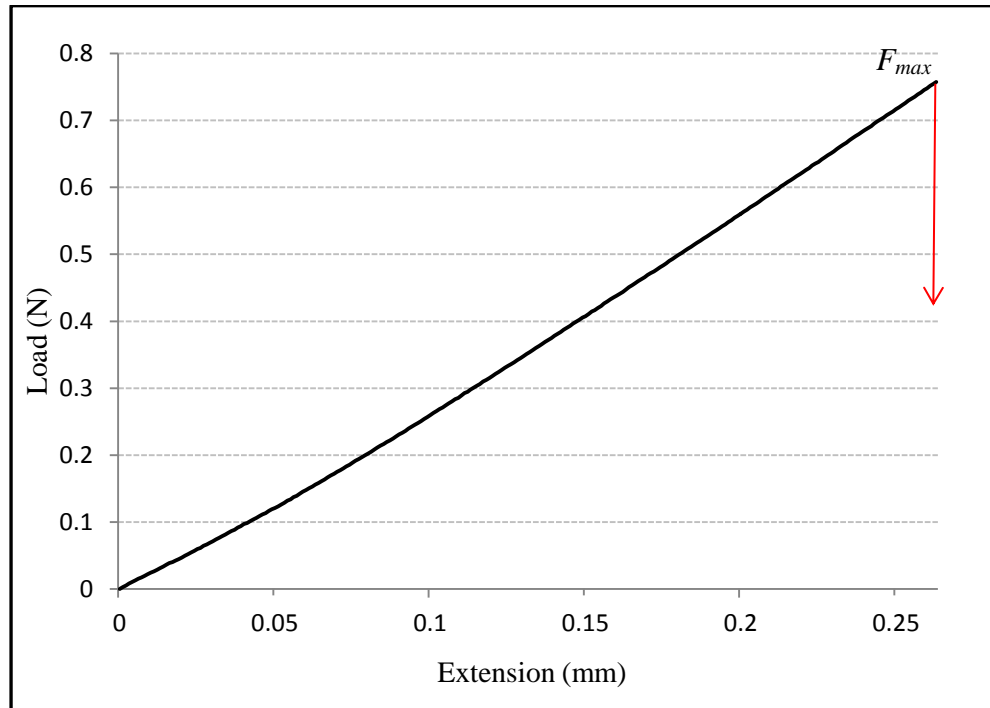


Figure 4.6: Typical load-extension curve for a selected single LAS glass ceramic fibre tensile test.

4.3.2.2 Data analysis

The tensile strength for each series of tests was analysed according to ASTM C1157-03 [155], with the exception that fibre diameters were measured at fracture areas rather than by means of a nominal or average fibre diameter due to the fragility of the samples. The fibre tensile strengths, σ_f of the samples were calculated by dividing the maximum force with the fibre cross-sectional area:

$$\sigma_f = \frac{F_{max}}{A} \quad [4.8]$$

Where F_{max} is the force at the failure location of the fibre (N) and A is fibre cross-sectional area (m^2) estimated by:

$$A = \frac{\pi D^2}{4} \quad [4.9]$$

where D is the fibre diameter. The fibre diameter was measured using a micrometer and was confirmed using scanning microscopy electron (SEM). The details of the measurement are described in **Section 4.3.3**. In this study, Young's modulus of fibre was not in the scope of the study.

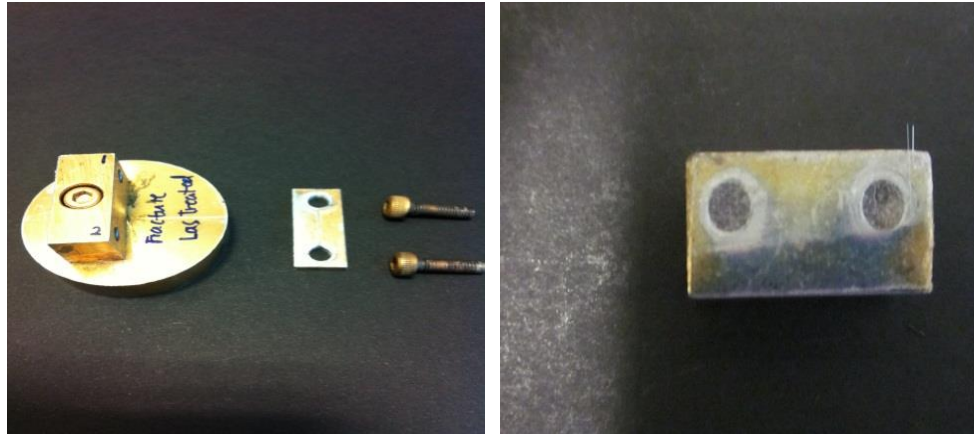
4.3.2.3 Weibull distribution

A statistical analysis of the fibre strength was performed using a Weibull distribution [96]. The results and analysis are presented according to ASTM C1239 [156]. The width of the distribution in strength was characterised by calculating the weibull modulus by applying a linear regression algorithm to the Weibull plot of $\ln(\ln(1/(1-P_f)))$ against $\ln(\sigma_f)$ (Equation 2.2). Details of this analysis procedure are shown in **Section 2.5.2**.

4.3.3 Measurement of fibre diameter

Fibre diameters were determined from areas of fibre breakage using a micrometer ($\pm 0.001\text{mm}$). In order to improve accuracy, firstly the fibres and depth gauge micrometer were cleaned from fracture debris. The digital readout, the surface of the anvil and the spindle were also cleaned with acetone each time 5 fibres had been measured.

For examination by scanning electron microscopy, the fibres from another half of tab were carefully cut from the end tab. This examination only applied for gauge length 60mm. A double sided tape (Sellotape) was applied on the surface of the sample holder (Figure 4.7a).



(a) Sample holder

(b) Fibre



(c) Gold sputter instrument EMSCOPE SC500 A

Figure 4.7: Sample preparation of fibre diameter measurement and observation surface fracture for SEM.

The fibres were placed onto the tape with the fractured area exposed as illustrated in Figure 4.7 (b). Then, the sample holder together with the fibres was rinsed with ethanol to remove any dirt. Diameters were observed close to the point of fracture for accurate measurement of the diameter and cross-section area, A . The fibres were assumed to be circular in cross-section due to the nature of laboratory preparation and heat-treatment. The samples were gold coated (Figure 4.7c) to increase the conductivity of the surfaces and prevent charge build-up by the electrons. The samples were examined using a FEI Nova200 FEG-SEM scanning electron microscope with an operating voltage of 15kV. Scanning electron

microscopy was conducted at the Materials and Engineering Research Institute (MERI) at Sheffield Hallam University.

4.3.4 Acoustic measurement

Ultrasonic velocity measurements are based on the propagation and reflection of sound waves through the thickness of a specimen. This technique utilised two types of transducer which gave longitudinal and transverse (shear) waves [47] in order to obtain Young's modulus.

4.3.4.1 Test specimen and test procedure

Samples of glass rod with length and diameter approximately of 5 mm were annealed and treated with the same heat treatment schedule as describe in Table 3.5. The samples were ground and polished using SiC grinding paper with grades of 400, 600, 800, and 1200, finished by surface polishing using diamond paste with grades of 6 μ m, 3 μ m, 1 μ m and 0.25 μ m. The length of the specimens were measured using a micrometer (\pm 0.001mm). The Young's modulus of each sample was determined via measurement of the longitudinal sound wave velocities using an EPOCH 500 series Olympus Ultrasonic Flaw detector as shown in Figure 4.8 and Figure 4.9. The frequency range used for measuring the modulus are between 0.1MHz to 20MHz depending on the width of the resonance curve.

Measurements were carried out at room temperature. Samples were pre-smeared with a glycerine (Panametrics Olympus-NDT) coupling medium to improve the transmission of sound waves between the transducer and the samples. The time-of-flight, or time taken for a wave to be emitted by the transducer, reflected by the sample and received by the transducer, was recorded for calculation of Young's modulus. The results of the time-of-flight were taken as mean values of three measurements.

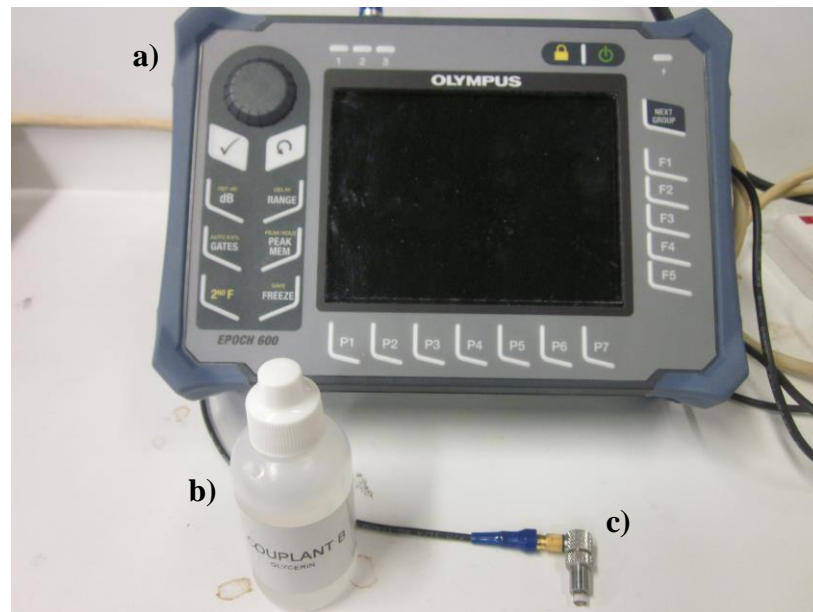


Figure 4.8: (a) The EPOCH 500 series Olympus Ultrasonic Flaw detector, (b) coupling medium and (c) transducer.

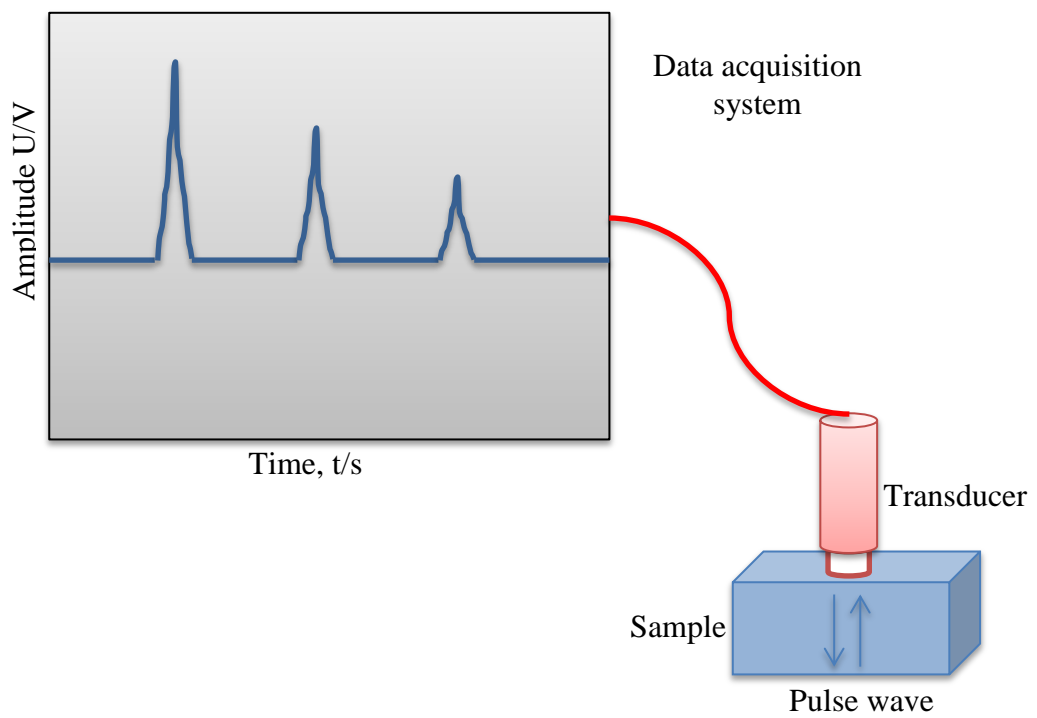


Figure 4.9: A schematic illustration of the acoustic device.

4.3.4.2 Data analysis

Acoustic measurements were undertaken according to the principles stated in the test standard ASTM E 494-95 [157]. The longitudinal velocity, v_l was determined by the transit time through the thickness of the samples by Equation [4.10]:

$$v_l = \frac{2 \times d(m)}{t(s)} \quad [4.10]$$

Where, v_l , d , and t are the longitudinal wave velocity, length of the sample and the time-of-flight, respectively.

From above measurement, the Young's modulus was calculated according to the following Equation [4.11]:

$$E = \rho v_l^2 \quad [4.11]$$

where ρ is the density of tested sample and v_l is the longitudinal velocity of each sample tested.

4.3.5 Fractography

Fractography is the study of the fracture surfaces of brittle materials in order to locate and characterise the origin of the fracture. Evaluation of the fracture surface was undertaken for selected fibres after tensile testing and was performed using scanning electron microscopy (SEM). The fibres were selected for further analysis in they failed in tension within the gauge length. The fractured areas were examined to identify the morphologies of failure surfaces. The samples were gold coated and were examined using a FEI Nova200 FEG-SEM with an operating voltage of 15kV as shown in Figure 4.9. Scanning electron microscopy was conducted at the Materials and Engineering Research Institute (MERI) at Sheffield Hallam University.

4.4 Characterisation of glass and glass ceramic fibre reinforced composite

4.4.1 Dynamic Mechanical Testing Analysis (DMTA)

In order to evaluate the mechanical properties mainly the moduli accompanied with small size of sample, a dynamic mechanical thermal analysis (DMTA) is used. DMTA provides a method for determining the storage modulus (E') and loss tangent ($\tan \delta$) as a function of temperature.

In this research, the test is conducted in a fixed frequency and constant amplitude (strain) mode. The results of the storage modulus and $\tan \delta$ are very useful in ascertaining the performance of the sample under stress and temperature. By using this DMTA in mechanical test, fibres embedded in resin are expected to interact with the mechanical stress.

In this experiment, the testing was performed in a three-point bending mode as shown in Figure 4.10, using a dynamic mechanical thermal analyser (DMTA) of Perkin Elmer Instruments, DMA8000. The measurements were performed from 0°C to 180 °C at a heating rate of 0.2 °C/min and fixed single frequency of 10 Hz. Meanwhile the sample geometry 8 x 30 x 1 mm³ (Figure 4.11) has been chosen and manufactured according to the available fibres. As such, the preparation was critical as obtaining a good result is heavily dependent on ensuring that the ends of the sample are perfectly parallel to avoid errors during testing. The dynamic storage modulus (E'), versus temperature traces for use range of composites made using MAS glass fibre, MAS glass ceramic fibre, LAS glass fibre ad LAS glass ceramic is plotted as presented in **CHAPTER 5** (Figure 5.34).

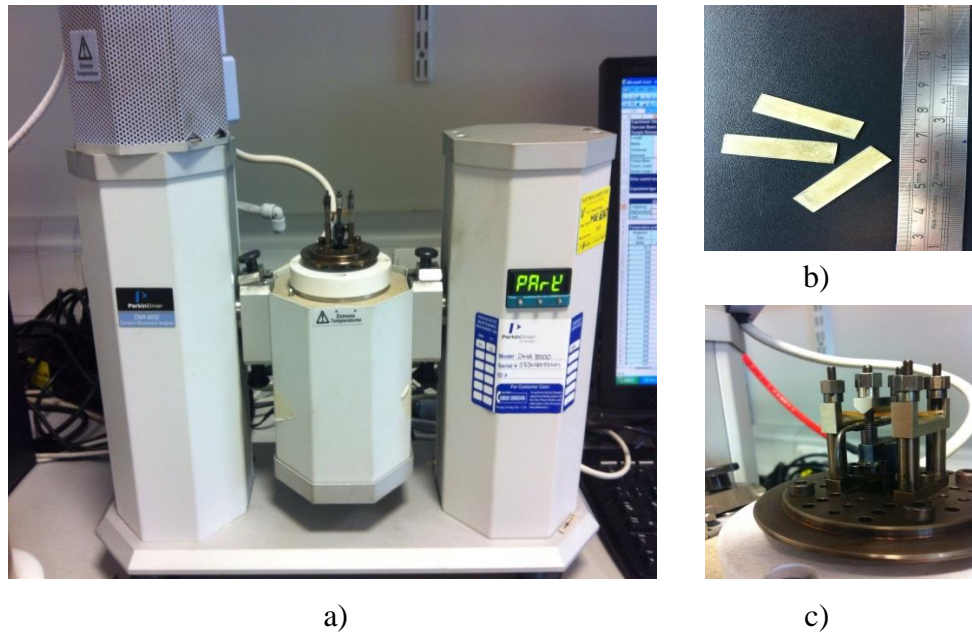


Figure 4.10: Schematic illustrations of a) Perkin Elmer Instruments, DMA8000 3, b) samples and c) three point bending mode.

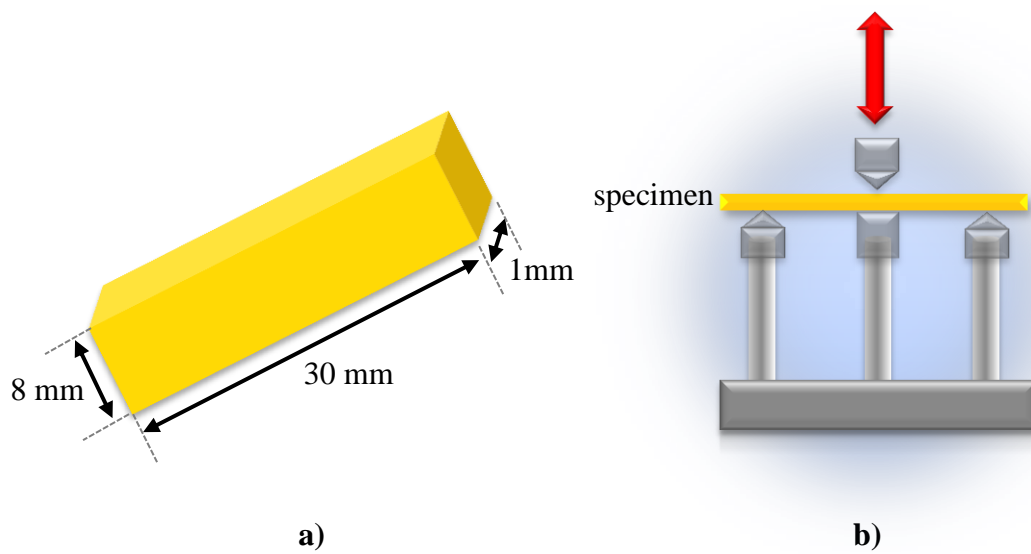


Figure 4.11: Schematic illustrations of a) specimen dimensions for b) three point bending mode.

4.4.2 Measurement of volume fraction

For this measurement, thermogravimetry analysis (TGA) was used to measure the weight fraction of the constituents in the composites. This value was used to determine the fibre volume fractions. The test measures the change in weight of the specimens as the specimen is progressively heated. In this study, TGA on a Perkin Elmer TGA 7 was performed at a controlled rate under controlled atmosphere. The test is conducted according to ASTM Standard E1131 [134]. Samples were tested with the Perkin Elmer TGA as shown in Figure 4.12(a) using heating profile illustrated in Figure 4.12(b).

A sample mass of 10 to 30 mg was heated from 25°C to 900°C at 10°C/min heating rate. Jumahat [170] heat-treated the sample in two stages. At first, it was heated from 25°C to 550°C at 10°C min⁻¹ heating rate in nitrogen at 50 ml/min. The temperature was then kept at 550°C for 1 hour to decompose the epoxy resin. In stage two, the N₂ gas supply was then switched to air and the temperature was increased to 1000 °C to decompose the carbon residue and/or graphite fibres. In this study, the residue was glass and glass ceramic fibres. Data was collected using TGA PYRIS software. The TGA curve plots showed the percentage weight change against the material's decomposition temperature. The isothermal temperature of 550 °C is selected as the optimum temperature to burn off the epoxy resin.



(a)

Stage	Heating programme
1	Temperature : 20°C ~ 550°C Heating rate : 10°C/min Gas : Nitrogen
2	Temperature : 550°C Held: 1h Gas: Nitrogen
3	Temperature : 550°C ~ 900°C Heating rate : 10°C/min Cooling rate : 10°C/min Gas: Air

(b)

Figure 4.12: Schematic illustrations of a) TGA and b) heating programme.

The basic equations given in ASTM Standard D3171-99 [135] were used to calculate the constituent contents of the glass and glass ceramic composite materials as follows:

- i. The fibre volume fraction

$$V_f = \left(\frac{m_f}{m_c} \right) \times \left(\frac{\rho_c}{\rho_f} \right) \times 100 \quad [4.12]$$

where m_f = mass of the fibre, m_c = mass of composite or initial mass of the specimen, ρ_f = density of the fibre and ρ_c = density of the composite.

- ii. The resin volume fraction

$$V_m = \left(\frac{m_m}{m_c} \right) \times \left(\frac{\rho_c}{\rho_m} \right) \times 100 \quad [4.13]$$

where m_m = mass of the epoxy resin, m_c = mass of composite or initial mass of the specimen, ρ_m = density of the epoxy resin and ρ_c = density of the composite.

- iii. The weight fraction of the constituents to the composite; $\left(\frac{m_f}{m_c}\right)$ and $\left(\frac{m_m}{m_c}\right)$ was obtained from TGA results.

4.4.3 Microvoid observation

In this study, the microvoid of the composite was observed using a Reichert-Jung POLYVAR MET optical microscope. Figure 4.13 shows a Polyvar B-Met optical microscope with the image analyser apparatus.

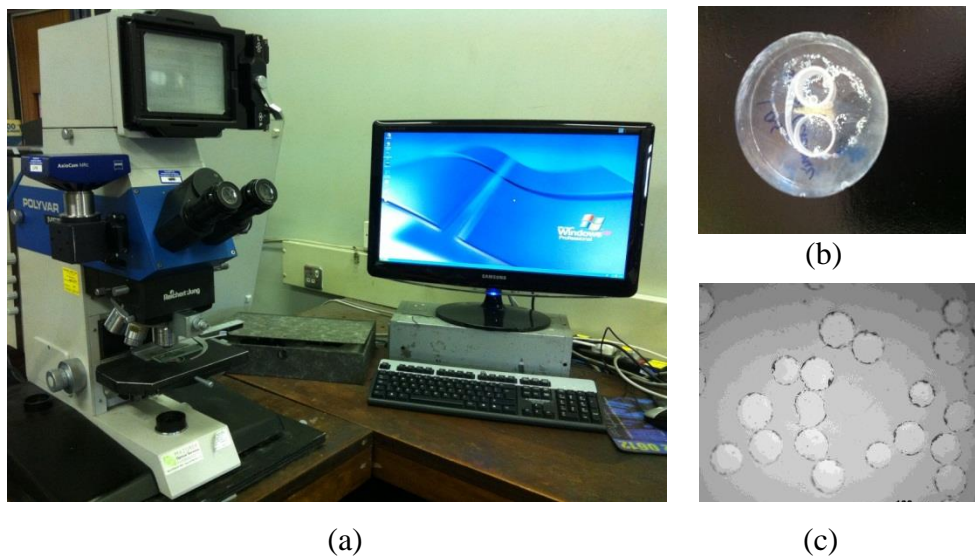


Figure 4.13: Schematic illustrations of a) optical microscope, b) specimen and c) micrograph of cross section of the sample.

For sample preparation, a small section of composite was sectioned at the centre specimen perpendicular to the fibre axis. The small section was prepared using a standard metallographic technique. The specimens were cast in epoxy resin and carefully manually ground with SiC paper 120, 240, 400, 800 and 1200 grits. Then the ground specimens were polished sequentially using diamond paste of $6\mu\text{m}$, $3\mu\text{m}$, $1\mu\text{m}$ and $0.25\mu\text{m}$. The surface of the polished specimen should

display a clear delineation between the fibres and the matrix. The possibilities of microvoid were observed under optical microscopy.

4.4.4 Density measurement

The densities of both cured epoxy and the composites of MAS and LAS were determined using Archimedes' technique with distilled water as the immersion medium. The densities were calculated according to the ASTM D792 [158], from the dry (m_1) and immersed (m_2) sample masses, density of distilled water ($\rho_{\text{distilledwater}}$) and the volume of the samples, as calculated by the following relations:

$$V_{\text{sample}} = \frac{m_1 - m_2}{\rho_{\text{distilledwater}}} \quad [4.14]$$

$$\rho_{\text{sample}} = \frac{m_1}{V_{\text{sample}}} = \frac{m_1 \rho_{\text{distilledwater}}}{m_1 - m_2} \quad [4.15]$$

4.4.5 Fracture observation

The methodology used to prepare the composite sample was to cryogenically freeze in the liquid nitrogen for 1 minute. The samples were then immediately subject to mechanical fracture by hand and the fracture surface samples were gold sputter coated (Figure 4.9(c)) for observation under SEM.

4.5 Concluding remarks

This chapter describes the experimental procedures that were used to obtain the experimental data. The overall performances of these systems were evaluated through physical observation, thermal and mechanical testing. SEM techniques were used to study the fracture mechanisms involved during mechanical testing. The glass ceramic fibre reinforced polymers composite were tested in bending mode to study their properties compared to the neat system. The quality of the composite was evaluated based on the fibre volume fraction, and microvoid observation was conducted using optical microscopy. The results obtained from the physical, thermal and mechanical testing and SEM observation of glass fibre, glass ceramic fibre, glass fibre composite and glass ceramic composite are presented and discussed in **CHAPTER 5**.

Chapter 5

Results and Discussion

5.1 Summary

In this chapter, experimental results are reported for the characterisation of raw materials, which focussed on the effect of heat treatment on the thermo-mechanical properties of the MAS and LAS glass ceramic systems. Correlation between the thermo-mechanical properties and crystalline phases of these materials is supported by microstructural analysis after heat-treatment at different temperatures. The fibre properties were measured with single fibre test and analysed using a Weibull distribution. Additional material properties were gained from the melt formation of fibres. The performance of polymer composites reinforced by the glass and glass ceramic fibres was evaluated. Overall discussion of these findings is also presented.

5.2 Characterisation of bulk glass

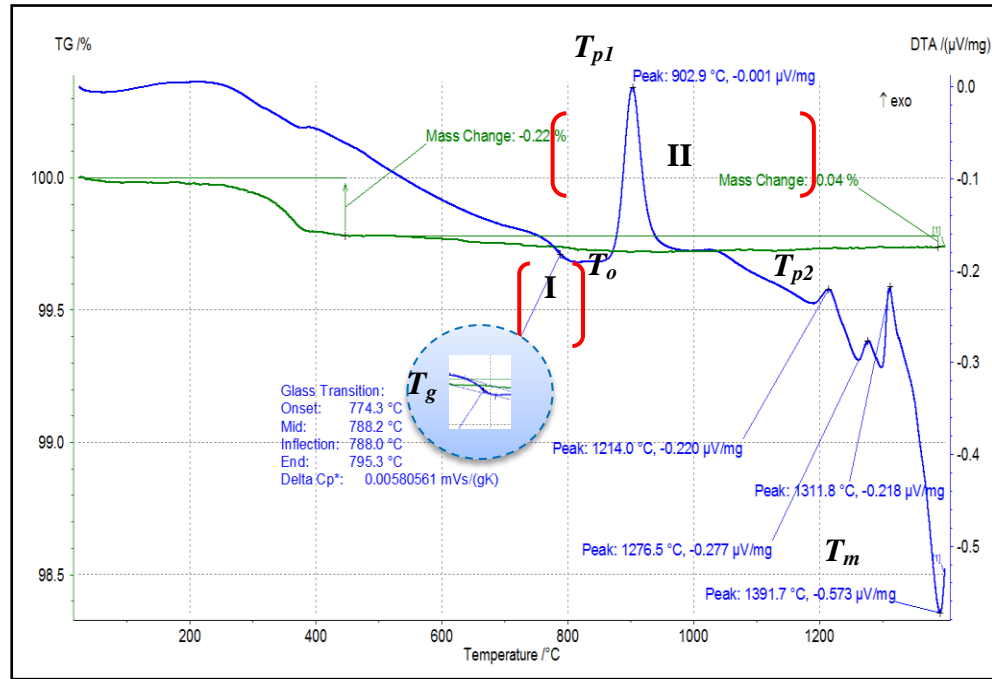
Bulk glass characteristics were studied as a function of temperature. Five methods were used to measure and analyse the thermo-mechanical properties of the microstructure and different phases of the parent glass and glass ceramic. These comprised differential thermal analysis (DTA), X-ray diffraction (XRD), density measurement, nanoindentation and scanning electron microscopy (SEM).

5.2.1 MgO-Al₂O₃-SiO₂ (MAS) glass

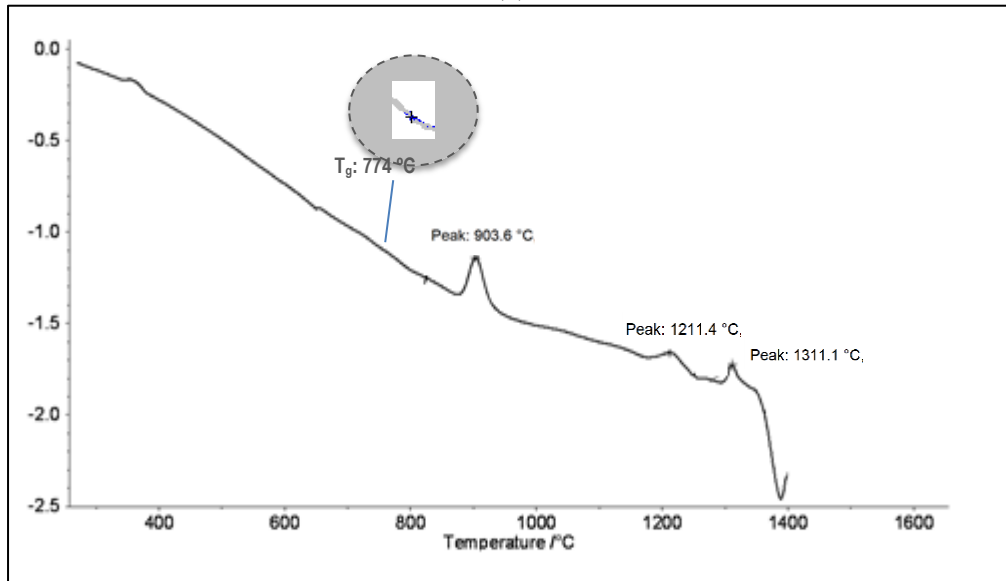
5.2.1.1 Differential thermal analysis

The differential thermal analysis (DTA) trace of the parent MAS glass obtained using the equipment at ALSTOM and Department of Materials Science and Engineering is provided in Figure 5.1(a,b). In Figure 5.1 (a), a series of endothermic reactions were observed over a temperature range of 20°C~1400°C. Upon heating the MAS glass powder to 1400°C at 10°C/min, samples exhibited one endothermic and two exothermic peaks which are represented as phases I and II. Phase I consists of a transition glass, T_g and onset temperature of peak crystallisation, T_o , whilst phase II indicates the nucleation temperature, T_n , and crystallisation temperature, T_c . The exothermic peak at 902.9°C is relatively sharp in comparison to the other broader peaks. The value of the glass transition temperature was determined from the intersection of two tangents at the start of the corresponding endotherm. The glass transition temperature was determined to be approximately at 788°C, as extrapolated from the start and end of the transition peak as shown in Figure 5.1(a). The melting endothermic peak (T_m) was at about 1391.7°C. Subsequent peaks are associated with the nucleation of crystal phases. The crystallisation temperature, T_c , is characterised by the exothermic peak with a high temperature shoulder. A low and flat endothermic reaction appeared after T_g , which indicated a thermal effect due to the rearrangement of molecules in the glass structure. The changes in the heat flow indicate that the initial formation of nuclei started at approximately 860°C which is in agreement with the literature [159]. Two exothermic peaks (T_{p1} , T_{p2}) were observed and are associated with the formation of different crystalline phases.

The glass transition temperature as shown in Figure 5.1(b).was determined earlier at Department of Materials Science and Engineering. It is shown that the T_g approximately at 774°C, as extrapolated from the start and end of the transition peak while the other peaks were observed slightly shifted compared to Figure 5.1 (a).



(a)



(b)

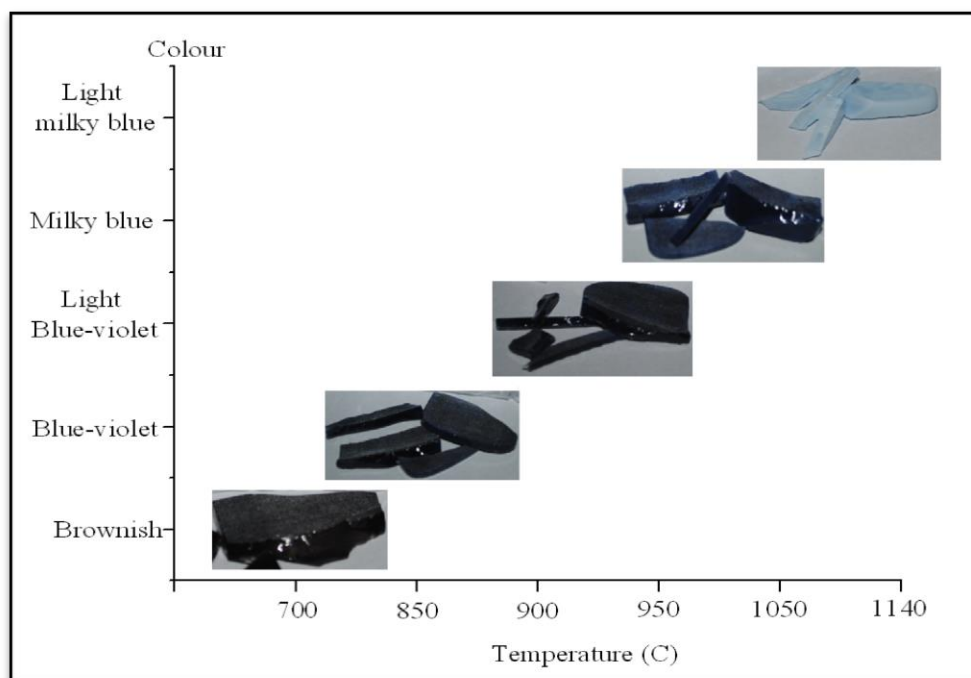
Figure 5.1: DTA traces of the parent MAS glass from a) Alstom and b) Department of Materials Science And Engineering

Based on the DTA results, both A (annealed at 700°C) and B (annealed at 570°C) samples were subjected to a two-step crystallisation process, including nucleation and crystal growth, as described in **CHAPTER 3**. These annealing temperatures are within the range 450°C to 700°C as suggested by [37] to allow the stress to be released. Different annealing temperatures were imposed in order to examine the

effect on materials properties, since the properties of glass ceramic materials are influenced by the temperature. From the results DTA (Figure 5.1a), nucleation was carried out at 720°C for 3 hours which is below the transition temperature followed by a crystallisation stage at different temperatures: 850, 900, 950, 1050 and 1140°C for 2 hours. It has been reported [24] that the nucleation growth suitable between the T_g and the crystallisation point. Since the present study is aimed to develop a heat treatment schedule and study the effect of heat treatment, the nucleation temperature was established at one low temperature, 720°C. Crystallisation of the glass ceramic phases are hugely influenced by sintering temperature and dwelling time [44]. Thus, the present of the peak at this low temperature could be attributed to the formation of the preliminary crystallisation phases (nucleation stages) representing as a weak broad peak even though no crystallise phases observed in sample A (Figure 5.3). Furthermore, a visual inspection showed the sample change in colour to opaque suggesting the sample transformed from glass material to glass ceramic material. Longer dwelling time at temperature 720 °C might be required to form a better nucleation as shown in LAS system (**Section 5.2.2**). The visible changes seen in the treated samples are summarised in Table 5.1 and Figure 5.2. The brownish colour seen in the as-annealed sample has previously been reported by Zdaniewski [40] and Wange et al.[16] and is probably due to the presence of TiO₂. However Quayang et al. [28] reported that an inclusion of 9wt% of TiO₂ resulted in a light purple colour [2009] which then became opaque white as the heat treatment temperature was increased. It was also reported [16, 40] that varying the amount of TiO₂ in the composition produced visible changes in the appearance.

Table 5.1: Effect of heat treatment on colour of MgO-Al₂O₃-SiO₂ glass.

Temperature of heat treatment (°C)/h	Remarks	
	Sample A	Sample B
Annealed	Brownish	Brownish
720 °C-3hr	Blue-violet	Dark blue-violet
720 °C-2hr, 850 °C-2hr	Blue-violet	Blue-violet
720 °C-2hr, 900 °C-2hr	Light blue-violet	Blue-violet
720 °C-2hr, 950 °C-2hr	Light blue-violet	Light blue-violet
720 °C-2hr, 1050 °C-2hr	Milky blue	Dark milky blue
720 °C-2hr, 1140 °C-2hr	Light milky blue	Milky blue

Figure 5.2: Effect of heat treatment on the colour of MgO-Al₂O₃-SiO₂ glass.

5.2.1.2 X-Ray diffraction

The crystalline phases formed were identified using X-Ray diffraction (XRD) analysis of cross sectioned samples. The samples were scanned over the range 5-80° 2θ at a rate of 2° 2θ/min. Figure 5.3 shows the XRD patterns of each glass after heat treatment. The complex crystalline phases in the MAS system analysed in this present study are abbreviated as T - magnesium aluminum titanate, M - magnesium aluminate, S - magnesium silicate, A - aluminum titanate and Q - quartz.

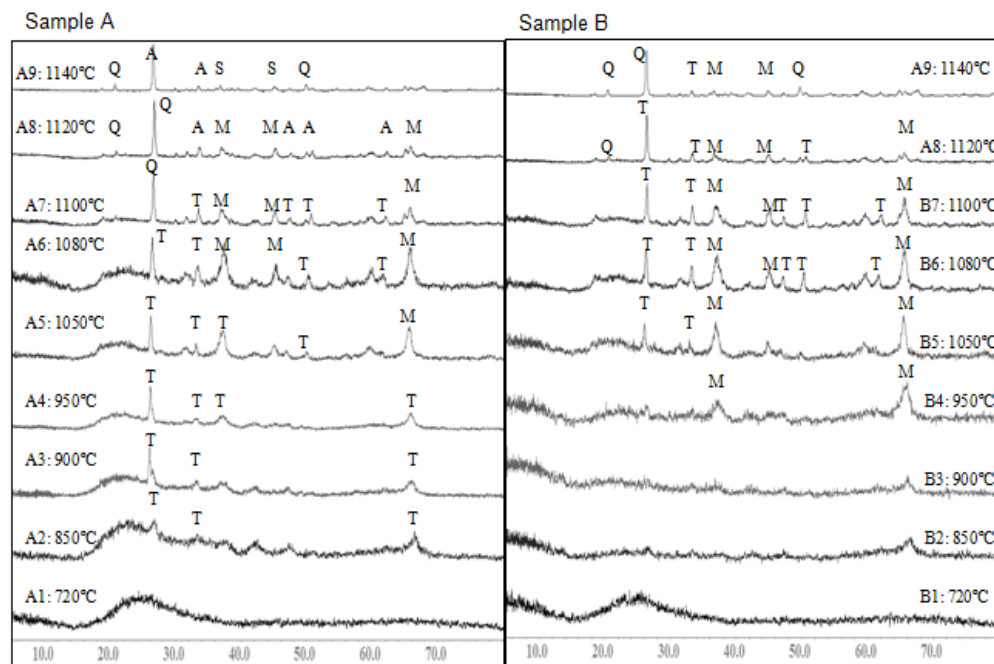


Figure 5.3: XRD patterns of heat treated glass of MgO-Al₂O₃-SiO₂ samples, annealed at 700°C (sample A) and 570°C (sample B) prior to the heat treatment. T - magnesium aluminum titanate; M - magnesium aluminate; S - magnesium silicate; A-aluminum titanate; Q-quartz.

Sample A

Sample A1 heat-treated at 720°C shows no indication of crystalline phases. The sample was XRD amorphous after the heat-treatment of 3 hours. Amorphous materials are characterised by the glass transition temperature (T_g) which separates the solid-like behaviour (below T_g) from the liquid-like behavior (above

T_g) [47]. Weak diffraction peaks are observed at 850°C, indicating mainly glassy phase and a small amount of crystalline phase, namely magnesium aluminium titanate (T), $MgAl_2Ti_3O_{10}$, (JCPDF card: 5-450). Wange et al. [16] reported the formation of quartz at 800°C followed by the formation of magnesium aluminium titanate ($Mg_2Al_6Ti_7O_{25}$), which is similar to the results presented in this work. Quyang et al. [28] also reported that magnesium aluminium titanate appears after heat treatments at 850°C and 900°C.

Referring to the diffractogram of sample A in Figure 5.3, it was found that the predominant crystalline phase at 900°C and 950°C was magnesium aluminium titanate ($MgAl_2Ti_3O_{10}$). Sample A shows more peaks compared to sample B with increasing temperature of heat treatment. The number of peaks is higher than those reported in the previous work [17], which can be correlated with MgO content of the glass. The MgO content used by Quyang et al. [28] and Shao et al. [17] was higher than in this composition, which according to Amista et al. [33], lowers the temperature of crystallisation. Heat treatment at 1050°C for 2 hours induces crystallisation of $Mg_2Al_6Ti_7O_{25}$ (JCPDF card: 5-451) and magnesium aluminium oxide (M), $MgAl_2O_4$ (JCPDF card: 73-1959).

The distinct peak at $26.14^\circ 2\theta$ indicated the presence of a quartz (β -QSS) solid solution with a high intensity. The intensity of this reflection slightly increased when the temperature was increased to 1080°C, and shifted to $26.46^\circ 2\theta$ corresponding to α -quartz solid solution (Q), SiO_2 (JCPDS card 81-65). The sample heat-treated at 1100°C indicates that the composition of magnesium aluminium titanate ($Mg_2Al_6Ti_7O_{25}$) transformed to $Mg_{0.3}Al_{1.4}Ti_{1.3}O_5$, which corresponds to an increased aluminium content and reduced magnesium and titanium content as compared with the original T phase. In contrast with the previous studies [16], little or no formation of magnesium aluminium silicate was observed.

After the heat treatment at 1140 °C (at the onset of the peak), the reflections due to magnesium aluminium titanate and magnesium aluminium oxide disappeared and the glass phase was also minimised. Instead aluminum titanate (A), Al_2TiO_5

(JCPDS card 70-1435) and α -quartz solid solutions (α -QSS) along with a small amount of magnesium silicate (S), Mg_2SiO_4 (JCPDS card 34-556) were observed, likely due to the disappearance of glass.

Sample B

XRD results show a glassy phase with a high background level and significant XRD peaks were not observed after heat treatment at the exothermic peak of crystallisation.

Glass B4 treated at 950 °C shows two broad peaks at 37.29° and 65.94° 2 θ corresponding to magnesium aluminum oxide (M) phase. This is a significantly different result compared with sample A4 that was heat treated at the same temperature. Heat treatments at 1050 °C and 1080 °C led to the precipitation of magnesium aluminium titanate, T ($\text{Mg}_2\text{Al}_6\text{Ti}_7\text{O}_{25}$) and magnesium aluminium oxide (MgAl_2O_4). The XRD pattern of B6 heat treated at 1080°C showed that the sharp peak at 26.09° 2 θ shifted to 26.30° 2 θ , which can be attributed to a change in the magnesium aluminium titanate composition to $\text{Mg}_{0.3} \text{Al}_{1.4} \text{Ti}_{1.3} \text{O}_5$. Small peaks appeared when the temperature increased by only 30°C. Increasing the temperature to 1140 °C showed that magnesium aluminium titanate (A) and magnesium aluminium oxide phases remained, the glass phase was minimised and high quartz was also formed.

5.2.1.3 Physical and mechanical properties

A. Density of bulk glass

Density is a function of the chemical composition of the glass and its thermal history. The densities of both the parent glass and glass ceramics of MAS system were determined using the Archimedes' technique with distilled water as the immersion medium. Figure 5.4 shows the absolute densities of MAS glass system as a function of heat treatment temperatures.

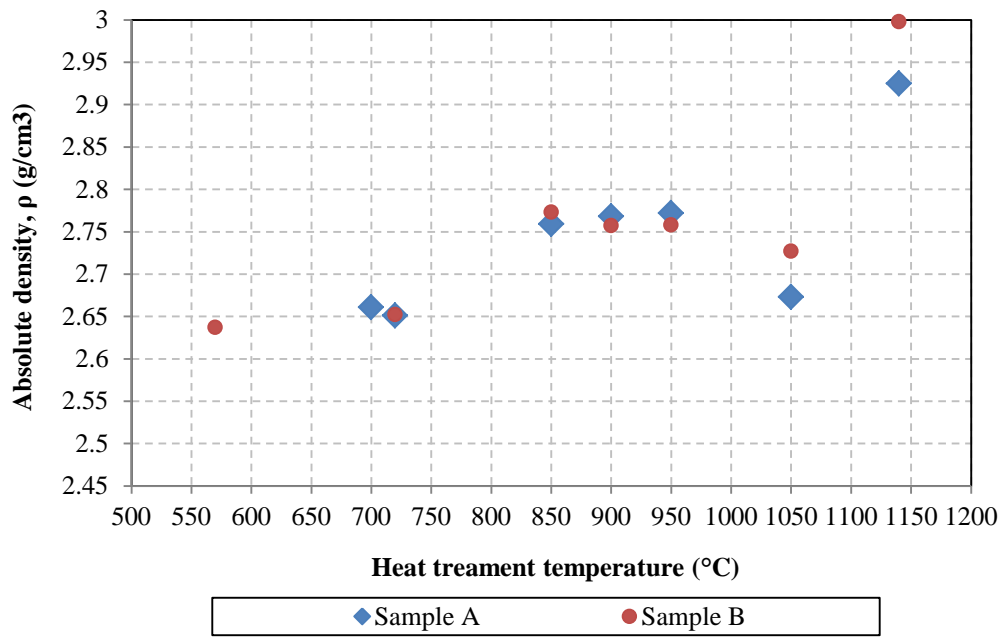


Figure 5.4: Densities of the treated MAS samples at various heat treatment temperatures.

Density increased with temperature of heat treatment from the amorphous glass phase towards the onset of the crystallisation temperatures for samples A and B and slightly decreased at the onset of the second peak of crystallisation. Density increased gradually from 1050-1140°C. The average difference in density between 1050°C and 1140°C is approximately 8.8% for both samples. The density profile of both samples is similar from 950°C to 1100°C [17, 16, 40] with the highest value found after crystallisation at 1140°C [16].

B. Reduced Young's modulus and hardness

Mechanical properties such as reduced Young's modulus and hardness have been measured. The reduced modulus, E_r , is obtained from nanoindentation. It involves elastic measurement of both the sample and indenter and thus cannot be considered comparable to the elastic modulus, E . Table 5.2 lists values of the reduced Young's modulus and hardness for both samples using the Oliver-Pharr method [154]. Figure 5.5 shows load-displacement curves for the original MAS glass and four glass ceramics produced in this work.

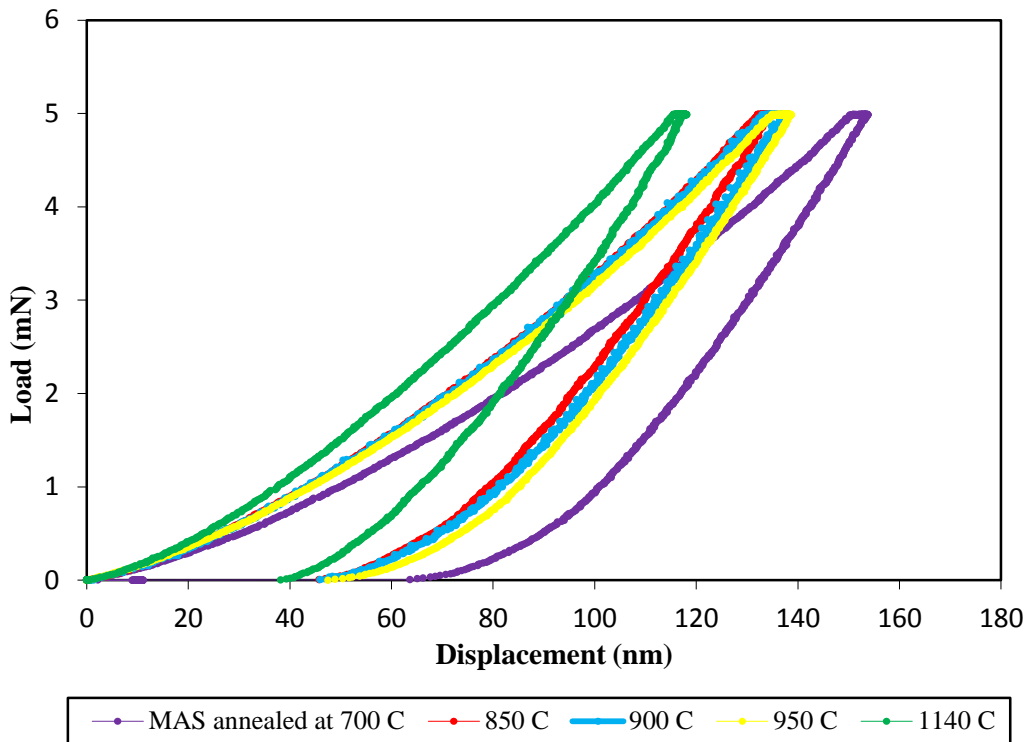


Figure 5.5: Load-displacement curves for MAS glass annealed at 700 °C (sample A) and further subjected to different heat-treatment temperatures (leading to formation of crystalline phases). The MAS sample annealed at 570 °C and LAS glass showed a similar behavior.

As the heat-treatment temperatures were increased, the depth of indentation decreased under the same load, reflecting an increase in sample hardness. No major differences were observed in the mechanical properties of the two different sample series (see Table 5.2). It may be deduced that samples from Group A exhibited slightly higher mechanical properties than samples from the B series of glasses, especially at a temperature of 1140°C.

Table 5.2: Reduced Young's modulus and hardness results of the selected MAS glasses from the nanoindentation tests.

Temperature (°C)	E_r (GPa)				H (GPa)			
	Sample A	Std	Sample B	Std	Sample A	Std	Sample B	Std
570	-	-	102.8	0.82	-	-	8.240	0.18
700	103.2	1.01	-	-	8.220	0.13	-	-
850	112.8	0.70	110.3	1.40	10.30	0.23	10.10	0.23
900	115.9	3.40	114.3	4.04	10.50	0.77	10.40	0.58
950	112.9	1.80	113.4	1.80	11.26	0.23	11.25	0.29
1140	137.2	2.26	129.6	7.89	13.80	0.49	12.93	1.16

The influence of the temperature of heat treatment on mechanical properties is shown in Figure 5.6 (reduced Young's modulus) and Figure 5.7 (hardness). These results show that the elastic modulus and hardness slightly increase with the increased heat treatment temperature. These results are improved than those of the parent glass [49]. These results are possible explained based on the development of the proportion of the major crystal phases as has been reported in the literature [25, 37]. In this study, this proportion is proved based on the number of peak crystal phases precipitated. The hardness and modulus of both samples is particularly comparable with other works [17, 16, 160].

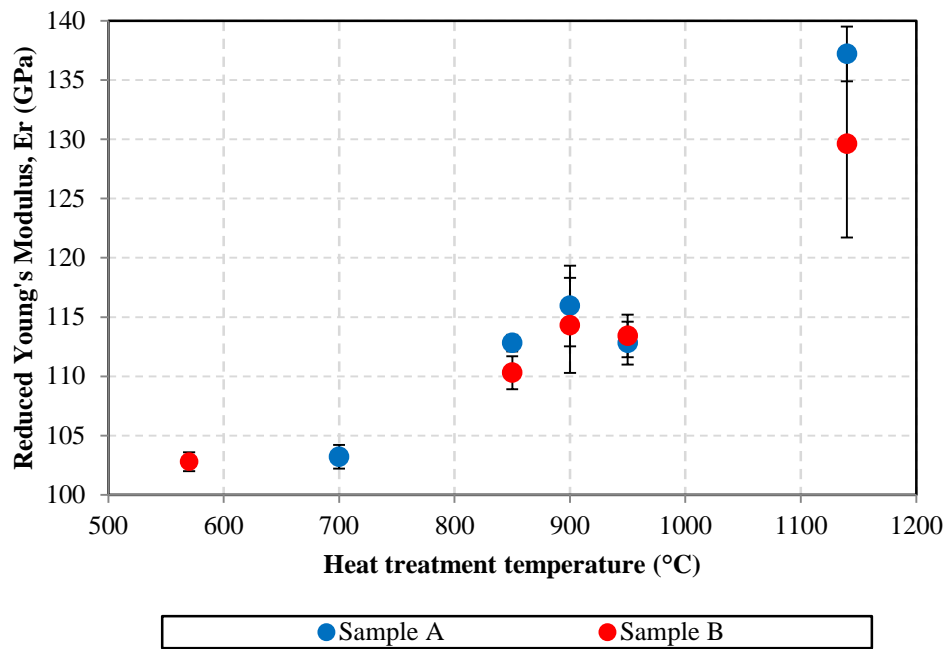


Figure 5.6: Reduced modulus values of MAS systems with various heat treatment regimes.

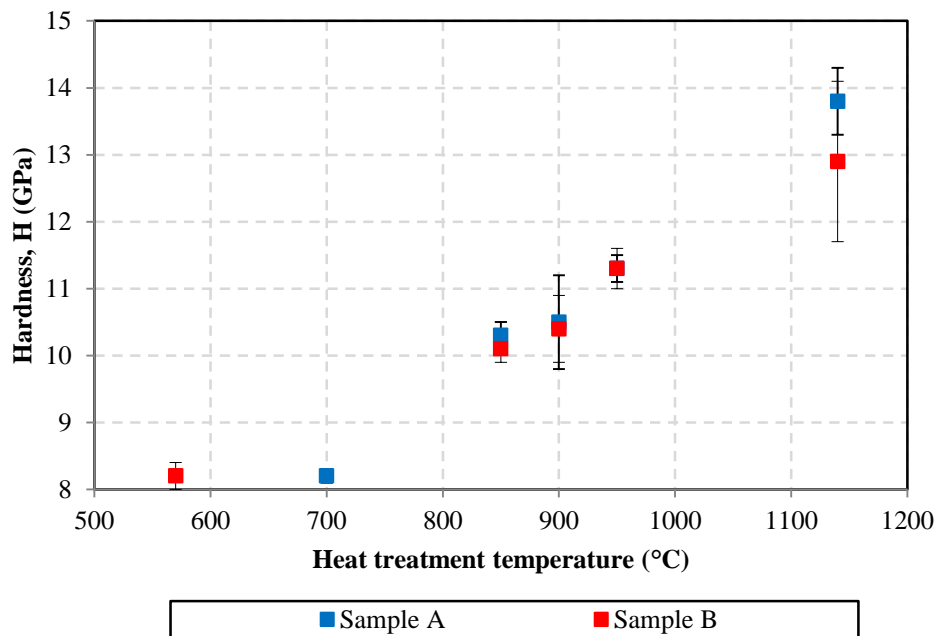


Figure 5.7: Hardness results of MAS systems with various heat treatment regimes.

5.2.1.4 Scanning electron microscopy

The morphologies of the crystalline phases developed during heat treatment of the glass samples were examined by scanning electron microscopy (SEM). From the SEM analysis presented in Figure 5.8 and Figure 5.9 (a-c) it can be seen that the increase in heat treatment temperatures had a strong influence on the microstructure and morphology of MAS glass ceramic studied in this work.

Heat treatment caused nucleation of crystals in the glass, which transformed the system into prominent droplet and glassy phases (as shown in dotted line). The crystals observed at 950°C were significantly larger than those depicted at 900°C, indicating that an increase in the crystallisation temperature enhanced crystal growth. The droplet-shaped phase separation initiated at around 900°C where MAT became apparent, detected by XRD as shown in Figure 5.8 (Sample A). Similar features also observed in Sample B.

The morphology of MAS glass ceramic scanned after heat treatment at 950°C showed that the crystal droplets (initiated at 900°C) increased in quantity and size and formed numerous boundaries. A similar phenomenon was reported in a different system using the same nucleating agent by Shyu et al. [63] and Minsheng et al. [64]. Figure 5.8 (c) shows the morphology of the sample that crystallised at 1140°C, where the quantity of droplet-shaped crystals increased, whilst decreasing in their sizes. A small number of crystals transformed into needle-like shapes as shown in sample A. The features morphology also discerned from sample B where the crystal increased with increasing heat treatment temperature (Figure 5.9 (c)). Moreover, the morphology of the dispersed phase seems to be slightly different than that of sample A which can be described that the magnesium aluminium titanate and magnesium aluminium oxide phases dominant with absence of aluminum titanate (Figure 5.8)

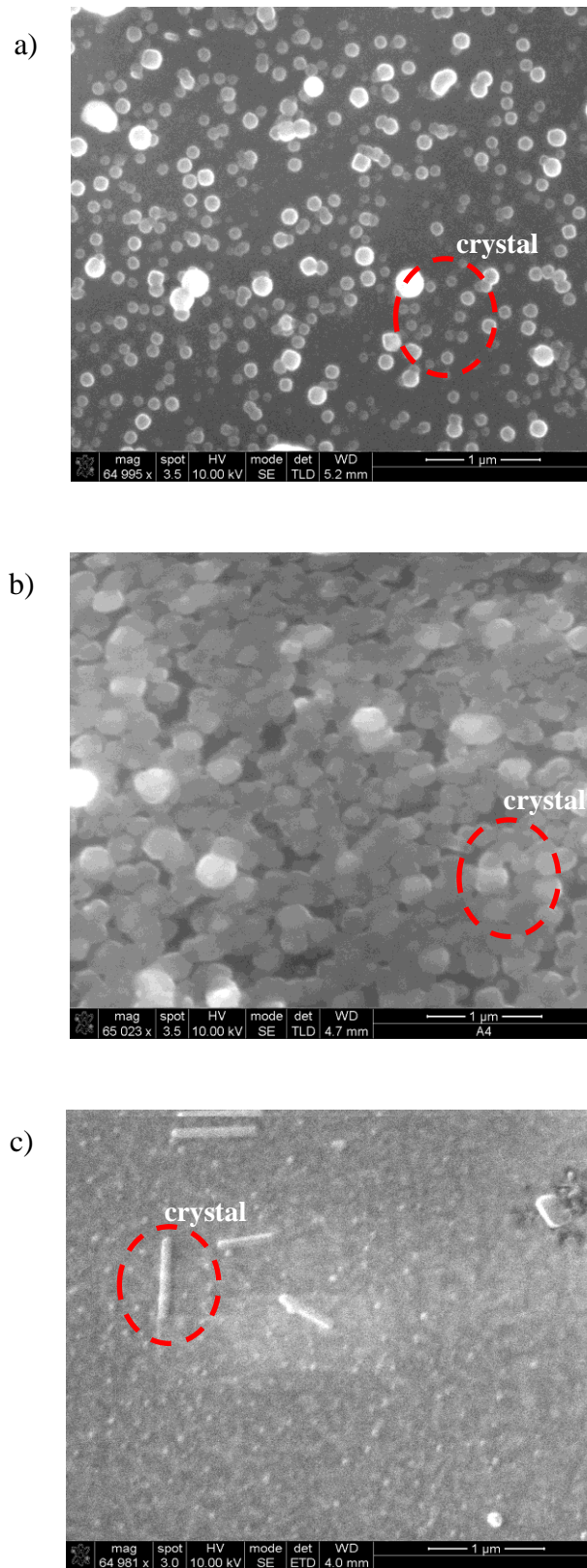


Figure 5.8: SEM micrographs of the crystallised $\text{MgO-Al}_2\text{O}_3\text{-SiO}_2$ at a) 900°C , b) 950°C and c) 1140°C (Sample A).

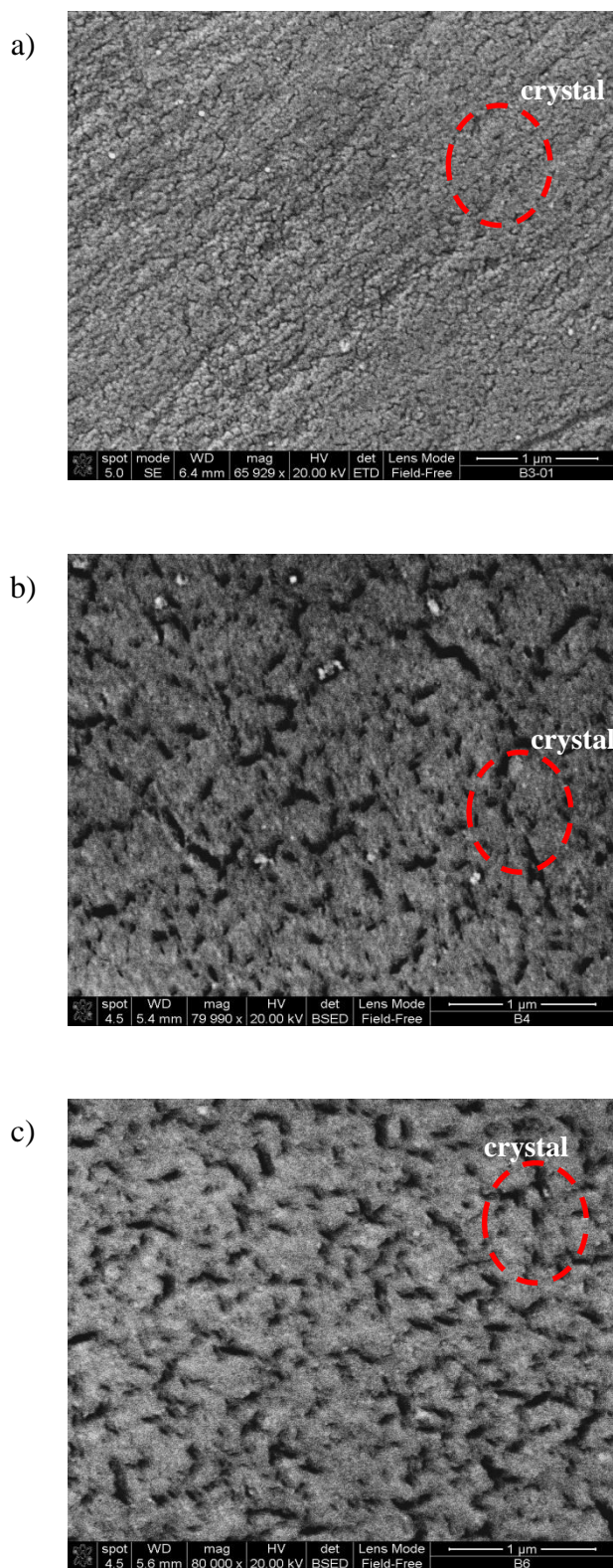


Figure 5.9: SEM micrographs of the crystallised $\text{MgO-Al}_2\text{O}_3\text{-SiO}_2$ at a) 900°C, b) 950°C and c) 1140°C (Sample B).

5.2.2 LiO₂-Al₂O₃-SiO₂ (LAS) glass

5.2.2.1 Differential thermal analysis

The DTA curve in Figure 5.10 for LiO₂-Al₂O₃-SiO₂ glass illustrates an endothermic deflection related to the glass transition temperature and an exothermic peak related to the crystallisation temperature. Two exothermic peaks were clearly detected at 750.2°C (T_{p1}) and 957.1°C (T_{p2}), where the latter is relatively sharp. An initial peak denoted as T_{p1} is not particularly distinctive as a point due to its broad shape. A small endothermic peak appeared after T_{p1} and is associated with the rearrangement of molecules in the glass structure, which is similar to the thermal effect observed in the MAS curve (Figure 5.1).

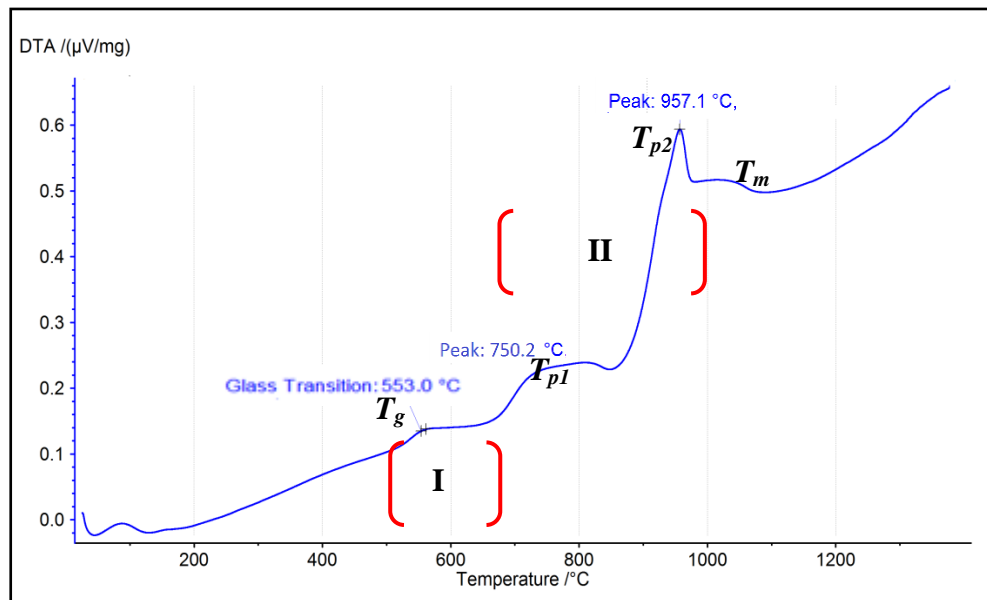







Figure 5.10: DTA traces of the parent LAS glass.

The nucleation temperature is generally expected to lay between T_g and the crystallisation temperature T_p [24]. The curve may be interpreted as two phases. Phase I covers the region from T_g until onset temperature T_{p1} for nucleation heat treatment followed by crystal growth in phase II. Following DTA analysis, the heat treatment of the parent glass was carried out in two-step process.

Table 5.3: Effect of heat treatment on colour of $\text{LiO}_2\text{-Al}_2\text{O}_3\text{-SiO}_2$ glass.

Temperature of heat treatment (°C-hour)	Images
LAS 1 Annealed	
LAS 2 Nucleation: 550 °C (100)	
LAS 3 Nucleation : 550 °C (100) Crystallisation: 750 °C (2)	
LAS 4 Nucleation : 550 °C (100) Crystallisation: 950 °C (2)	
LAS 5 Nucleation : 600 °C (2) Crystallisation : 750 °C (2)	

Nucleation and crystallisation temperatures were determined corresponding to T_g and T_p , respectively. Thus, the nucleation treatment was carried out at 550°C for 100 hours based on data collected from ALSTOM followed by 2 hours heat treatments at 750°C and 950°C, respectively. A melting endothermic peak (T_m) was observed after the crystallisation peak. Table 5.3 shows little difference in sample appearance after the heat treatment, although it is expected that colour

responses occur when glass is heat treated [161]. The LAS 2 and LAS 3 sample were slightly more opaque than LAS 4 but seemd to contain relatively good amount of glassy phase as can be seen from Figure 5.11.

5.2.2.2 X-ray diffraction

Figure 5.11 shows XRD patterns for all samples. Samples LAS 1 and LAS 2 show no indication of crystalline phases. These samples were XRD amorphous after heat treatment. Weak diffraction peaks are observed at LAS 3 and LAS 4 which demonstrates the prevalence of glassy phases with a smaller presence of crystalline phases.

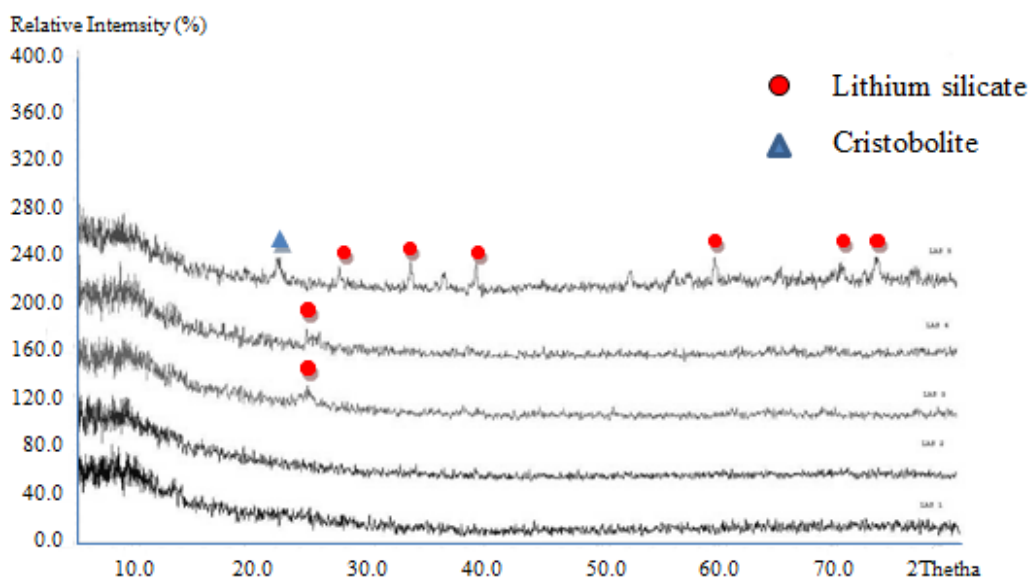


Figure 5.11: XRD patterns for glass ceramic in LAS system.

Crystalline peaks corresponding to different crystalline phases are marked with different symbols. Major crystalline phases consisting of lithium silicate, Li_2SiO_3 (JCPDF card 30-766), were identified by XRD in all samples. These results are in agreement with those found in the literature [162,163] concerning the crystallisation of lithium aluminosilicate. The presence of crystalline phases appeared to increase with the crystallisation temperature. This is borne out by the observation of an additional peak corresponding to cristobolite, SiO_2 (JCPDF card 39-1425) in the XRD pattern of LAS 5 glass ceramic. It is notable that the

intensity of cristobolite started to increase at a higher temperature than lithium silicate, which appeared with a lower intensity at 750°C.

5.2.2.3 Physical and mechanical properties

A. Density of bulk glass

Figure 5.12 shows the densities of parent LAS glass and glass ceramic. The density of LAS glass slightly increased with heat treatment. As expected, the first nucleating stage of heat treatment increased the density. This finding may be attributed to the proportional relationship between the dwell time and the proportion of major crystal phases.

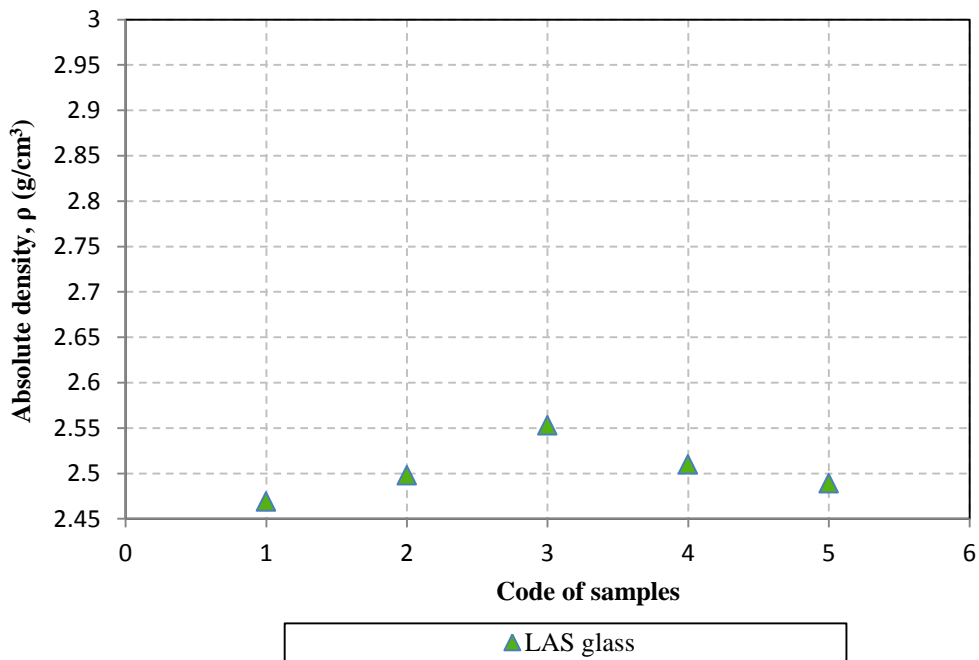


Figure 5.12: Densities of the LAS samples at various heat treatment temperatures.

The density for LAS glass system gradually decreases from the onset of the second peak crystallisation temperature (950°C). Figure 5.11 also shows that the nucleation temperature has shifted up 50°C from 550°C and that the density decreased to 2.489 g/cm³. Additionally, the crystallisation dwell time was virtually unchanged between the LAS 4 and LAS 5 samples. This also indicates

that the density in this LAS system is proportional to the nucleation dwell time and the developed microstructure.

B. Reduced Young's modulus and hardness

The results for the reduced Young's modulus and hardness of the LAS system are presented for each sample type. Results of the nanoindentation tests in Table 5.4 show variation in values for both modulus and hardness. Table 5.4 also emphasises the difference in properties acquired by different heat treatments. These include nucleation at 550°C for 100 hours followed by crystallisation at 720°C for 2 hours and nucleation at 600°C with crystallisation at 750°C for 2 hours.

Table 5.4: Reduced Young's modulus and hardness results of the selected LAS glasses from nanoindentation test.

Temperature (°C)	Reduced Young's Modulus (GPa)		Hardness (GPa)	
	E_r	Std	H	Std
LAS 1	79.40	1.30	6.64	0.20
LAS 2	84.98	3.24	7.08	0.80
LAS 3	93.01	2.86	8.06	0.48
LAS 4	89.85	2.99	8.28	0.23
LAS 5	81.07	2.32	7.34	0.38

In Figure 5.13, the hardness of the LAS glass sample is shown as a function of the heat treatment temperature. Sample LAS 4 was the hardest (8.28GPa) with a nucleation at 550°C for 100 hours and crystallisation at 950°C for 2 hours. Hardness decreased to 7.34GPa with a nucleation temperature of 600°C for 2 hours and crystallisation temperature to 750°C for 2 hours. This value shows to be slightly different to that of annealed glass. This finding agrees with a previous study conducted by Hu et al. [164]. They found that the hardness decreased with an increase in nucleation temperature and showed that an increase in dwelling time during nucleation produced a smaller grain size and contributed to an

increase in hardness. The ability for LAS glass ceramic to maintain hardness at an acceptable level is thus dependent on annealing time.

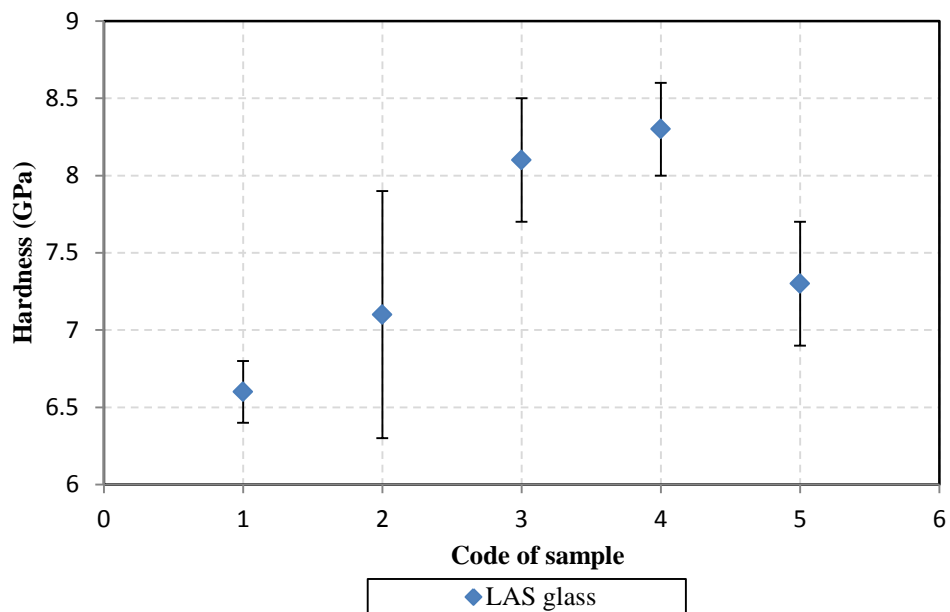


Figure 5.13: Hardness of LAS system at various heat treatment regimes.

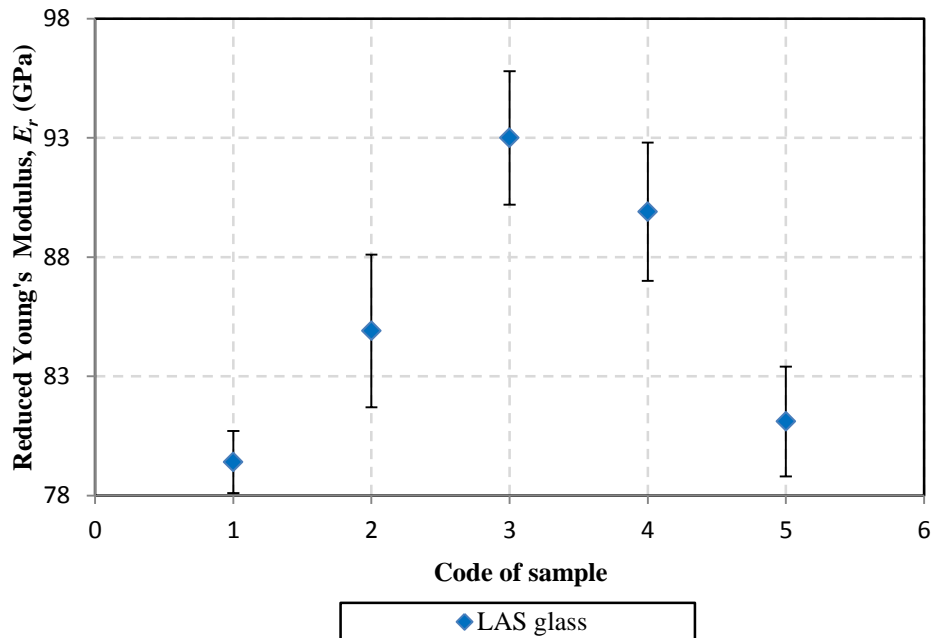


Figure 5.14: Reduced modulus results of LAS systems for various heat treatment regimes.

As shown in Figure 5.14, the reduced Young's modulus is a function of the heat treatment temperature. The highest modulus was recorded for the sample nucleated at 550° (LAS 3), while the lowest was exhibited by the sample nucleated at 600°C (LAS 5). The value of the sample LAS 5 which nucleated at 600°C is notably similar to that of annealed glass (LAS 1). However, the reduced Young's modulus of samples LAS 3 and LAS 4 nucleated at 500°C for 100 hours were strongly influenced by the annealing time during nucleation, but were not highly dependent on the crystallisation temperature. These values are in the same range as those reported in the literature for other lithium aluminosilicate glasses. Guo, et al. [66] found values in the range of 78.4 to 95.2GPa for glasses from $\text{LiO}/\text{Al}_2\text{O}_3/\text{SiO}_2/\text{MgO}/\text{Na}_2\text{O}/\text{TiO}_2/\text{K}_2\text{O}/\text{MgF}_2$ systems. Hu et al [164] found values in the range of 93.4 to 93.7GPa for glasses $\text{LiO}/\text{Al}_2\text{O}_3/\text{SiO}_2/\text{MgO}/\text{ZnO}/\text{TiO}_2/\text{ZrO}_2$ systems. The new findings presented in Figure 5.14 are in good agreement with latter literature values.

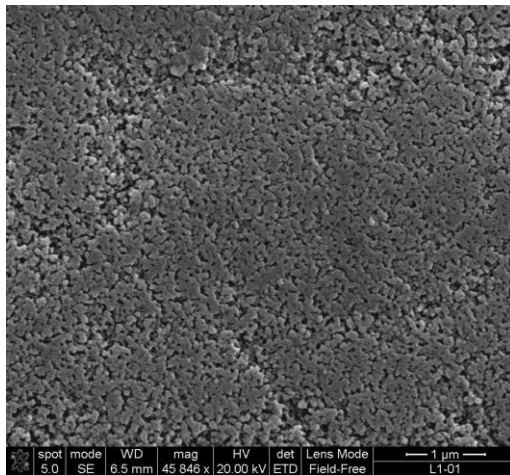
5.2.2.4 Scanning electron microscopy

The morphologies of the crystalline phases developed during heat treatment of the glass samples were examined by scanning electron microscopy (SEM). From the SEM analysis presented in Figure 5.15 (a-d), it can be seen that the increase in heat treatment temperatures had a notable influence on the microstructure and morphology of LAS glass ceramic studied in this work. However, in this system the selection of the parameters heat treatment (e.g temperature and dwelling time) have been selected by ALSTOM and it is bounded by confidential agreement.

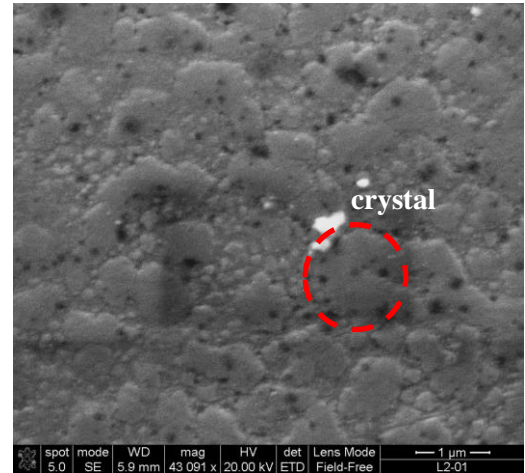
Heat treatment caused nucleation of crystals in the glass, which transformed the system into prominent droplet and glassy phases. The crystals observed at LAS 2 (nucleated at 550°C for 100 hours) were significantly larger than those depicted at sample LAS 1 (annealed at 500°C for 15mins), indicating that an increase in the crystallisation temperature enhanced crystal growth. The spherules-shaped phase separation initiated at around 750°C where lithium silicate, Li_2SiO_3 became

apparent, was detected by XRD as shown in Figure 5.15 (sample LAS 3 nucleated at 550°C for 100 hours, crystallised at 750 °C for 2hours).

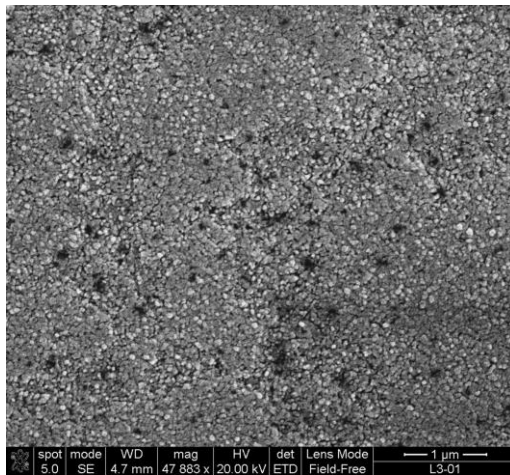
The morphology of LAS glass ceramic scanned after heat treatment at 950°C (LAS 4 nucleated at 550°C for 100 hours, crystallised at 950°C for 2 hours) showed that the tiny crystals uniformly dispersed (initiated at 750°C) were increased in quantity and formed numerous circular boundaries which appeared as a black spot. This indicated that the temperature increase preceeded the changes in the microstructure, rather than difference in the dwelling time. A similar phenomenon was reported in the same system when different nucleating agents were employed with the varied heat treatment by Xingzhong et al. [162] and Ananthanarayanan et al. [164]. In contrast, LAS 5 shows clear granular crystals after being nucleated at 600°C and crystallised at 750°C for 2 hours, respectively. The microstructure also showed increases in hole-shapes, whilst decreasing in crystal sizes which was also observed in [36]. These holes are believed to result in both densities of LAS 4 and LAS 5 decreasing as shown in the results (Figure 5.12).



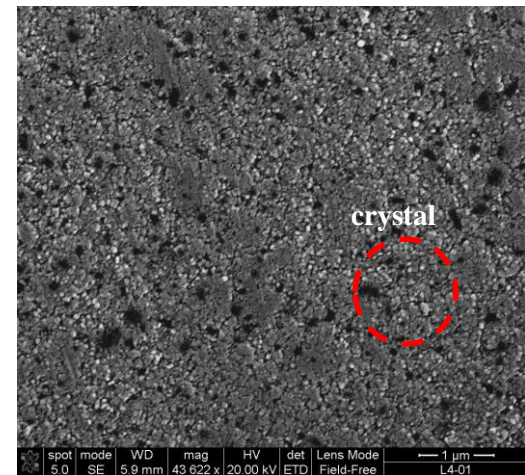
a) LAS 1



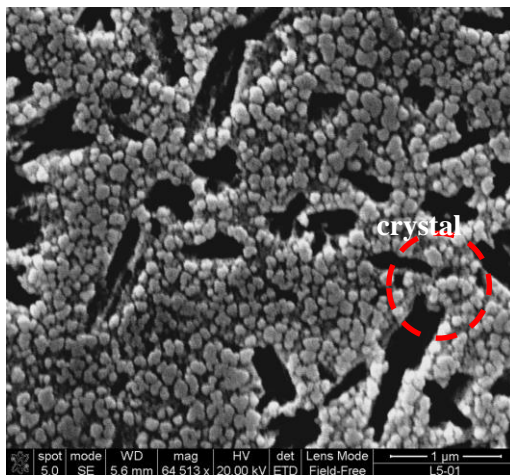
b) LAS 2



c) LAS 3



d) LAS 4



e) LAS 5

Figure 5.15: SEM micrograph of LAS systems at various heat treatment regimes.

5.3 Fabrication of glass fibre

Two methods of fabrication are used depending on the feasibility of the drawing. For MAS system, glass fibres were formed using up-drawing from supercooled melts and LAS glass fibres were produced from down-drawing using glass rod. Both glass fibres were fabricated on a laboratory scale.

5.3.1 Feasibility of the melt drawing process

Figure 5.16 illustrates necking of the crystallised preform after drawing and demonstrates the incompatibility of continuous drawing with the MAS system. The MAS preform was transparent with a light brownish colour before drawing (Figure 5.16a). Drawing trials were conducted to determine suitable parameters for processing, including the temperature of drawing and the feed rate for producing acceptable fibres with a consistent diameter size. The process was started by heating a preform near to the heater coil at the softening temperature (T_d) of approximately 850°C to generate a localised heat point. The range of drawing temperatures covered up to the working temperature [62] was determined from a dilatometry curve (Figure 5.17). The resultant dilatometer curve shows the curve terminating at approximately 900 °C, which represents softening of the glass. The preform gradually started to soften and a considerable external force was applied to initiate fiberisation.

Unfortunately, a light blue colour was observed after glass rod started necking, which showed that the fibre surface had crystallised before it was drawn into a fibre. It can be seen from Figure 5.16c that the crystallised preform deformed into a symmetrical cone shape. This deterioration occurred after several trials up to the working temperature at 1000 °C. A relatively narrow softening temperature to the onset crystallisation temperature (T_c) enabled crystallisation at lower drawing temperatures using the continuous drawing method. Difficulties in fibre drawing may be encountered due to the narrow thermal stability range of MAS glass fibres. Better glass fibres are therefore obtained from melt drawing below the liquidus temperature.

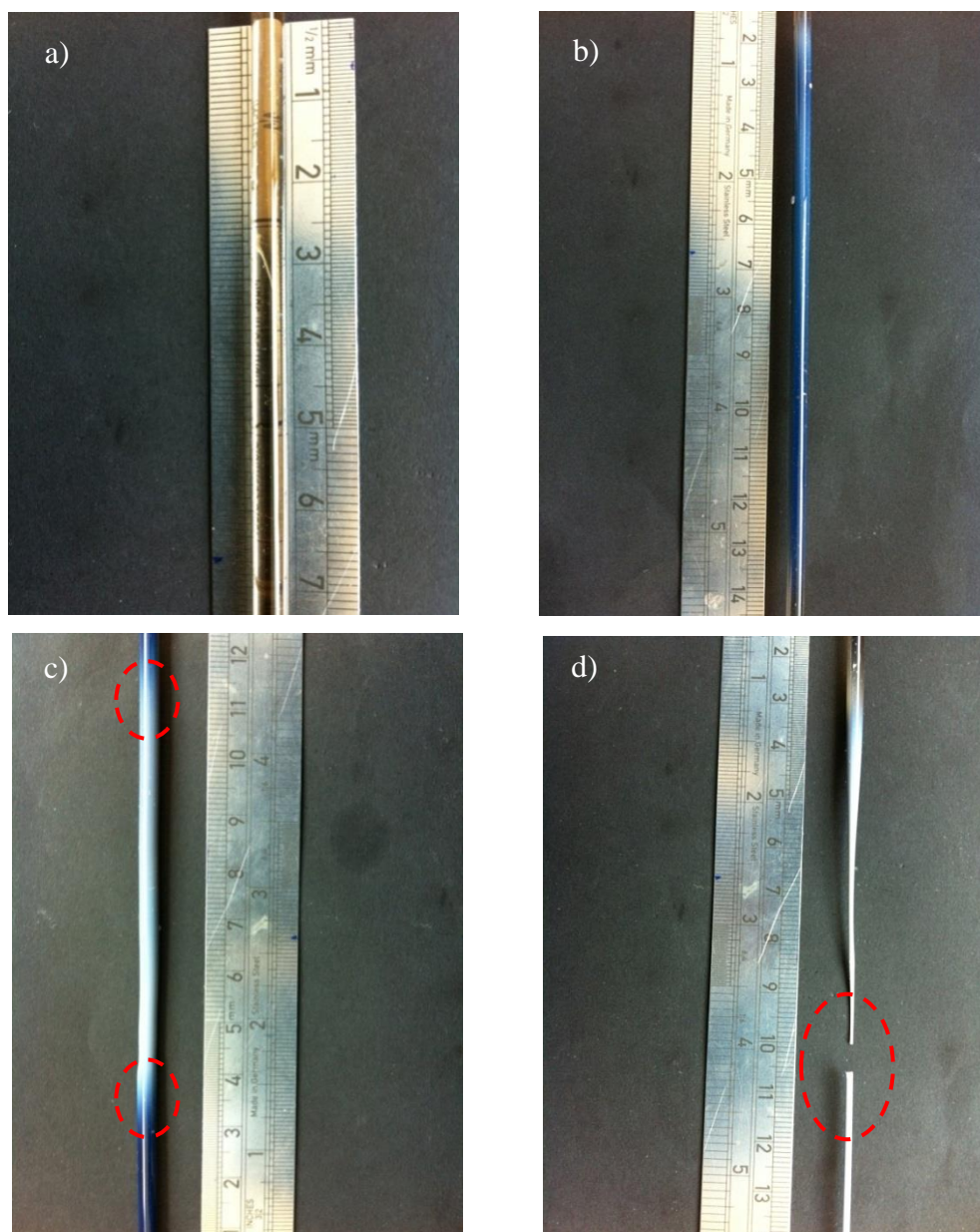


Figure 5.16: Photographs of the glass rod before and after continuous drawing trials a) before drawing, b) 850°C, c) 950°C and d) 1000°C.

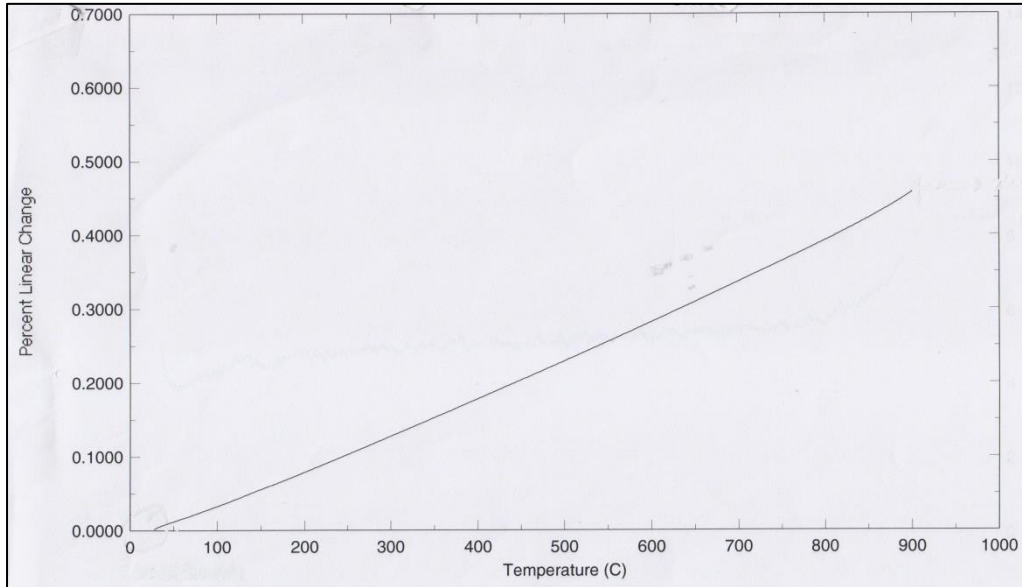


Figure 5.17: Dilatometer curve showing the onset of softening temperature.

Optimal glass fibre formation may be assessed by experimental determination of the melt viscosity, which was beyond the scope of this investigation. In the absence of empirical data, it has been noted that the melt viscosity may be assumed to be of the order of 10^3 Pas for a given composition at the drawing temperature of 1240°C at which the fibres were obtained [62]. Variation was found in the diameter of fibres successfully drawn with a length above 1.5m. This variation was expected due to the magnitude of the melt viscosity and the speed of hand pulling. These fibres were divided into groups according to diameter. In addition, MAS glass fibre showed good drawing formability in comparison with continuous drawing. The fibres which were free from deformation and visible inconsistencies were selected for glass ceramic fibres.

4.3.2 Feasibility of continuous drawing process

This process was used to produce a total length of approximately 1800m of fibre (as shown in Figure 5.18b). The fibre was wound onto a 30cm x 30cm frame. Several such frames of fibres were produced for each drawing speed. In order to avoid disturbance of the drawing process, the system did not have any instrumentation to directly measure the glass preform temperature. Upon drawing,

LAS glass rod started to soften at 650 °C, which is well below the onset crystallisation temperature of 750°C, as tabled in Table 5.5. The viscosity is approximately 10^5 Pas at this stage of processing [62]. The drawing speed, which is controlled by feed rate, was as high as 700 mm/s.

Several optimisation trials were performed in order to consistently obtain a minimal fibre diameter. This process succeeded in producing two fibre diameters; 50 and 70 μ m. These fibres did not show any sign of crystallisation to the naked eye (Figure 5.18b) and we can also observe the regular shape of the preform and the absence of defects and crystalline phases from its surface.

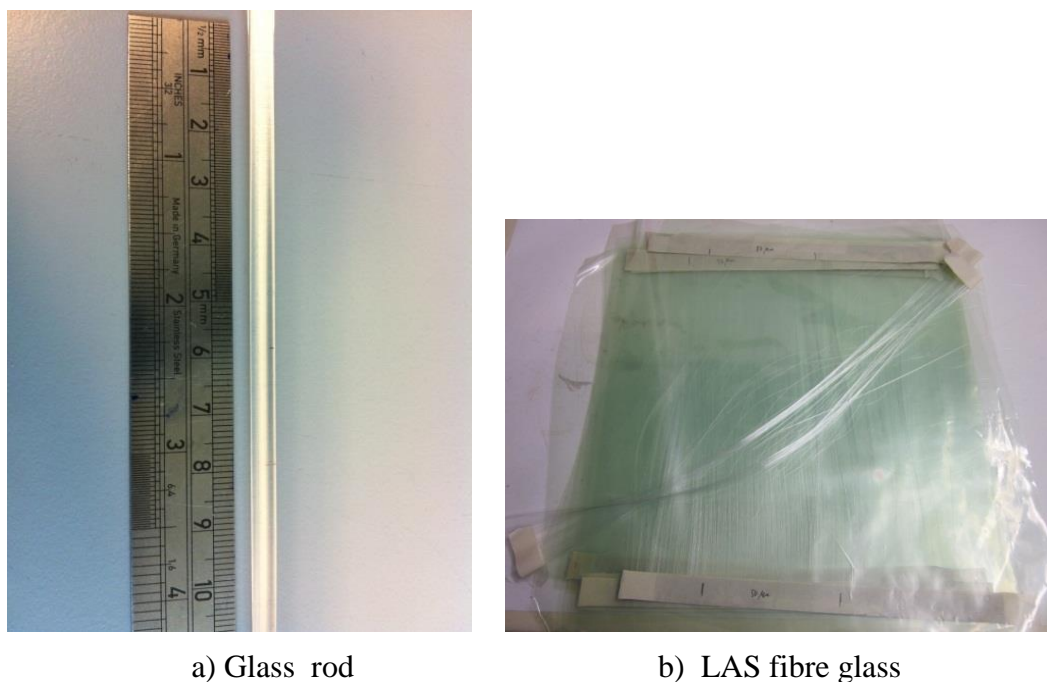


Figure 5.18: Photographs of the a) glass rod before drawing and b) fibre glass after being drawn.

The diameters of the obtained fibres measured using scanning electron microscopy are reported in **Section 4.5.1** together with the respective values obtained through micrometer measurement. The obtained diameters agree to within 5 μ m of the values recorded from SEM imaging. The small standard

deviation within this dataset indicates the consistency of fibre diameters obtained through this drawing process.

Table 5.5: Process parameters for drawing of LAS glass ceramic.

Diameter of fibre (μm)	Drawing temperature ($^{\circ}\text{C}$)	Feed rate (mm/s)	Drum speed (mm/s)
50	650	600	50
70	650	700	50

5.3.3 Characterisation of drawn glass fibre

The typical appearances of the drawn fibres are represented by the SEM micrograph illustrated in Figure 5.19. The amorphous nature of the fibre gives rise to its smooth surface. All the fibres have the same external appearance with circular cross sections, smooth surfaces and featureless surface morphologies.

Inferior samples were also obtained in the course of trials in which drawing yielded frail fibres with white droplets on coarse surfaces, resulting in deteriorated fibres as shown in Figure 5.20. With regards to the previous results in **Section 5.2.1.1**, there are two possible explanations for this phenomenon. The first involves rapid cooling of the molten causing droplets of crystallisation, which can usually be suppressed due to the molten viscosity. This may have occurred if drawing was not performed at the working temperature, at which the viscosity slightly increased. This may have been caused by a drop in temperature during transfer to the crucible. The second reason may be variation in the drawing speed due to control by hand pulling. These factors may explain the behaviour of defects with respect to nucleation and crystallisation points, which lay above the softening temperature.

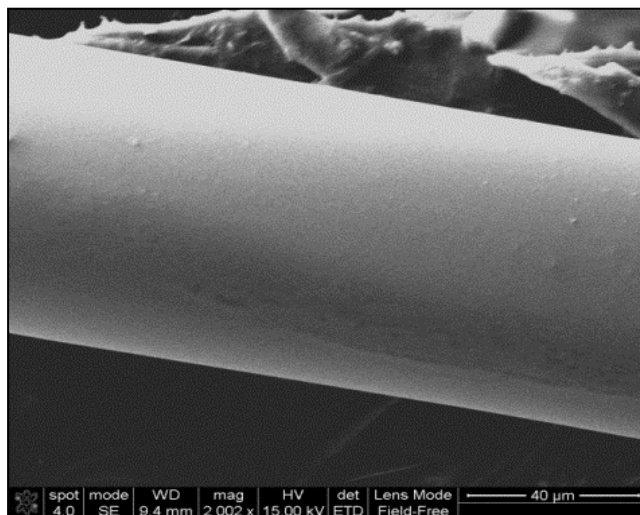


Figure 5.19: SEM micrograph of MAS glass fibre surface after drawing.

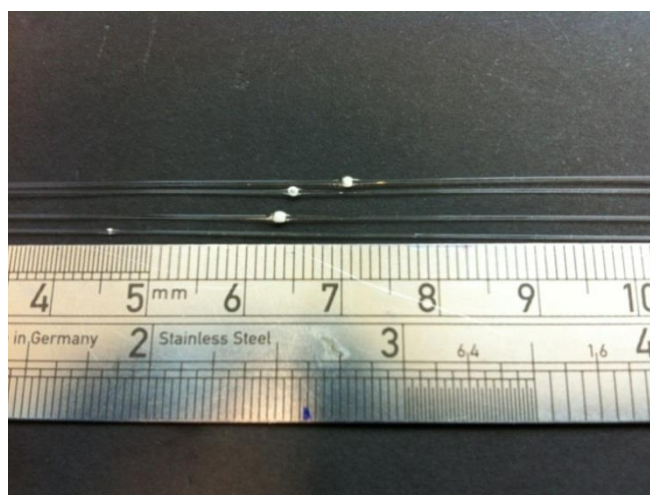


Figure 5.20: Droplet crystallisation on the surface of MAS glass fibre during trials.

The drawing of LAS produces uniformity of the shape and circular cross section of the glass fibres without pores, as shown in Figure 5.27. This indicates that the shape of the fibres was maintained during drawing without a significant decrease

in diameter size. This was expected as the process was automatically controlled. Furthermore, the fibres were also flexible, as shown in Figure 5.21, where the mean diameter of the fibres is approximately 50 μ m. It is clear from these results that drawing protocols and conditions influence the physical appearance of the glass fibres and that these factors dictate the feasibility of both glass systems.



Figure 5.21: Bent LAS glass fibres with a mean diameter of 50 μ m.

5.4 Fabrication of glass ceramic fibre

In this section, the glass fibres of both systems were converted into glass ceramic fibres in order to improve mechanical properties. The heat treatment of the glass fibres were studied in order to identify optimal treatment conditions and to prevent thermal distortion.

5.4.1 Heat treatment trials

Fibres from the MAS system are shown in Figure 5.22a. A heat treatment trial was conducted by varying the temperature for the same dwelling time. The appropriate heat treatment range was determined from differential thermal analysis measurement, such as the one shown in Figure 5.1 (Section 5.2.1.1). In

addition, the optimal temperature was determined by measurement of the reduced Young's modulus, which was found to increase at higher temperatures.

The chosen heat treatment for MAS started with reheating in the vicinity of the sharp crystallisation peak at 900°C and 1140 °C and held for a dwelling time of 2 hours after the nucleation process at 720°C. The glass ceramic fibre shown in Figure 5.22b was heated at 900°C for 1 hour. This heat treatment resulted in a slight colour change from light brown to transparent grey. In addition, no significant distortion or shrinkage was observed. This demonstrates that the chosen temperature satisfied the dwelling time criterion.

A trial heat treatment at 1140°C for 1 hour produced more significant changes in physical appearance, as shown in Figure 5.22c. Figure 5.22c represents a series of fibres at different diameters and illustrates great distortion and colour change to opaque white. These changes indicate that the thinner fibre experienced the worst distortion and shrinkage. This suggests that the rate of crystal growth was comparable to the rate of nucleation. This change in structure was observed to significantly affect fibre strength in single fibre testing.

The dwelling time used in this process is lower than that used for the bulk heat treatment. A previous study by Tick et al. [81] proposed that the optimal dwelling time should be experimentally determined and suggested that fibre distortion could be avoided by control of the dwelling time [74]. The 1 hour dwelling time for crystallisation was arbitrarily selected.

The heat treatment schedule for the LAS system was quite different to that of the MAS system. The first trial was performed at the temperature utilised by LAS 3, which contributed the highest recorded reduced Young's modulus. The dwelling time in the nucleation stage was reduced to 2 hours from 100 hours and the crystallisation rate was kept at 1 hour. Heat treatment resulted in a significant change to a white colour without ancillary physical changes, as can be seen in Figure 5.23. The colour change indicates that the sample has been crystallised at a higher temperature (950°C) than the bulk sample (LAS 5). This means that

nucleation dominated the crystal formation at this temperature and that the faster rate growth mechanism was promoted. It is very important to control fibre shrinkage during heat treatment to avoid fibre distortion.

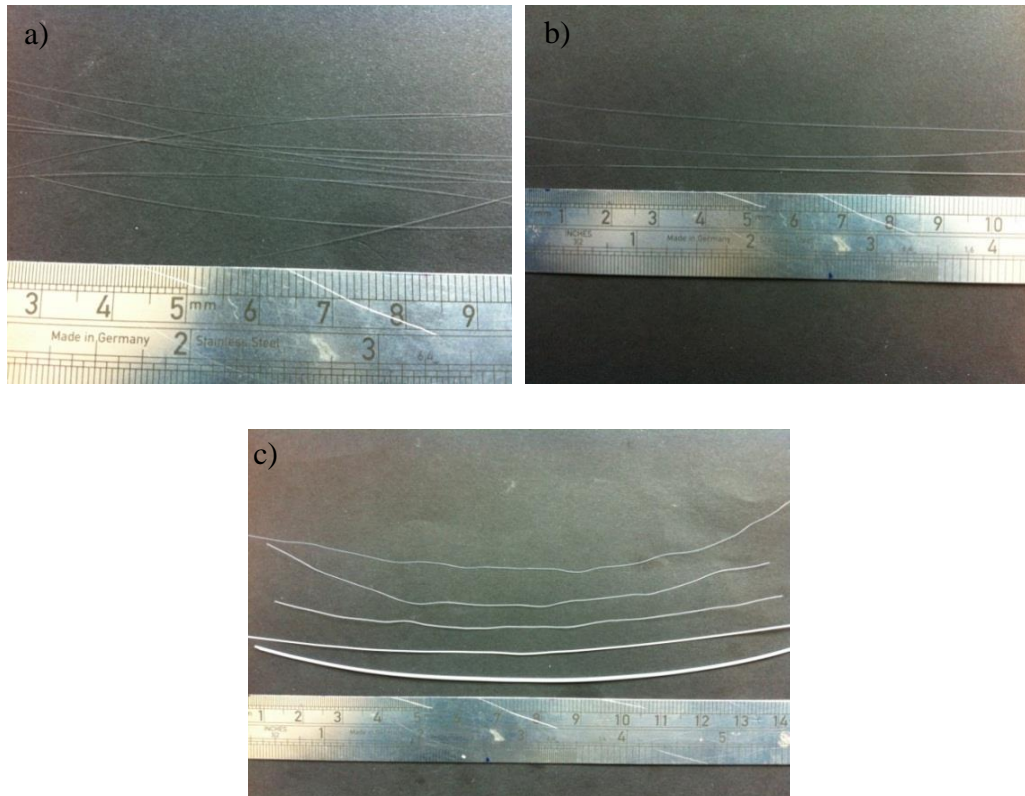


Figure 5.22: Photographs of the MAS glass fibres after the heat treatment a) after annealing temperature, b) at 900 °C and c) at 1140 °C for different diameters.

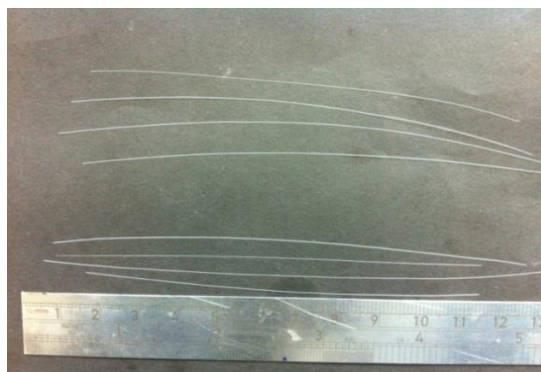


Figure 5.23: Photographs of the LAS glass fibres after the heat treatment at 750°C.

Therefore, based on the observation of physical changes, it was concluded that for the production of these two glass ceramic fibre a heat treatment at 900°C represented the most appropriate route for processing of the MAS system and LAS system with 750°C were chosen for the further investigation.

5.4.2 Characterisation of glass ceramic fibre

5.4.2.1 Density

The density of the fibres was measured using density balance equipment with an accuracy of ± 0.0001 g. Table 5.6 shows the density recorded for each group.

Table 5.6: Density of the glass fibre.

Group	Density (g/cm ³)
MAS glass	2.7280 \pm 0.01
MAS glass ceramic	2.8430 \pm 0.01
LAS glass (50 μ m)	2.4730 \pm 0.01
LAS glass ceramic (50 μ m)	2.9100 \pm 0.01
LAS glass (70 μ m)	2.7460 \pm 0.01
LAS glass ceramic (70 μ m)	2.9700 \pm 0.01

The heat treatment had slightly increased the density of the glass ceramic fibres in comparison with the density of the glass fibre, which were measured using Archimedes' principle. However the density in LAS glass with 50 μ m diameter was slightly different from LAS glass with 70 μ m. This may be explained by the precipitation of crystal phase. Usually precipitated crystals are even in geometry and size, however due to the diameter changes, it is believed that heat treatment may produce a different effect. As expected, the heat treatment introduced increases in density for both glass systems which was related to the degree formation of the promoted crystalline phases [55,159].

5.4.2.2 X-ray diffraction

The glass fibres were characterised using XRD to examine the effect of heat treatment on the formation of crystalline phases. The samples were scanned over a range of 5-80° 2 θ at a rate of 2° 2 θ /min. Results for the LAS glass ceramic fibre are shown in Figure 5.24. The XRD pattern for LAS glass ceramic fibre illustrates that the crystalline phases identified by X-ray diffraction analyses are lithium silicate with a minor proportion of cristobalite, SiO₂. Furthermore, no major changes in phases were observed in comparison with the bulk system. In addition, it has been shown that the identified phases are not dependent on the dwelling time of crystallisation.

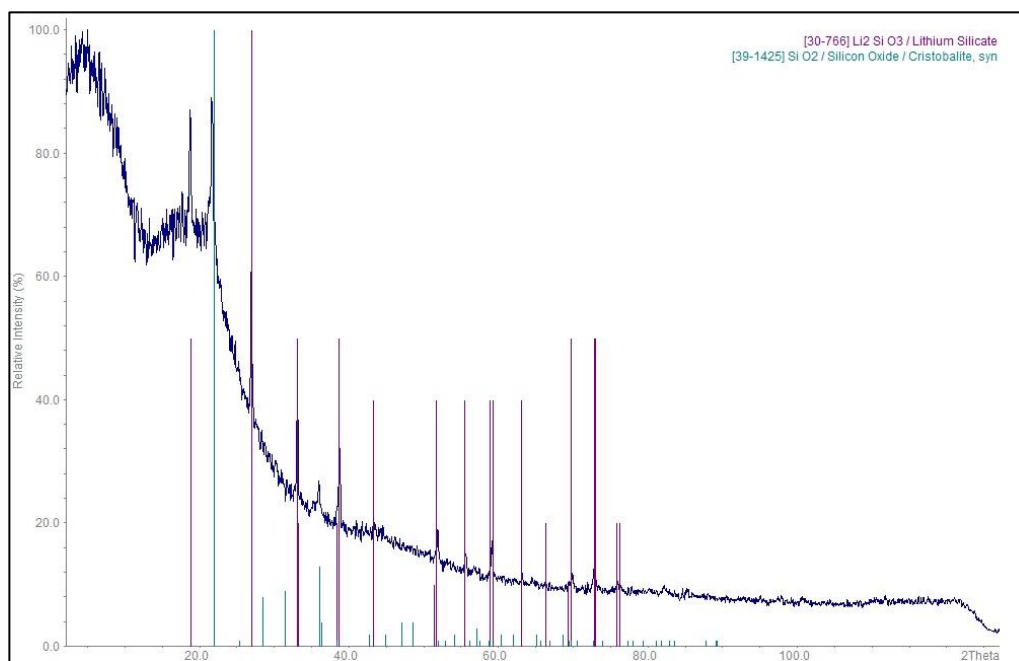
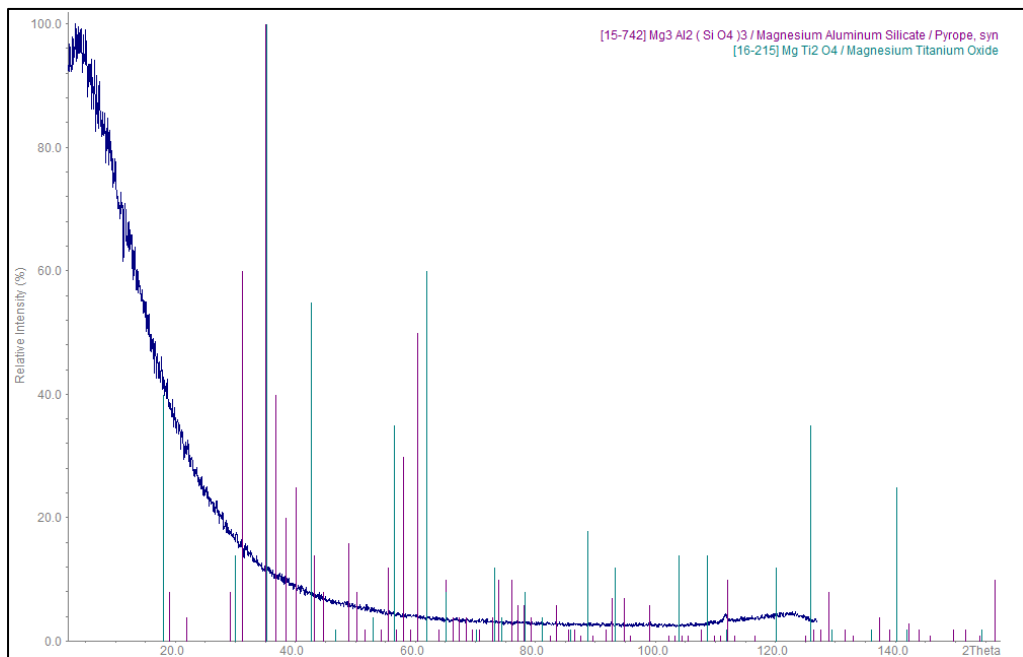


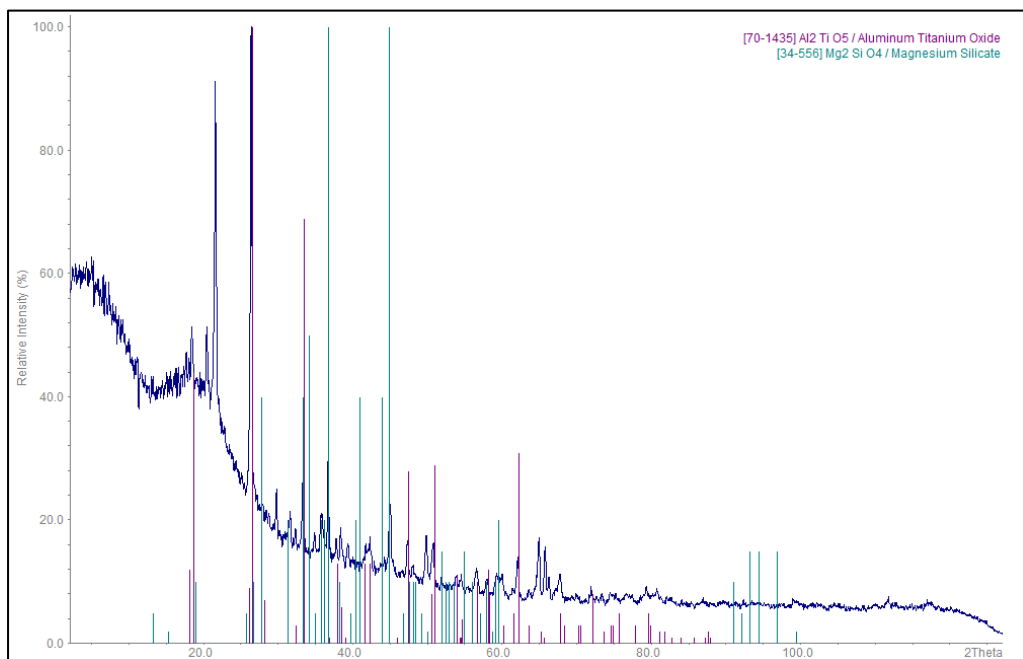
Figure 5.24: XRD diffraction patterns of LAS glass fibre treated at 750°C.

Figure 5.25 shows the XRD patterns of MAS glass after heat treatment. The identified crystalline phases were compared with the bulk glass phase in the glass ceramic. The XRD results show a glassy phase with a high background level and weak XRD peaks were observed after heat treatment at the peak of exothermic crystallisation. No significant peaks appeared in contrast to the bulk phase. This fibre treated at 900 °C shows one broad peak at 115.94° 2 θ corresponding to the magnesium aluminum oxide phase. This is a significantly different result in

contrast to the sample bulk glass B3 heated at the same temperature with a different dwelling time of crystallisation.



a) 900 °C



b) 1140 °C

Figure 5.25: XRD diffraction patterns of MAS glass fibre a) treated at 900°C and b) treated at 1140°C.

The XRD pattern of B3 showed that the broad peak at $65.94^\circ 2\theta$ shifted to $115.94^\circ 2\theta$ which can be attributed to a change into magnesium aluminium titanate. This difference is presumably due to the size of the sample being different, where finer sample possesses higher surface area and greater surface to volume ratio.

Therefore, it is seen that the fibre more intensively crystallised compared to the bulk form. In addition, it is also believed that the less compact and non-uniform arrangement of fibres within the sample holder and the surface roughness of the fibre in comparison with the polished bulk glass sample contributed to the unclear peak. However, an unexpected broad peak was observed in addition to small peaks that appeared between $20^\circ\sim 80^\circ 2\theta$ when the temperature increased to 1140°C . The XRD pattern showed that while the glass phase decreased, magnesium aluminium oxide phases remained and a high proportion of quartz was formed. This confirmed that no significant changes had occurred after the dwelling time of crystallisation was reduced to 1 hour.

5.5 Properties of glass fibre

Glass and glass ceramic fibres that were free from distortion to the naked eye were selected from those produced by melt drawing and continuous drawing.

5.5.1 Measurement of fibre diameter

Fibre diameters at or near the point of failure location were measured by SEM (D_{sem}) and micrometer (D_{mic}). Figure 5.26 illustrates the variations in diameter as measured by single fibre of both MAS and LAS glasses. As shown in Figure 5.26, diameter values recorded using SEM at failure locations were slightly lower than those measured by micrometer. A digital micrometer relates its measurement of distance to the number of rotations of a ratchet, which stops in response to the pressure exerted by the fibre surface on a spindle. Thus the fibre diameter was obtained from the displacement made by a fibre between the anvil and spindle.

Fibre cross-sections were reasonably circular after testing, as is shown in Figure 5.27.

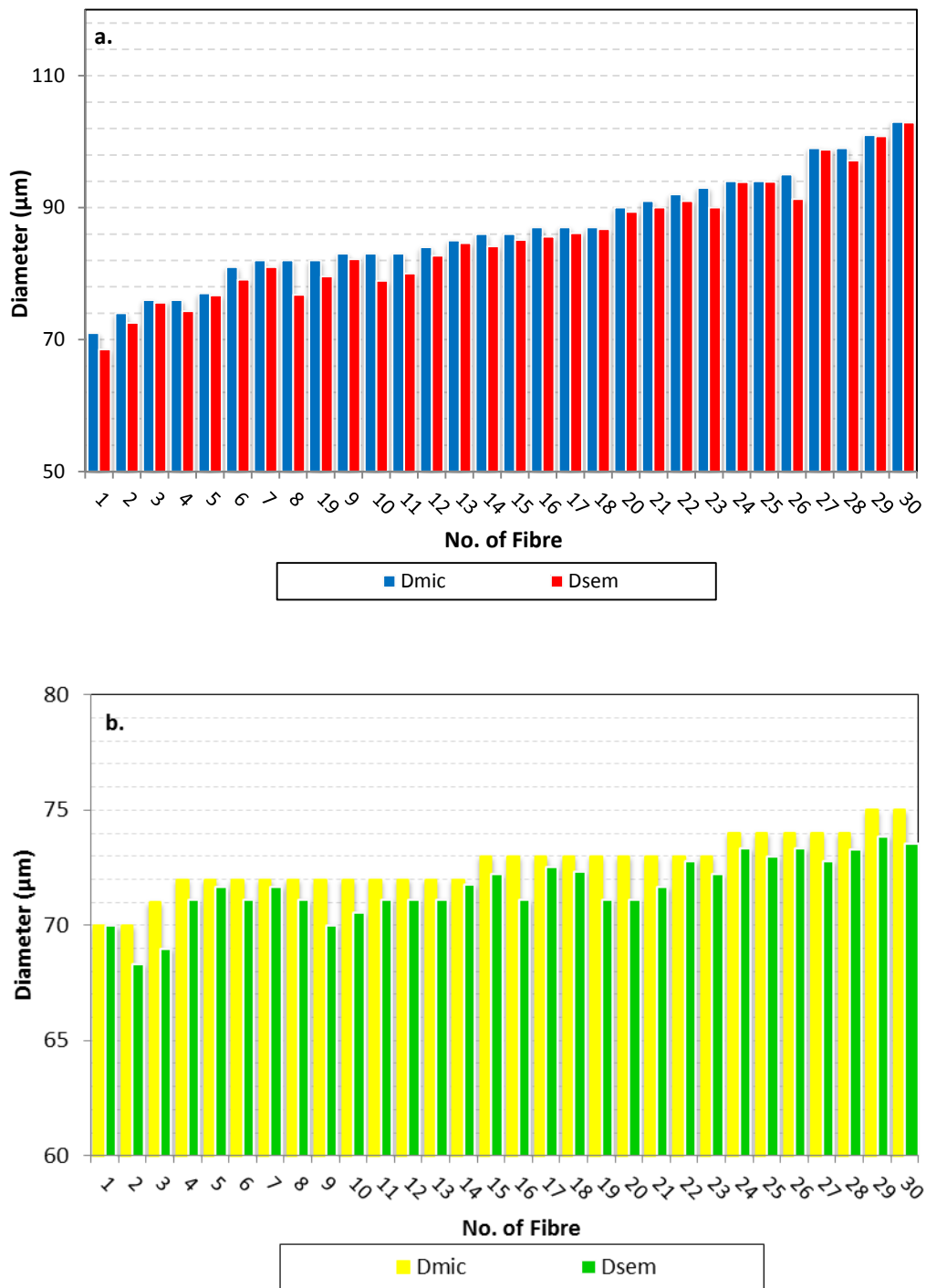


Figure 5.26: Diameter variations detected by SEM and micrometer for a) MAS and b) LAS with a 60mm gauge length.

The histogram in Figure 5.28 shows that the diameter distribution of MAS glass and glass ceramic fibres used in the present work. There was a large variation in fibre diameters produced. MAS fibres were produced using a melt drawing technique, where fibre diameter was controlled by melt viscosity and the speed of hand pulling. This is due to the equivalent fibre diameters before and after heat treatment were measured after tested for a group of 30 random fibres from each glass system before grouped by in intervals with fibre diameter values between 60-79, 80-89 and 90-110 μm . The diameters of fibres were assorted due to the inconsistent diameters produced during the drawing process, that may have influenced the subsequent results.

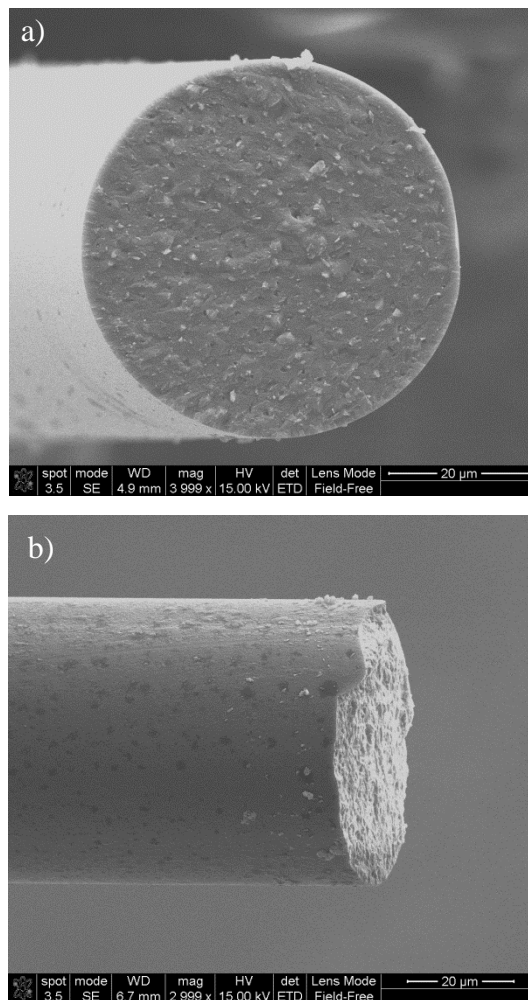


Figure 5.27: a) External aspect of the fibres at room temperature as they appear circular in cross section and b) Longitudinal view of the LAS fibre.

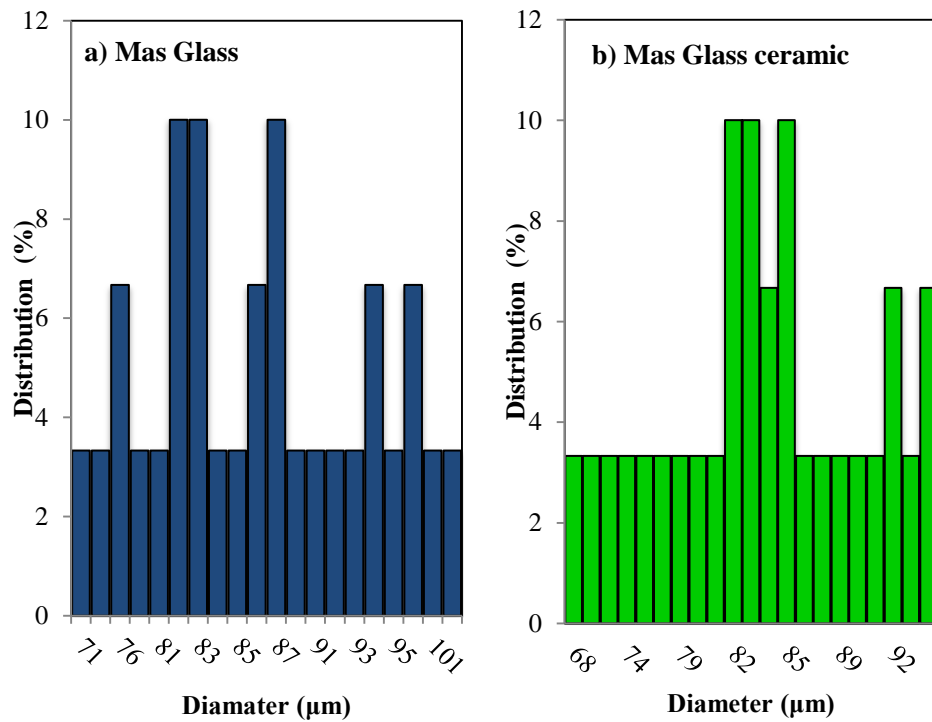


Figure 5.28: Percentage of distribution for the equivalent diameters of MAS fibres with a gauge length of 60mm.

5.5.2 Tensile strength

5.5.3.1 Fibre strength

The tensile strength of both fibre glass systems were evaluated from single fibre tensile tests. It has been reported earlier that microscopic flaws critically affected mechanical properties, especially fibre strength [24, 84]. Figure 5.29 shows the average tensile strength for both systems. The average tensile strength of both types of fibres was seen to decrease with the increasing gauge length, implying that the possible glass surface flaws caused the stress concentration along the gauge length. The results for LAS system and MAS system yielded the same trend in terms of gauge length effects on fibre properties. This trend has been also reported by other researchers [97,99] and is related to the increase in probability of finding a larger defect with the increasing gauge length. The comparison between the data of strength glass fibre and glass ceramic fibre as illustrated in

Figure 5.29 (a) and (b) seems to be in agreement with the [85, 89] that these differences are directly related to the amount of damage sustained by the surface during sample preparation handling especially for glass ceramic fibre. The amount of surface damage in the glass ceramic fibres might be expected to be significantly greater than that in glass fibres due to higher degree of handling during the heat treatment. This may be the source of scatter in the strength data as the defects were created during placement of the fibres onto the plate before and after the heat treatment process. Therefore, it is possible that increasing the gauge length will cause strength reduction in glass ceramic fibres. However, the average strength for LAS and MAS system slightly decreased as the diameter increased in both glass and glass ceramic fibres, however to a lower degree compared with the influence of the gauge length. The results for LAS system show a smooth gradual decrease, due to the consistent fibre diameter produced through automated drawing process. For MAS system, the average strength results were slightly more inconsistent. Different failure modes observed in these fibres, as revealed by diameter grouping, suggested that the effect of diameter was small compared with the effect of gauge length, due to the manual drawing process involved. This seems to be in agreement with the earlier conclusion [93,94] that the tensile strength of glass fibre could be affected by the variation of the diameters particularly for non-uniform fibres.

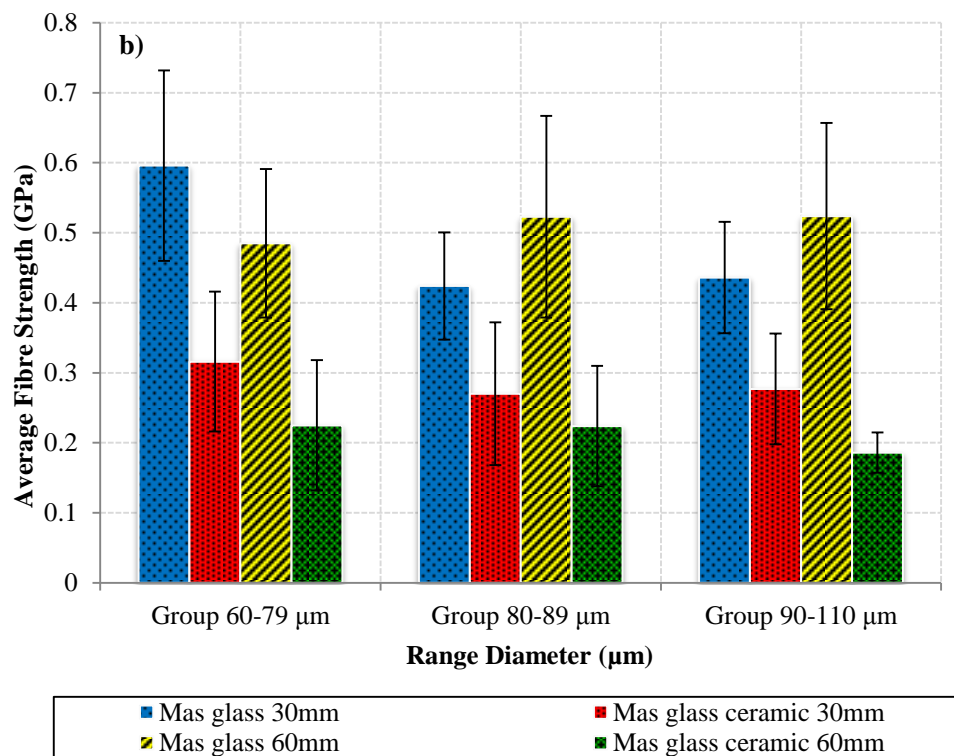
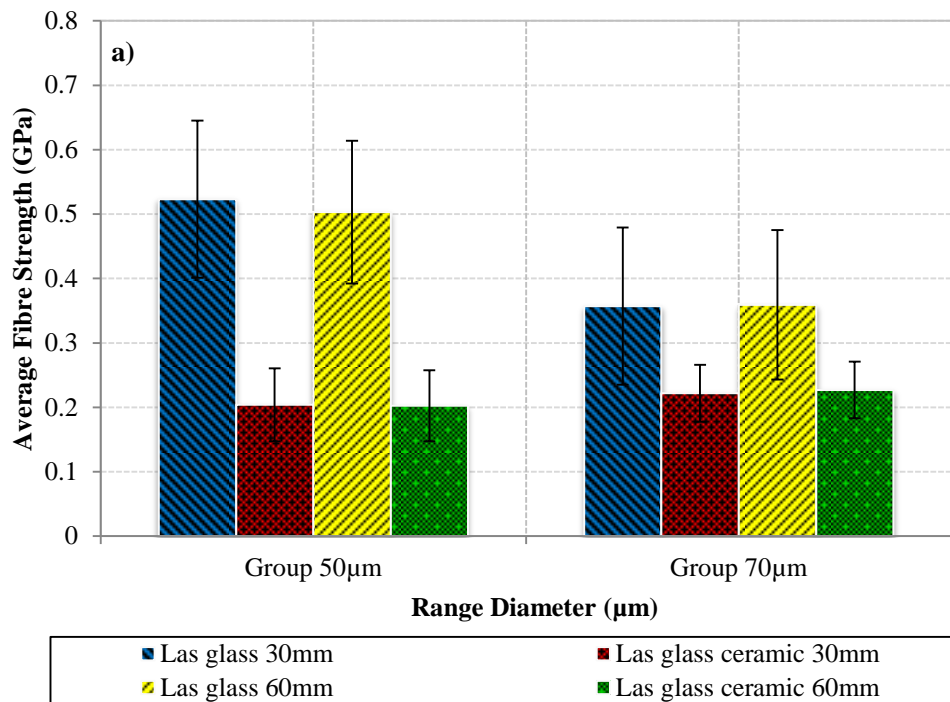


Figure 5.29: Average fibre strengths of a) LAS system and b) MAS system.

5.5.3.2 Weibull distribution

The Weibull distribution parameters from single fibre testing were determined by the weakest link theory method (WLT). A summary of the Weibull parameter values at the gauge lengths tested are listed in Table 5.7 and Table 5.8.

The Weibull moduli for both systems were calculated for each gauge length according to Eq. [2.2]. The plots for LAS and MAS systems at each gauge length are shown in Figure 5.30 and Figure 5.31. The results clearly show that LAS has the higher Weibull moduli and therefore have more consistent strength. This indicates that the failure is at a higher stress. A low value of m indicates a broad distribution in strength which indicates that there is a wide range of flaw sizes in the fibres.

The modulus, m for all observed systems shows a reduction for the higher gauge length, and for a certain group of glasses, σ_0 was larger for the lower gauge length. However, it was expected that the strength would be lower in the glass ceramic fibres due to the crystallisation process. This trend has been discussed by Morimoto et al [100] and Virk et al [101], where they indicated a similar trend. The lower strength is likely to be caused by the introduction of further surface flaws during processing and handling, mainly during conversion to glass ceramic. Weibull modulus reduction indicated a similar phenomenon reported in the earlier studies [102-103], potentially related to flaws in microstructure. A visual inspection of the fit of the glass and glass ceramic fibre shows a better fit to the strength data where the value in all groups, the R^2 coefficient was between 0.83 and 0.98. As can be seen from Table 2, the R^2 ($R^2 = 0.9132$, [166]) coefficients are close to 1, indicating a good degree of linearity except for MAS glass ceramic at 60mm gauge length.

Table 5.7: Weibull characteristic of LAS glass fibre.

Glass system	Gauge Length <i>L</i> (mm)	Weibull Modulus <i>m</i>	Characteristic Strength (σ_0) (GPa)	R^2
Las Glass 50 μ m	30	10.1	0.67	0.96
Las Glass ceramic 50 μ m	30	5.8	0.30	0.96
Las Glass 70 μ m	30	5.7	0.51	0.92
Las Glass ceramic 70 μ m	30	9.1	0.29	0.91
Las Glass 50 μ m	60	4.7	0.57	0.98
Las Glass ceramic 50 μ m	60	4.2	0.23	0.98
Las Glass 70 μ m	60	3.0	0.40	0.97
Las Glass ceramic 70 μ m	60	5.9	0.24	0.96

Table 5.8: Weibull characteristic of MAS glass fibre.

Glass system	Gauge Length, <i>L</i> (mm)	Weibull Modulus <i>m</i>	Characteristic Strength (σ_0) (MPa)	R^2
Mas Glass	30	4.7	0.53	0.92
Mas Glass ceramic	30	3.6	0.32	0.93
Mas Glass	60	4.8	0.56	0.94
Mas Glass ceramic	60	3.4	0.24	0.83

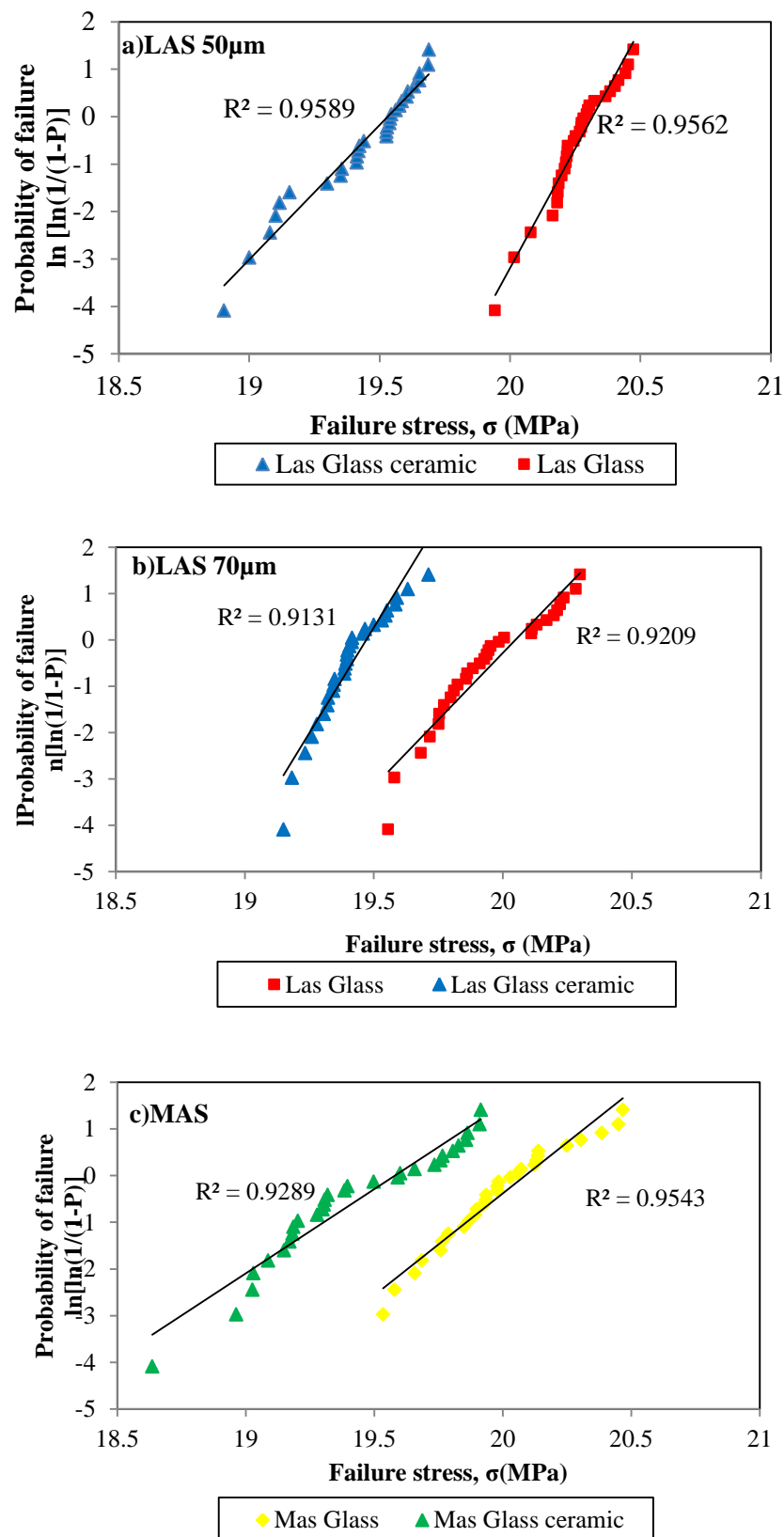


Figure 5.30: Weibull plots for tensile strength of a) LAS 50µm system, b) LAS 70µm system and c) MAS system at gauge length of 30mm.

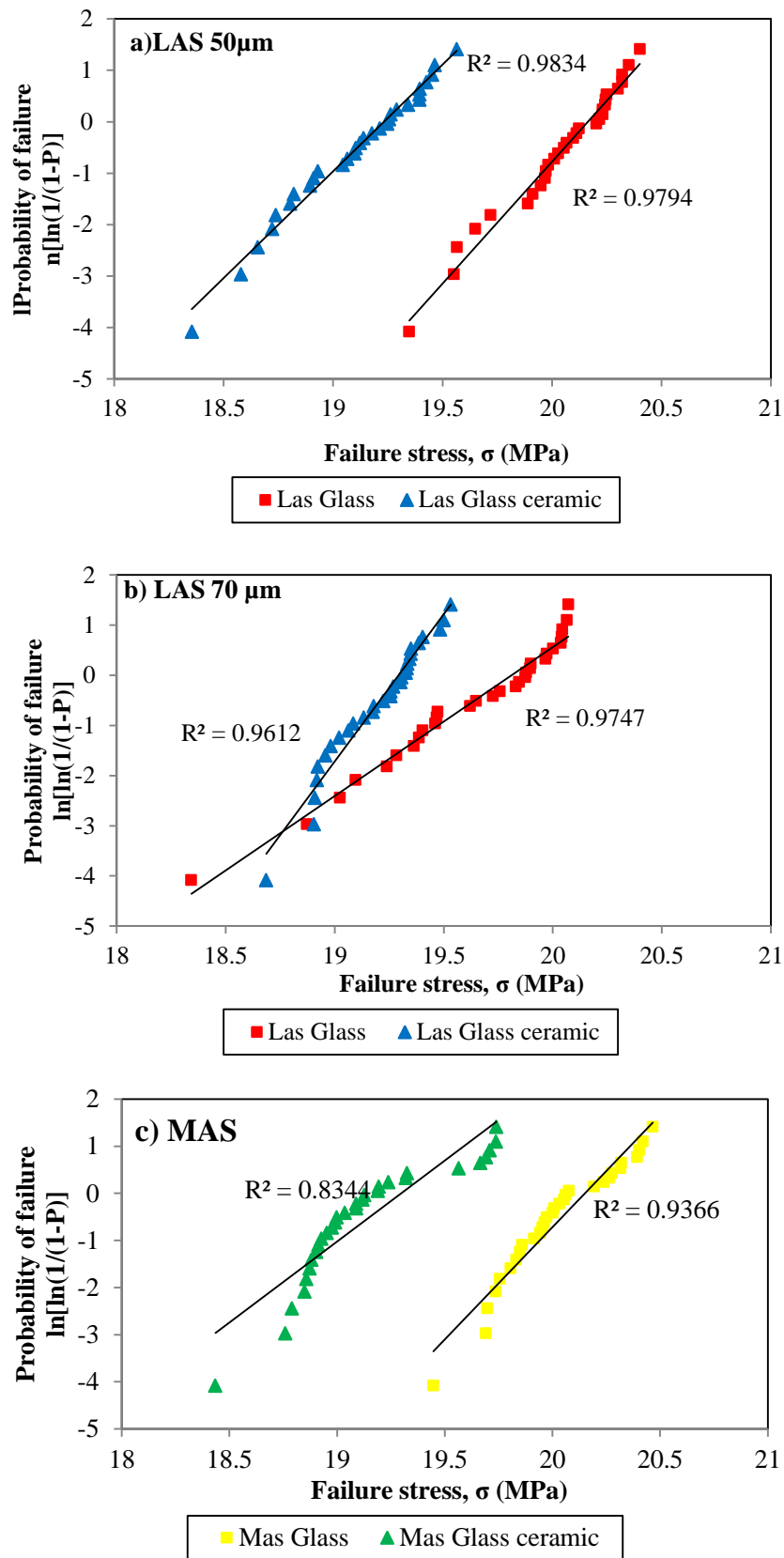


Figure 5.31: Weibull plots for tensile strength of a) LAS 50 μ m system, b) LAS 70 μ m system and c) MAS system at gauge length 60mm.

5.5.3 Acoustic measurements

In this current work, the Young's modulus was further measured by wave generated ultrasound. This method was used in order to measure Young's modulus of fibre by using a glass rod and it was expected that the values would approximate the results obtained from the nanoindentation [54]. From a measurement of the ultrasonic velocity, the effective Young's modulus has been calculated as described in **Section 4.3.4**. The results are shown in Table 5.9. Both systems were heat treated as described in Table 3.5, CHAPTER 3. It was found that the LAS glass ceramic system had a lower modulus than the MAS glass ceramic system, which was in agreement with our earlier results [167] of reduced moduli of 115GPa and 93GPa respectively. These differences between the two glasses may also be directly related to the chemical composition [25]. Wallenberger & Brown reported that the reduced Young's modulus of glass decreased with the decreasing alumina content [168] whereas MAS had a greater alumina and magnesium content in this study compared to LAS system. The results from the acoustic measurement showed to be slightly higher compared to the nanoindentation data shown in brackets. It was observed that these differences appeared due to the method of measurement. The value of Young's modulus from acoustic measurement involved elastic waves which could be influenced by the presence of internal defects.

Table 5.9: Young's moduli of both glass systems measured using acoustic approach.

System	Glass (GPa)	Glass ceramic (GPa)
MAS	117 (102)	120 (115)
LAS	90 (79)	106 (93)

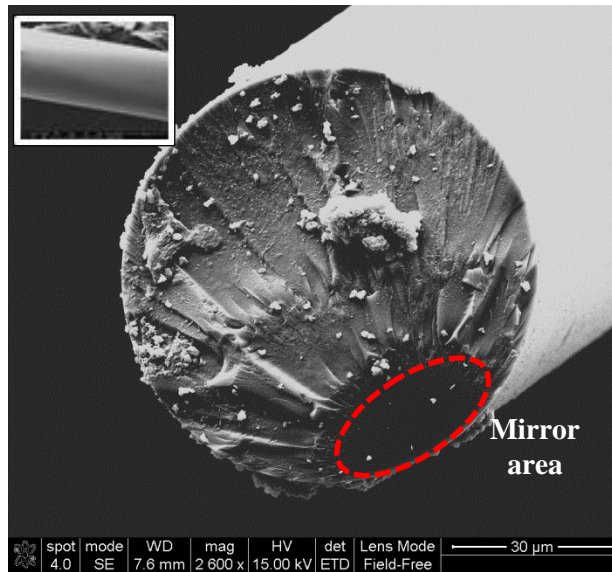
* () Value from indentation

5.5.4 Fractography

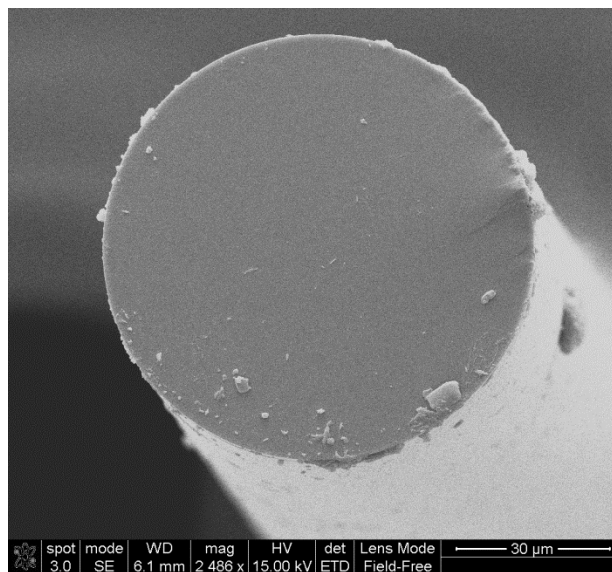
SEM images of tested MAS and LAS fibres are presented in Figure 5.32 (a,b) and Figure 5.33 (c,d), respectively. In this part, morphological differences in fractured samples were not observed along the gauge lengths for all the fibres. Differences were observed between glass and glass ceramic fibres. In the MAS glass ceramic fibre (Figure 5.32b), the heat treatment led to nucleation of crystals in glass, transforming the system into prominent spherical and glassy phases [167], in contrast with the glass fibre which remained amorphous (Figure 5.32a). A similar phenomenon was observed in LAS glass ceramic fibres. It can be seen (Figure 5.33a) that the surface of the glass fibre appeared glassier and smoother than that of the glass ceramic fibre.

The fracture surfaces in Figure 5.32a and Figure 5.33a display certain features that indicate that the glass fibres failed at different stresses in the dotted marked area, prior to the failure propagation across the full cross-section in both MAS and LAS glass fibres. SEM examination of the fracture surfaces revealed the presence of fracture-inducing flaws located at the surface of the fibre.

Both MAS and LAS glass fibres show classic mirror/mist/hackle fracture patterns [169] that are centred on surface defects. The equivalent glass ceramics do not exhibit any particularly obvious fracture origins and the fracture surface is textured, probably indicating intergranular fracture between fine crystals in the microstructure. Additionally, MAS glass ceramic is more finely grained than the LAS glass ceramic.

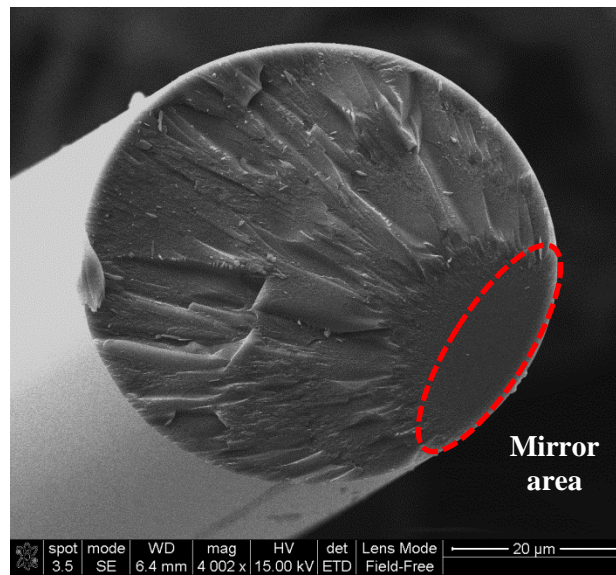


a)

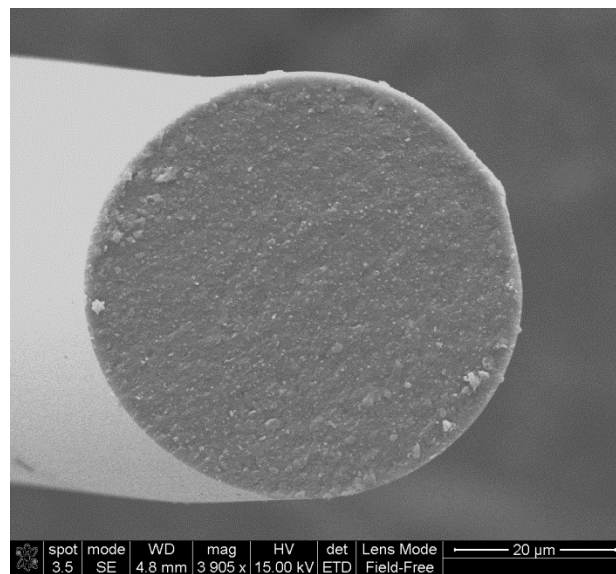


b)

Figure 5.32: Fracture morphology of MAS a) glass fibre and b) glass ceramic fibre.



a)



b)

Figure 5.33: Fracture morphology of LAS showing a) brittle fracture morphology of the glass fibre at room temperature and b) glass ceramic fibre.

5.6 Glass ceramic reinforced polymer composite

The dynamic mechanical performance of the unidirectional glass ceramic fibre composites was studied in this section. The dynamic mechanical thermal analysis was used to assess the viscoelastic performance of the glass ceramic fibres reinforced in epoxy resin systems. This technique was chosen as an alternative tool for measuring the elastic properties of glass ceramic fibre composites of a limited size. The quality of composite was observed using an image analysis technique and the volume fraction of fibres was determined using thermogravimetric analysis (TGA). Scanning electron microscope (SEM) was used to study the morphology of the composites and the quality of the adhesion at the interface.

5.6.1 Dynamic mechanical thermal analysis

Dynamic mechanical thermal analysis (DMTA) provides a method for determining the storage modulus (E') and the loss tangent ($\tan \delta$) as a function of temperature. Tests were conducted with a fixed frequency at a constant amplitude (strain) mode. Analyses of the storage modulus and $\tan \delta$ have been used in ascertaining the performance of the sample under stress and temperature.

The experiments were performed in a three-point bending mode from 0 to 180°C at a heating rate of 2°C/min and at a fixed frequency of 10 Hz, using 8 x 30 x 1 mm³ specimens. Plots of the dynamic storage modulus (E') against temperature were recorded for the range of composites with MAS glass fibre, MAS glass ceramic fibre, LAS glass fibre and LAS glass ceramic as shown in Figure 5.34. A gradual decline in E' with the increasing temperature from 0°C to 180°C was observed. It is noted that the incorporation of LAS glass fibre into the matrix material results in a remarkable increase in the storage modulus over the entire investigated temperature range, especially at temperatures below T_g (~150°C) which can be relate with the bonding between fibre and matrix. The incorporation of glass fibre into matrix material remarkably enhanced its stiffness.

A low and broad peak appeared closely before T_g (denoted in dotted line), which indicated a possibility of the post-curing process.

Incorporation of LAS glass ceramic fibres decreased the storage modulus compared to LAS glass fibre system. However, E' of MAS glass ceramic composite showed no significant change when the composite was in its glassy zone (below 150°C). In the glass transition zone (above 150°C) MAS glass ceramic composite demonstrated a surprisingly sharp decrease in storage modulus.

Figure 5.35 shows that $\tan \delta$ curves follow a similar pattern. $\tan \delta$ is a damping coefficient that can be related to the impact resistance of a material [128]. Since the damping peak occurs in the region of the glass transition where the material changes from a rigid to a more mobile state, it is associated with the movement of small groups and chains of molecules within the polymer structure, all of which are initially frozen in. The higher the peak $\tan \delta$ value, the greater the degree of molecular mobility. As expected, the peak $\tan \delta$ values were higher for pure matrix material (1.31) than that for other composite. The $\tan \delta$ peak of MAS glass ceramic composite (0.32) was lower and shifted by approximately 10°C from that of matrix material (I). Denser composites possessed peaks at lower temperatures, indicating that although the fibres were not misaligned, they were not perfectly bonded to the matrix. In addition to the low modulus value, (red arrow as shown in Figure 5.34) these composites were therefore observed to be less crosslinked with weaker interfaces, which agreed with the study by Kuzak and Shanmugam [129]. It can be seen that MAS glass composites (0.37) and LAS glass composites (0.40) provided a separation area between the matrix and fibre as shown **Section 5.6.4**. LAS glass composites showed the highest T_g followed by LAS glass ceramic composites, MAS glass composite, matrix material and MAS glass ceramic composites. Not much variation in T_g was expected between the composites since the matrix and the preparation was the same for each sample (Section 3.5.2.1). The arrangement of fibres in the composites may have also contributed to the shift in $\tan \delta$ to lower temperatures on account of change of the localised fibre volume fraction. In addition, some variation in storage modulus

between the composites may be attributed to the different mechanical properties of reinforcing fibres.

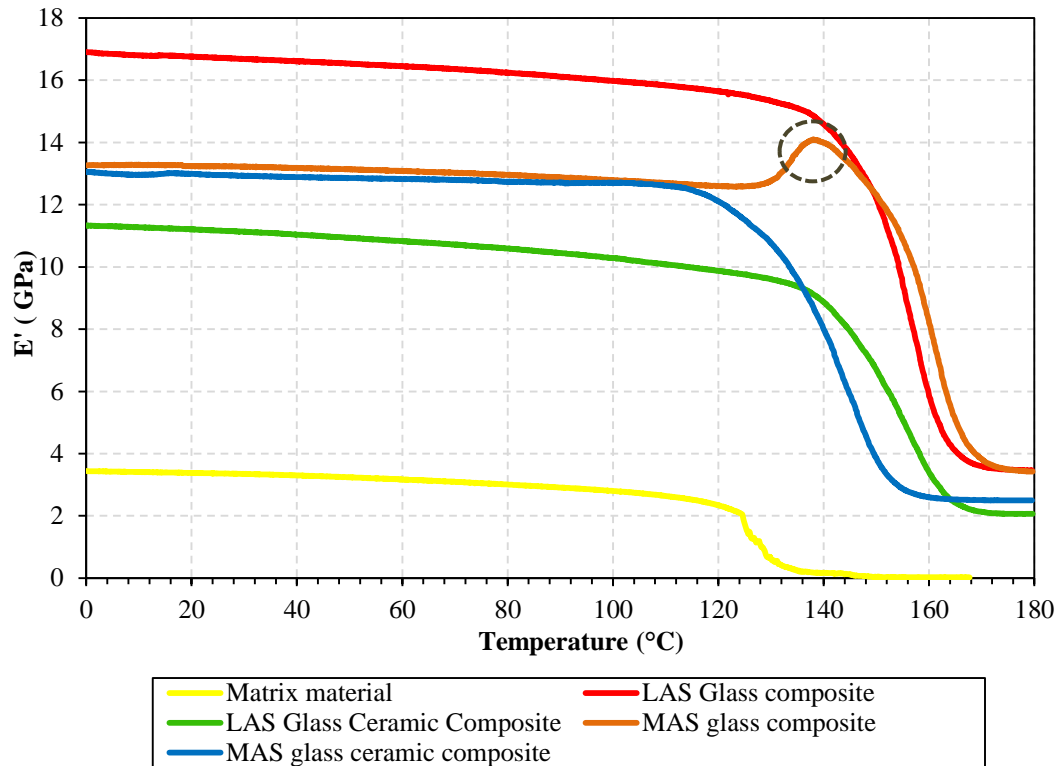


Figure 5.34: Storage modulus (E') for matrix material, LAS glass fibre, LAS glass ceramic composite, MAS glass fibre composite and MAS glass ceramic fibre composite between a temperature range of 0 to 180°C.

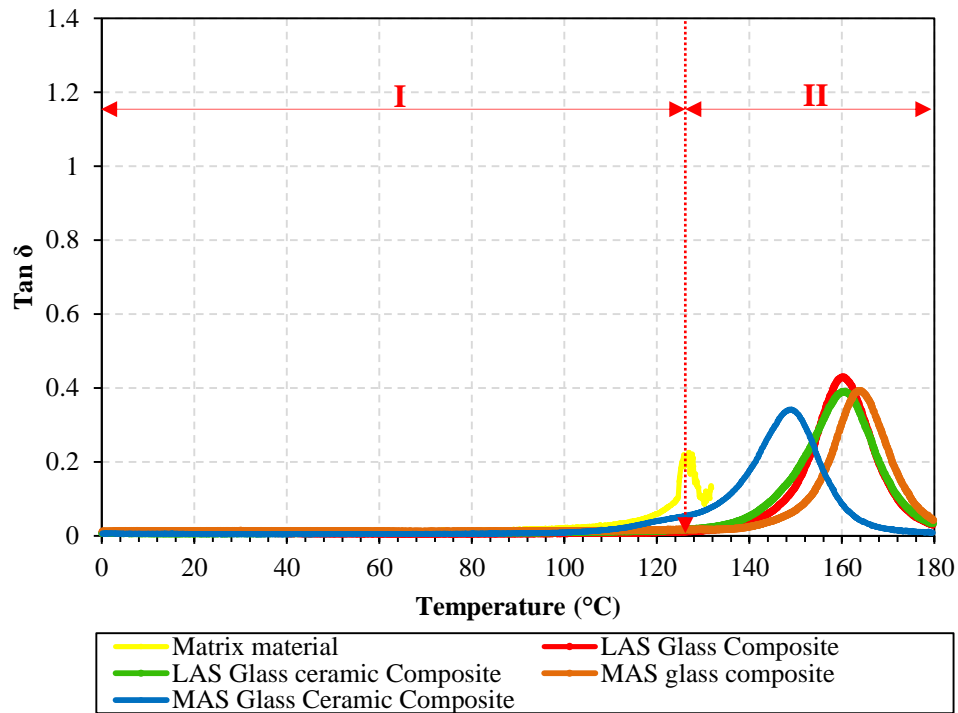


Figure 5.35: Temperature dependency of $\tan \delta$ at 10Hz for all range composites.

5.6.2 Density and microvoid content

Table 5.10 summarises the densities of neat matrix material, LAS glass composite, LAS glass ceramic composite, MAS glass composite and MAS glass ceramic composite using Archimedes' method. A density of 1.23 g/cm^3 was measured for the neat matrix. As expected, the inclusion of comparatively denser fibres increased the density of composites relative to the epoxy resin. However, the density of the composites was slightly lower compared with the theoretical density. This is due to the fact that some of the LAS and MAS fibres may have lost mass during trimming as some of the fibres are not perfectly embedded within the matrix. This happened in cases where the embedded fibres for both glasses system were not firmly compacted during the curing cycle, which lacked in pressure. Reinforcement by fibres at a volume fraction of 30% increased the density of matrix where LAS glass glass ceramic was the highest. This is because

the density of the LAS glass ceramic fibre, $\rho_{LASGC} = 2.9 \text{ g/cm}^3$, is greater than that MAS glass ceramic fibre.

Table 5.10: Average density of neat matrix and composites.

Composite system	Density, ρ_c (calculated using rule of mixtures; $\rho_c = \rho_m V_m + \rho_f V_f$) (g/cm ³)	Density, ρ_c (measured by density balance) (g/cm ³)
LAS glass	1.60	1.59 ± 0.03
LAS glass ceramic	1.73	1.70 ± 0.03
MAS glass	1.68	1.65 ± 0.03
MAS glass ceramic	1.71	1.69 ± 0.01
Matrix	1.23	1.23 ± 0.01

Structural morphology was examined in order to relate the properties of the composites with the effect of glass fibre inclusion. Specimens with a dimension of 5mm x 3mm x 1mm were cut directly from the composite coupon and examined in an optical microscope at high magnification and some light scratches revealed. This was undertaken in order to confirm that the composites were well consolidated and to check for any microvoids that may have formed in the matrix as a result of the lay-up process. Moreover, the presence of microvoids may be attributed to imperfections in the composite which may be difficult to eliminate due to the brittleness of the fibres. In addition, microvoids have the potential to generate microcracks due to the local stress concentration.

Optical microscopy images of the internal structure of the composite are presented in Figure 5.36- 5.37. At low magnification (20X) the images (as shown in Figure 5.36- 5.37((a) and (c)) illustrate the uniform circular cross-section of the fibres. This confirmed the previously held assumption of circular cross-sections used to calculate the surface area of the fibres. The diameter of the glass fibre for composite systems were selected randomly within the range of respective fibre groups. The degree of consolidation of the fibres was determined using images as shown in Figure 5.36-5.37 ((b) and (d)) at higher magnification (100X). These images show the distribution of glass fibres within a section cut normal to the fibre direction and appear to be essentially void free and well consolidated for all

specimens. However, voids can be seen away from the fibre direction. It is notable that the density of voids was closely related to the heat treatment of the fibre where the fibres appeared to be brittle. This suggested that grinding and polishing caused cracking of the edges of fibres, which led to the formation of some large voids around the fibre edge.

In this study, none of the fibres were treated with sizing. Study of the effect of size on the remaining fibres is outside the scope of this study. The LAS and MAS composites possessed resin-rich regions interspersed with regions of high and low fibre packing fraction. These composites were essentially non-uniformly distributed where fibres were loosely arranged and fibre diameters were much inconsistent. Hence, the void concentration can be claimed to be low with some confidence.

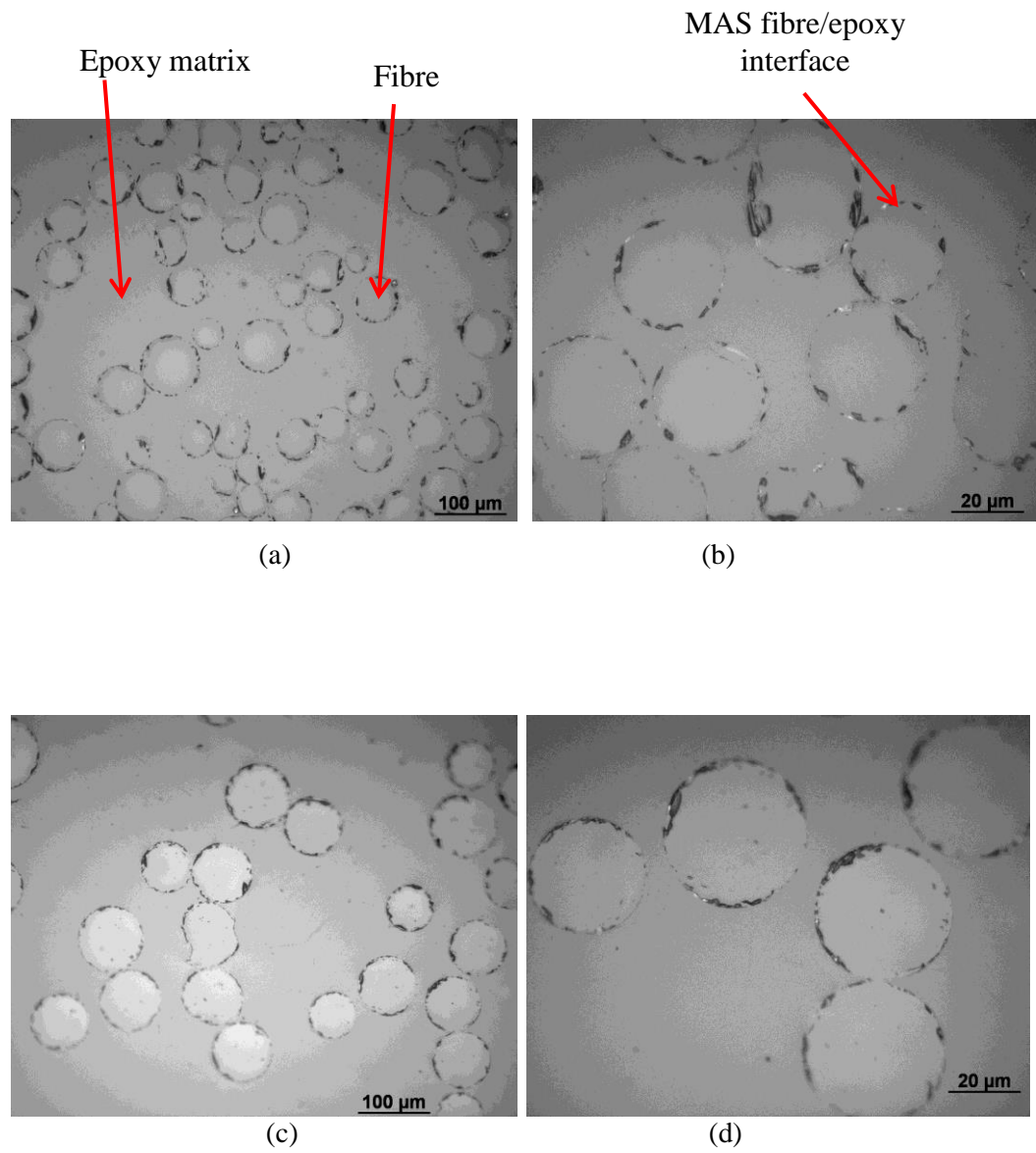


Figure 5.36: Morphology of MAS a-b) glass and c-d) glass ceramic composite system observed with optical microscopy.

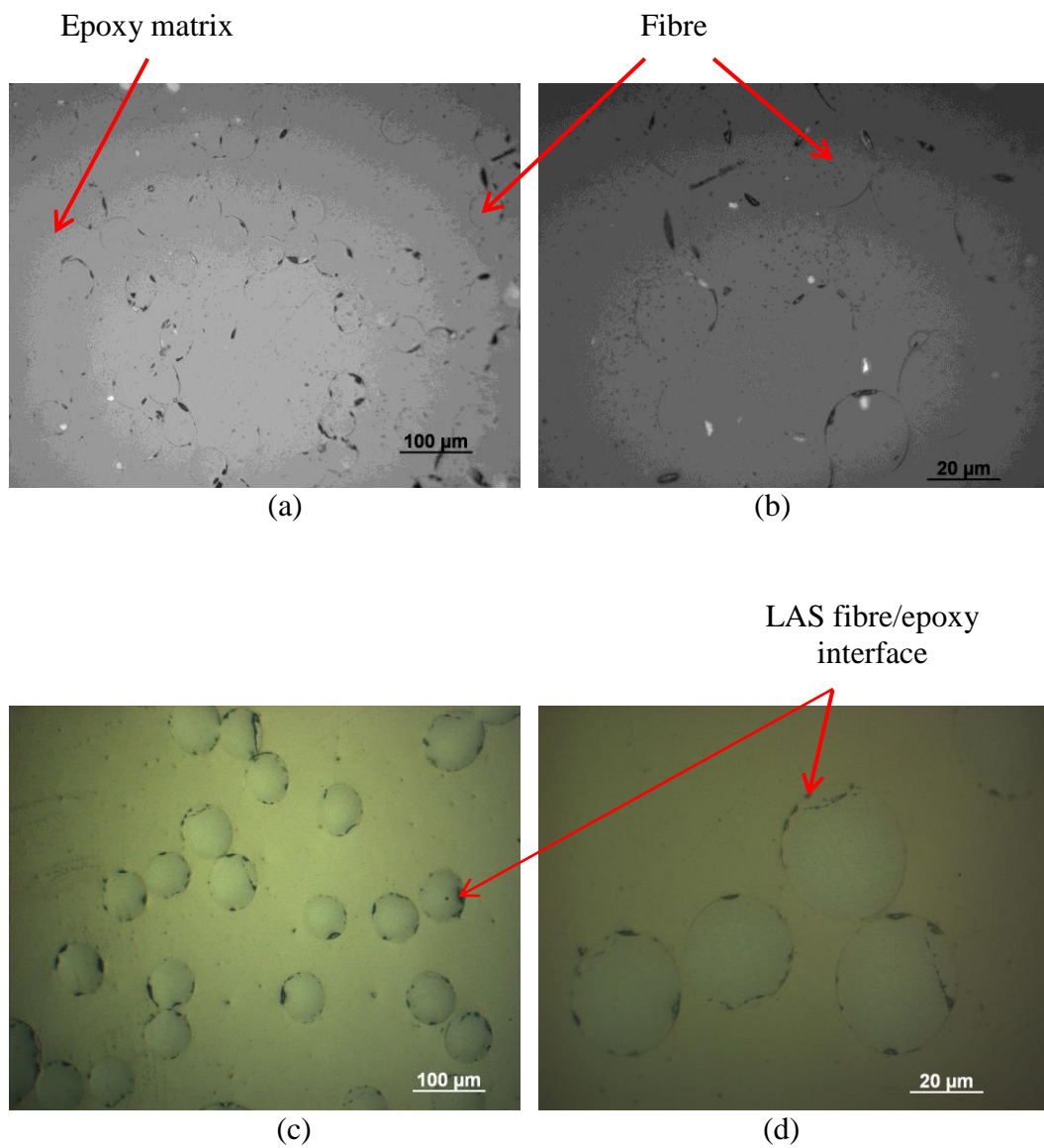


Figure 5.37: Morphology of LAS a-b) glass and c-d) glass ceramic composite system observed with optical microscopy.

5.6.3 Fibre volume fraction measurements.

The quality assurance of novel composite materials consists primarily of examination of the required fibre content. Fibre content is an important criterion in control of the mechanical properties. In this section, the amount of glass fibre content in the unidirectional (UD) composite was determined using the thermogravimetry analysis TGA method as described in **Section 4.3.7**. The thermal stability of pure epoxy and composite systems were also studied using TGA. This method was used due to the range of the quantity mass suitable for this limited weight of samples [133]. In this study, unidirectional fibres were used because of the simplest arrangement of fibres. Figure 5.38 illustrates the thermal degradation behaviour of pure matrix material and composites which were burned in nitrogen, N₂ gas from 30°C to 550°C at 10°C/min then held at 550°C for 1 hour followed by heating in air to 1000°C at 10°C/min. The trend observed in Figure 5.38 indicate that the matrix starts to degrade at 250°C and its combustion is completed at 637°C. The TGA profile represents a series of thermal effects (denoted as A, B, C and D). In this figure, the decomposition mechanism starts (A) with the initial weight loss of in average 0.5-1.0 wt% for all the system. This effect occurred due to vaporisation of moisture in the composite [132-133]. The degradation shows that all composite samples start to burn at slightly higher temperature than that of the pure system, indicating that composite systems exhibited better thermal stability. Between 380°C to 550°C the samples lost weight gradually and the second stage (B) is related to the decomposition of the epoxy resin in the nitrogen atmosphere. After holding at 550°C for 1 hour, the purge gas flowing over the sample was automatically switched to air. Based on Jumahat's work [170] on carbon fibre composites, this temperature was employed as an isothermal temperature due to the higher amount of matrix residue burned in N₂ and the SEM micrograph of the sample residue, collected at 550°C, showed that the marix remained deposited on the carbon fibres. Therefore the actual amount of matrix residue can be estimated at 550°C. Stage C showed at char decomposition occurred prior to the last inflection indicating that the matrix residue started to burn approximately at 570°C and finished at 637°C. The sample was heated to 1000°C in air to remove the matrix residue. Figure 5.40 illustrates

the maximum degradation temperature of the matrix and its residues occur at 410°C (marked as X) and 611°C (marked as Y), respectively. In this figure, the maximum degradation temperature of the glass fibre was not identified by the peak of the rate of weight loss versus sample temperature curve, as glass fibre degraded above 1000°C. However, low degradation temperature of LAS glass fibre composite were observed compared to other composites. Finally, stage D showed that the material remaining after 637°C corresponded to the weight fraction of glass fibres in the composite (marked as W).

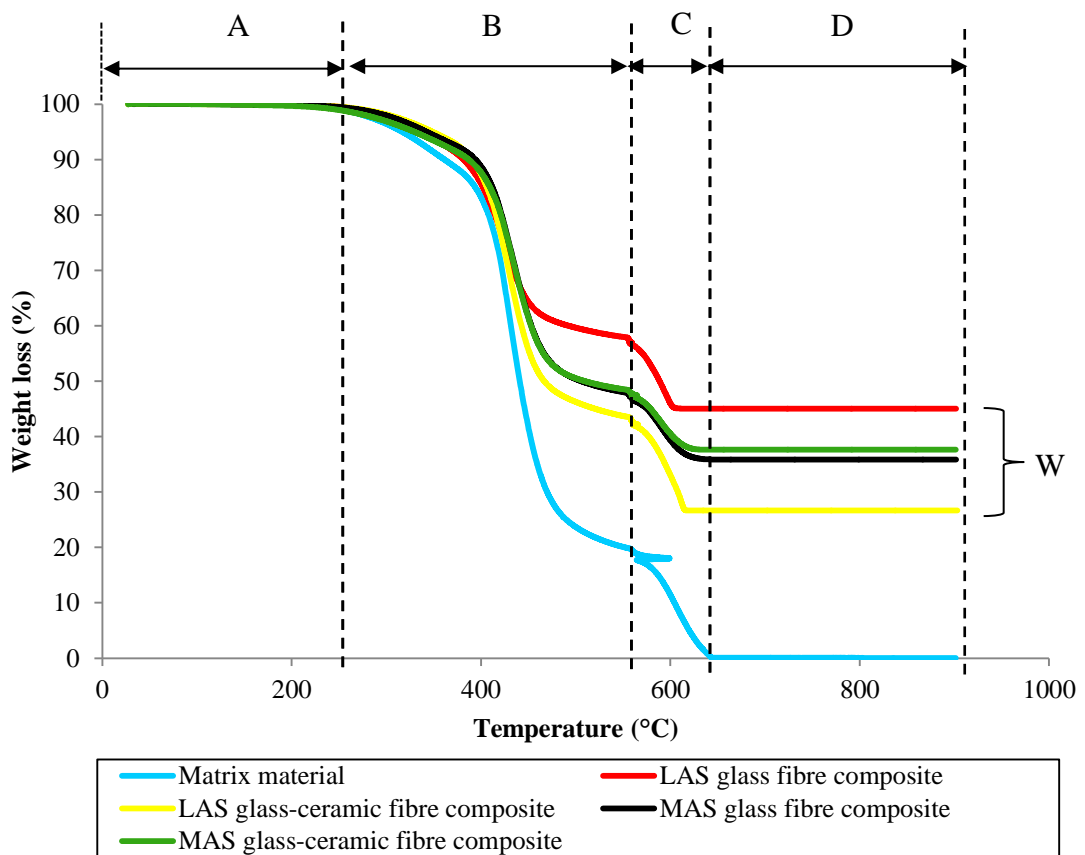


Figure 5.38: Typical TGA results illustrating percentage of weight loss versus temperature of matrix material and the composite specimens.

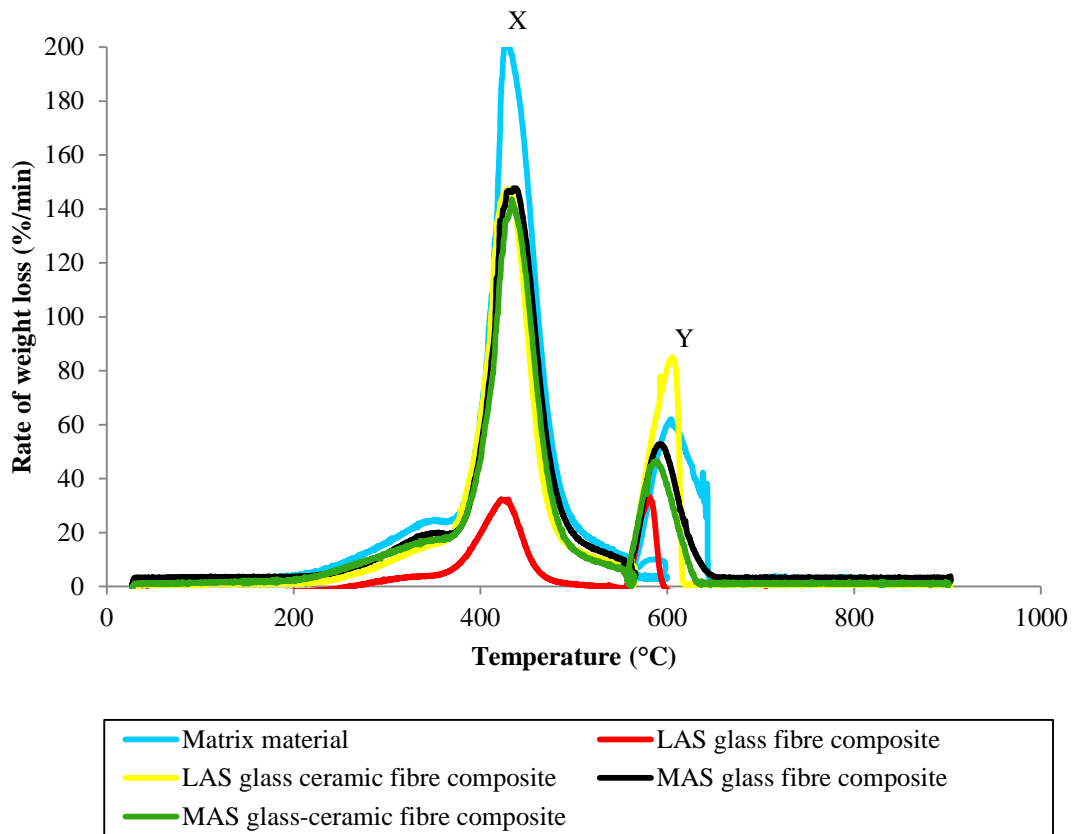


Figure 5.39: Typical TGA results illustrating rate of weight loss versus versus of matrix material and the composite specimens.

The fibre volume fractions in each of the composite systems were tested at three different areas. All the results were calculated in accordance to ASTM standard D3171-99 and shown in Table 5.11. Table 5.11 shows that the average weight fraction of the MAS glass fibre was 34.7 wt%. The average density of MAS glass fibre composite, which was determined using a density balance, was 1.65 g/cm³. The fibre volume fractions in the MAS glass composite were 21 vol. %. In practice, fibres were not perfectly aligned as the process involved was manual. Maximum volume fraction mostly depends both on the fibre form and method of manufacture. For other forms of reinforcement, maximum volume fraction also depends on the detailed arrangement of the fibres. Madsen et al [171] suggested that the void fibre composites expected appeared from fibre which intended causes void. This consists of fibre/matrix interface void and impregnation void where the reinforcement architecture denies the matrix resin access to inter-fibre

spaces as shown in Figure 5.36-5.37. Table 5.11 summarised the measured average weight fraction of fibre in each of the composite systems. The measured volume fractions of fibre glass in the composite systems were calculated using the equation given in **Section 4.4.2**.

Table 5.11: Volume fibre fraction and volume void fraction in MAS glass fibre composite (MASG), MAS glass ceramic fibre composite (MASGC), LAS glass fibre composite (LASG) and LAS glass ceramic fibre composite.

Properties	Matrix		MASG composite		MASGC composite		LASG composite		LASGC composite	
	Value	Std	Value	Std	Value	Std	Value	Std	Value	Std
Density composite, ρ_c (g/cm ³)	1.23	0.01	1.65	0.03	1.69	0.01	1.59	0.03	1.70	0.03
Density fibre, ρ_f (g/cm ³)	-	-	2.728	0.01	2.843	0.01	2.473	0.01	2.916	0.01
Weight fraction, W_f (wt%)	-	-	34.7	0.01	37.7	0.01	43.3	0.02	27.7	0.01
Volume fraction of fibre, V_f (vol%)	-	-	21	0.61	22.4	0.31	27.8	1.03	16.1	0.56

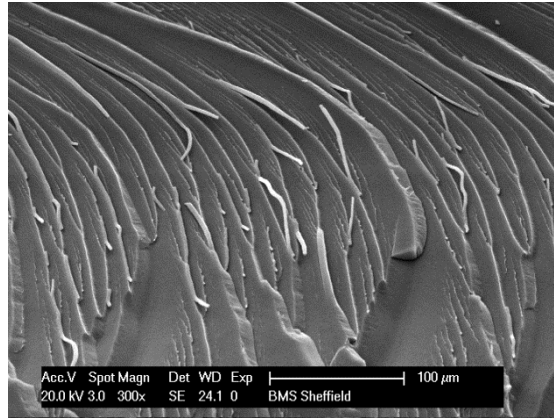
5.6.4 Failure analysis

Figures 5.40-5.42 illustrate the fractured surfaces of matrix, MASG composite, MASGC composite, LASG composite and LASGC composite, respectively. The samples were cryogenically frozen in liquid nitrogen for 1 minute before being subjected to mechanical fracture by impact. The SEM images show that two-phase morphology is clearly visible in all composite systems. The fibres were observed to fail randomly within the matrix. The fibre alignment plays a crucial

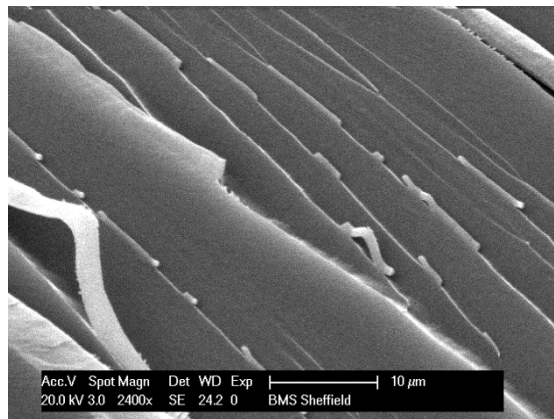
role in improving the mechanical properties especially the mechanical strength and moduli. Figures 5.41-5.42 show that the fibres were not uniformly arranged.

Figure 5.41 and 5.42 indicated MAS and LAS glass fibres showed different types of failure mechanisms. The failure indicated that the fibre breakage was responsible for the failure without the evidence of pull-out. The images from Figure 5.41(a) and 5.42(a) show that the fibre/matrix interface appeared weaker since there was no sizing employed. Surprisingly, MAS and LAS glass ceramic fibre composites showed good adhesion between the fibre and the matrix without the application of sizing. Closer inspection showed that the interfacial region was well wetted as shown in Figure 5.41 (b) and 5.42 (b).

The overall analysis indicated that the glass ceramic fibres are acceptable reinforcement in advanced composite materials and the next step would involve their application in high temperature resins and metallic matrices. Compared to their commercial counterparts, E-glass, GC fibres impart higher mechanical properties and a simple extrapolation would illustrate their beneficial influence on Al, Li, and other aerospace materials which currently possess excellent impact resistance and ductility, and could benefit from the additional reinforcement.



(a)



(b)

Figure 5.40: Fracture surface of the matrix material.

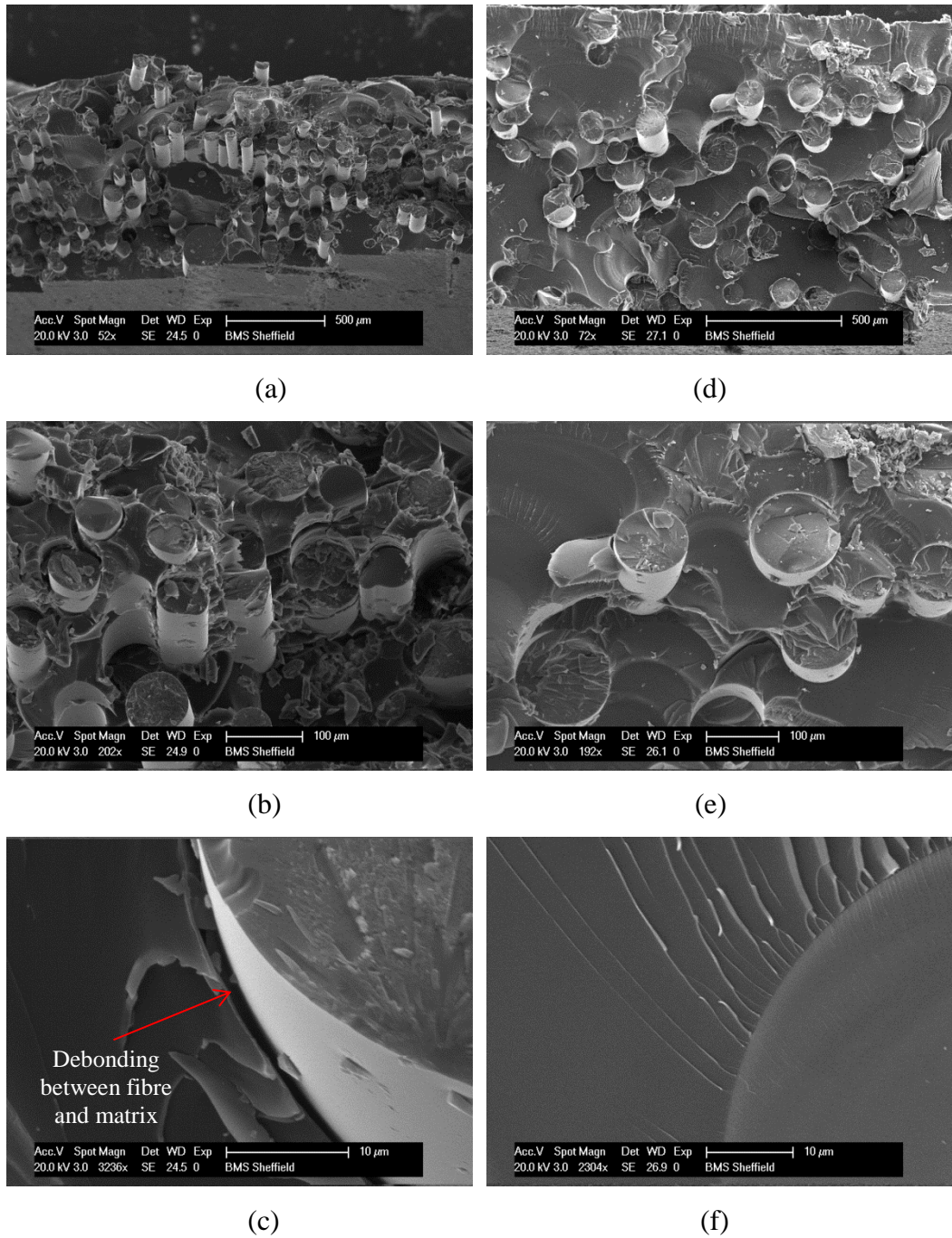
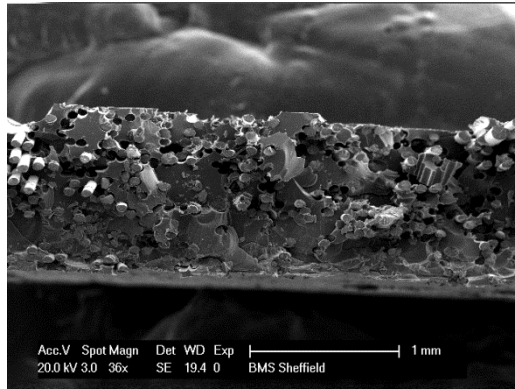
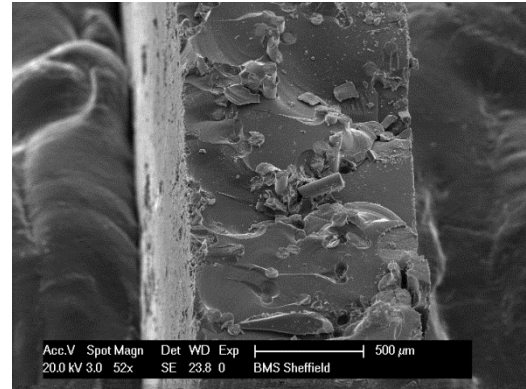


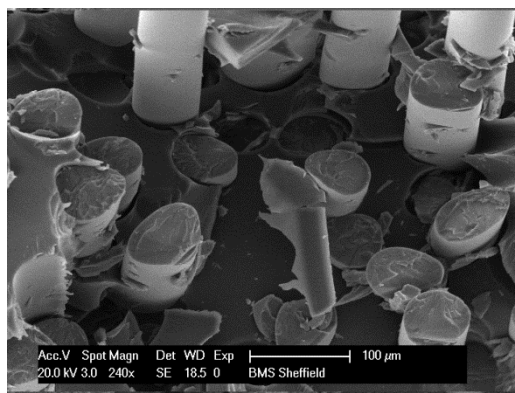
Figure 5.41: Fracture surface of a-c) MAS glass fibre and d-f) MAS glass ceramic fibre composite after bending.



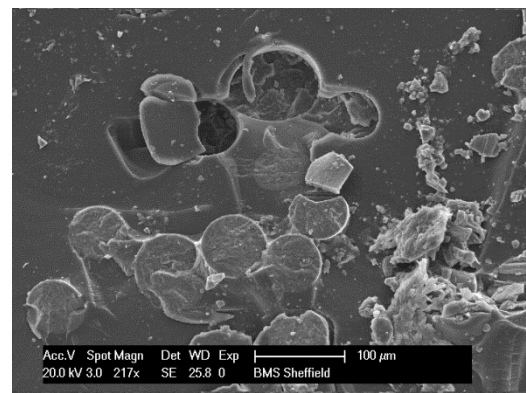
(a)



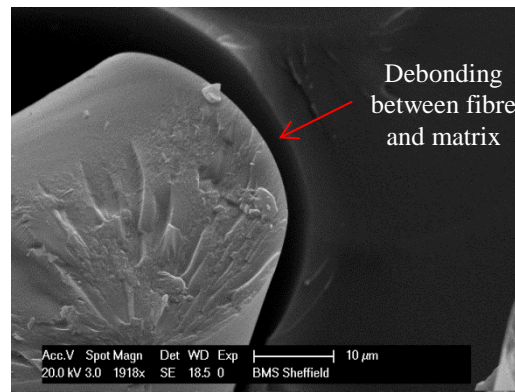
(d)



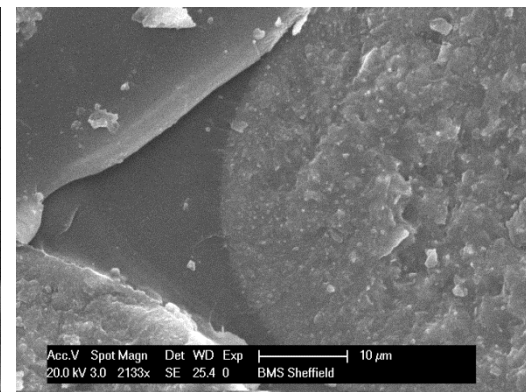
(b)



(e)



(c)



(f)

Figure 5.42: Fracture surface of a-c) LAS glass fibre composite and d-f) LAS glass ceramic composite after bending.

5.7 Concluding remarks

This chapter presented and discussed the results from the experimental investigation of the novel composite systems obtained from the glass ceramic fibres developed and manufactured in this study. The first section described the heat treatment optimisation and the subsequent thermomechanical properties of the bulk systems. The results showed that the highest modulus was obtained for MAS system, in the range of 137 GPa, and LAS system resulted in 99 GPa after the recommended heat treatment schedule. It is important to mention that the high modulus of elasticity was not the sole aim of this investigation, and it needed to be accompanied with the optimised manufacturing process that would enable preservation of the consistent structure in the extreme temperature environment. An optimum schedule of heat treatment temperature and time was developed based on their overall physical observation and used as a benchmark for fabrication of glass ceramic fibre.

The second part of this study covered the manufacturing of MAS and LAS glass-ceramic fibres, including the characterisation through the standard single fibre tests of hundreds of manually produced fibres in this study, both before and after crystallisation, using the ASTM standard. The results showed that LAS had higher Weibull modulus while MAS had lower values within the same gauge length. A low value of m indicated a broad distribution of measured strength which is attributed to a large number of flaws and various inconsistencies in the fibres. The modulus m for all observed systems showed a reduction with longer gauge lengths and for a certain group of glasses, σ_0 was larger for smaller gauge lengths. LAS glass fibres had flaws evenly distributed throughout the fibres. Both MAS and LAS glass fibres showed classic mirror/mist/hackle fracture patterns that were centred around surface defects where SEM was used to study the fracture mechanisms produced during the mechanical tests.

Finally, in the third part, the glass ceramic fibre reinforced polymer composites were fabricated using a wet lay-up technique. The results obtained from the physical, dynamic mechanical thermal analysis, optical microscopy and SEM

observation summarised that in the lay-up process presence of voids is inevitable. However, an introduction of unsized glass ceramic fibres in the matrix revealed a good adhesion between the fibre and matrix. The SEM micrograph showed a good bonding was achieved during the fabrication between the glass ceramic fibres and the matrix. Considering that glass fibres have an excellent thermal properties as showed from the DTA, these fibres have potential to be use as reinforcement at high thermal application. However further analysis at high temperature environment need to be carried to make the finding more conclusive. These results are very promising in the direction of developing a GCFRP system using appropriate fabrication method.

Chapter 6

Conclusions

The properties of glass ceramics and their fibres are principally influenced by their heat treatment [24]. Therefore, the potential usage of glass ceramic fibres, namely MgO-Al₂O₃-SiO₂ (MAS) and LiO₂-Al₂O₃-SiO₂ (LAS) systems, has been investigated. In order to achieve the main objectives of this study, processing and testing were carried out involving the characterisation of the heat treatment on bulk glass ceramics, fabrication of the glass and glass ceramic fibres, single fibre testing and the manufacture of glass ceramic fibre reinforced polymer composites.

There is a correlation between the properties and crystallisation behaviour of MAS and LAS glass ceramic systems. In these systems, increased temperature enhanced the rigidity of glass structures, thereby enabling higher density, nanohardness and reduced Young's modulus. These properties were successfully obtained in both systems, which were prepared with different heat-treatment regimes. The thermo-mechanical properties correlated with the crystalline phases of the selected system. Observations showed that there was a significant variation in the morphology of the crystalline phases with the changes in the heat treatment temperatures and dwelling times in MAS and LAS systems. An optimum heat treatment scheduled has been successfully developed based on the results from the reduced modulus. The highest values recorded were 137GPa for the MAS system and 93GPa for the LAS system, as measured by the nanoindentation method.

In this work, MAS fibres were prepared using melt drawing and LAS fibres were prepared by continuous drawing. These techniques have been successfully employed to fabricate MAS and LAS glass fibres. The drawing temperature for

the MAS system was higher than 1200°C and LAS glass fibres were drawn at a temperature below the crystallisation temperature of 750°C. MAS glass fibres were produced in a limited quantity and their diameters varied between 60-100µm due to manual processing at high temperatures. In contrast, the diameters of LAS glass fibres were automatically controlled in the range of 50-70 µm. The glass drawing method presented in this study is well suited to the fabrication of glass ceramic fibres.

Based on the heat treatment of bulk systems, glass fibres were subjected to a series of thermal treatments in order to optimise temperatures and dwelling times. The challenges of controlling the temperature and dwell time for the heat treatment of glass ceramic fibres were overcome in samples where physical observation indicated an absence of distortion.

Correlations between the properties of glass ceramic fibres and heat treatment conditions were clearly demonstrated by changes in density and average strength. The Young's moduli of the glass and glass ceramic fibres were obtained by measuring bulk material using the acoustic approach. Glass ceramic fibres were tested using the single fibre test method in order to obtain and evaluate their mechanical properties before and after the crystallisation. Data for the tensile strength was analysed statistically using the Weibull method. The results showed that the distributions of fibre strength and variation in the Weibull parameters correlated with the gauge lengths. Moreover, handling and test procedures were major concerns for the fabrication of fibres and the measurement of tensile strength. It has been reported [14] that all of the thermomechanical properties of fibres are dependent on fabrication conditions.

MAS and LAS glass ceramic fibres were successfully used in the manufacture of unidirectional glass ceramic fibre reinforced polymer composites by wet lay up techniques. Due to the limited and fragile nature of the fibres, single ply composites were cautiously prepared by hand lay-up. Both glass ceramic fibre composites were tested using dynamic mechanical thermal analysis. The results showed an unmistakable difference in the storage modulus, E' and $\tan \delta$ between

composites reinforced with MAS and LAS fibres. This indicated that the presence of fibres of an appreciable fibre alignment significantly influenced the results for dynamic thermo-mechanical properties.

Investigation of failure mode by using fractography indicated a correlation between the properties of composites with the crystallinity of their fibres. SEM photomicrographs displayed visibly good interfaces for all uncoated glass ceramic fibre systems in which glass ceramic fibres were well bonded with the epoxy. However, the SEM photomicrographs of LAS and MAS uncoated glass fibre composites revealed a weaker interface due to variable interfacial adhesion. Fibres consequently debonded from the epoxy and generated voids. It is therefore conclusive that the glass ceramic fibres have a future for composite applications.

Chapter 7

Recommendations for future work

The results obtained in this study were investigated in order to provide fundamental data on glass ceramic fibre reinforced polymer composites. It was shown that uncoated glass ceramic fibres bonded well to the matrix. These findings encourage further investigation in order to study GCFRP in a more detail. The following are recommendations for future work:

- Establishing standardised parameters for the heat treatment of glass ceramic fibres that could serve as the basis for processing and handling protocols during fabrication. This would be useful due to the strong dependence of mechanical properties on these parameters, especially the Young's modulus. A selective range of temperatures, dwell times and heating rates could be improved upon for better feasibility in forming glass ceramic fibres.
- The present study only used two different gauge lengths. Further investigation of the tensile strength at different gauge lengths and diameters would help elucidate the maximum tensile strength and Young's modulus for glass ceramic fibres.
- Improved manufacturing techniques must be further explored in order to produce high quality GCFRP owing to the current lack of information about the manufacturing methods of brittle fibre composites. The improved method of fabrication of the glass ceramic fibre composites

would involve facility to optimise cost-effective yet advanced manufacturing process.

- Preliminary work has been conducted in this study to investigate the performance of commercial matrix material reinforced with glass ceramic fibres using dynamic mechanical thermal analysis. A comparative study on the strength of the composite should be extended in order to investigate the effect of reinforcement and the relationship between strength and the morphology of the interphase.
- Further work should also consider reinforcement of lightweight metallic alloys to explore the possibility to exploit the high-temperature capability of glass ceramic fibres, and their excellent mechanical properties at high temperatures, both during the manufacturing process, and in service.

References

- [1] **Lawrence, C.W.** and **Briggs, G.A.D.** Acoustic microscopy of ceramic-fibre composite, *Journal of Materials Science*, 1993, **28**, 3645-3652.

- [2] **Reich, C.H,** **Brückner, R.** Effect of preparation parameters on the properties of unidirectional SiC-fibre reinforced MAS and BMAS glass-ceramics, *Composites Science and Technology*, 1997, **57**, 533-541.

- [3] **Yilmaz, R.,** and **Taylor, R.** Effect of heat treatment in air on the thermal properties of SiC fibre reinforced composite: Part 2 A magnesium aluminium silicate (MAS) matrix glass ceramic composite, *Journal of Materials Science*, 2007,**42**, 4115–4119.

- [4] **Ahn, J.M.,** and **Mall, S.** Frequency effects on fatigue behavior of a silicon carbide fiber-reinforced glass–ceramic composite (SiC/MAS), *International of Journal Applied Ceramic Technology*, 2009, **6 [1]**, 45–52.

- [5] **Bacon, J.F.** *Glass compositions with a high modulus of elasticity.* United States Patent, 1971, 683465.

- [6] **Booth, C.L.** and **Rindone, G.E.** Surface nucleation and crystal orientation in lithium silicate glass fibres. *Journal of American Ceramic Society*, 1964, **47**, 25-29.

- [7] **Ashbee, K.H.G.** Anisotropic glass-ceramics produced by extrusion through opposed dies, *Journal of Materials Science* , 1973, **10**, 911-917.

- [8] **Jones, R.W** and **McMillan, P.W.** The structure/property relationship glass-ceramic fibres, *Journal of Non-Crystalline Solids*, 1980, **38/39**, 1705-1709.

- [9] **Benedetti, A., Cocco, G., Fagherazzi, G., Locardi, B. and Meriani, S.** X-ray diffraction methods to determine crystallinity and preferred orientation of lithium disilicate in Li-Zn-silicate glass-ceramic fibres, *Journal of Materials Science*, 1983, **18**, 1039-1048.
- [10] **Benedetti, A., Cocco, G., Fagherazzi, Meriani, S. and Scarinci, G.** Mechanisms of nucleation and crystallisation of lithium disilicate in Li-Zn-silicate glass-ceramic fibres, *Journal of Materials Science*, 1983, **18**, 1099-1058.
- [11] **Sakamoto, A. and Yamamoto, S.** Fabrication of $\text{Li}_2\text{O-Al}_2\text{O}_3\text{-SiO}_2$ glass-ceramic ferrules by precision drawing of crystallised preforms, *Journal of Materials Science*, 2003, **38**, 2305-2310.
- [12] **Onishi, M., Kyoto, M. and Watanabe, M.** Properties of Bi-Pb-Sr-Ca-Cu-O Glass-ceramic Fibres Formed by Glass-Drawing Method. *Japanese Journal of Applied Physic.* 1991, **30**[6A], 988-990.
- [13] **Komatsu, T., Hirose, C., Ohki, T. Sato, R. and Matusita, K.** Preparation of Ag-coated superconducting $\text{Bi}_2\text{Sr}_2\text{CaCu}_2\text{O}_x$ glass-ceramic fibres, *Applied Physic of Science*, 2003, **38**, 2305-2310.
- [14] **Prabhat, K.G.** *Glass fibres for composite materials*, in Fibre reinforcements for composite, Bunsell A.R., Editor, Elsevier, Amsterdam. 1988.
- [15] **Gregory, A.G., and Veasay, T.J.** The crystallisation of cordierite glass - Part 3 Experimental studies of the crystallisation of a cordierite-type glass and the effects of oxide additions on the devitrification characteristics. *Journal of Materials Science*, 1973, **8**(3), 324-332.
- [16] **Wange, P., Höche, T., Rüssel, C., and Schnapp, J.D.** Microstructure-property Relationship in High-Strength $\text{MgO-Al}_2\text{O}_3\text{-SiO}_2\text{-TiO}_2$ Glass-Ceramics. *Journal of Non-Crystalline Solids*, 2002, **298**, 137-145.

-
- [17] **Shao, H., Liang, K., Zhou, F., Wang, G., and Hu, A.** Microstructure and Mechanical Properties of MgO-Al₂O₃-SiO₂-TiO₂ Glass-Ceramic. *Materials Research Bulletin*, 2005, **40**, 499-506.
- [18] **Bach, H.** *Low thermal expansion glass ceramics*, Springer, New York 1995.
- [19] **Serbena, F. C., Soares, V. O., Oscar, P., Pinto, H., Muccillo, R. and Zanotto, E.D.** Internal residual stresses in sintered and commercial low expansion LiO₂-Al₂O₃-SiO₂ glass-ceramics. *Journal of American Ceramics Society*, 2011, **94**[4], 1206-1214.
- [20] **Al-Harbi, O.A., Hamzawy, E.M.A., and Khan, M.M.** Effect of different concentrations of titanium oxide (TiO₂) on the crystallisation behavior of LiO₂-Al₂O₃-SiO₂ glasses prepared from local raw materials. *Journal of Applied Science*, 2009, **9**(16), 2981-2986.
- [21] **Zonotto, E.D.** A bright future for glass-ceramics. *American Ceramic Society Bulletin*. 2010, **89**(8), 19-27.
- [22] **Sakamoto, A. Asano, H., Wada, M., Takeuchi, H. and Yamamoto, S.** Durability of glass ceramic jacketed optical fibre, *Glass Technology*, 2004, **45**, 84-87.
- [23] **Sakamoto, A. Asano, H., Wada, M., Yamamoto, S. and Nishi, J.** Mechanical and optical properties of silica glass optical fibre with low-expansion glass ceramic jacket, *Journal of the Ceramic Society of Japan*, 2003, **111**[9], 640-644.
- [24] **McMillan, P. W.** *Glass-ceramic*, Academic Press, London, 1979.

- [25] **Halváč, J.** The technology of glass and ceramic; An introduction, Elsevier, Amsterdam, 1983.
- [26] **Hwang, S.P., and Wu, J.M.** Effect of composition on microstructural development in MgO-Al₂O₃-SiO₂ glass-ceramics. *Journal of American Ceramic Society*. 2001, **84**, 1108-1112.
- [27] **Owate, I.O. and Freer, R.** The electrical properties of some cordierite glass ceramics in the system MgO-Al₂O₃-SiO₂-TiO₂. *Journal of Materials Science*, 1990, **25**, 5291-5297.
- [28] **Quyang, X.Q, Xiao, Z.H., and Lu, A. X.** Phase transformation and microstructure of MgO-Al₂O₃-SiO₂ system glass-ceramics under different heat treatment conditions. *Advances in Applied*, 2009, **108**, 178-182.
- [29] http://serc.carleton.edu/research_education/equilibria/ternary_diagrams.html)
- [30] **Strand, Z.** *Glass-ceramic materials*, Elsevier, Amsterdam, 1986.
- [31] **Weaver, D.T., Van Aken, D.C. and Smith, J.D.** The role of TiO₂ and composition in the devitrification of near-stoichiometric cordierite, *Journal of Materials Science*, 2004, **39**, 51-59.
- [32] **Rawson, H.** *Properties and applications of glass*, Elsevier, New York, 1988.
- [33] **Amista, P., Cesari, M., Montena, A., Gnappi, G., and Lan, L.:** Crystallisation behaviour in the system MgO-Al₂O₃-SiO₂, *Journal of Non-Crystalline Solids*, 1995, **192&193**, 529-533.

- [34] **Riello, P., Canton, P., Comelato, N., Polizzi, S., Verità, M., Fagherazzi, G., Hofmeister, H., and Hopfe, S.** Nucleation and crystallisation behavior of glass-ceramic materials in the $\text{LiO}_2\text{-Al}_2\text{O}_3\text{-SiO}_2$ system of interest for their transparency properties, *Journal of Non-Crystalline Solids*, 2001, **288**,127-139.
- [35] **Beall, G.H. and Pinckney, L.R.** Nanophase glass-ceramics, *Journal of American Ceramic Society*. 1999, **82**, 5-16.
- [36] **Kim, K., D., Lee, S., H., Hwang, J., H. and Seo, W.S.** Nucleation behavior and microstructure of Al_2O_3 -poor LAS glass-ceramics, *Journal of Materials Science*, 2007, **42**, 10180-10187.
- [37] **Lewis, M., H.** *Glasses and glass-ceramics*, New York, Chapman and Hall, 1989.
- [38] **Eppler, R.A.** Glass formation and recrystallization in the lithium metasilicate region of the system $\text{LiO}_2\text{-Al}_2\text{O}_3\text{-SiO}_2$, *Journal of American Ceramic Society*. 1963, **46**, 97-101.
- [39] **Beall, G. H., Karstetter, B. R. and Rittler, H. L.** Crystallisation and chemical strengthening of stuffed β -Quartz glass-ceramics, *Journal of American Ceramic Society*. 1967, **50**, 181-190.
- [40] **Zdaniewski, W.** Crystallisation and structure of a $\text{MgO-Al}_2\text{O}_3\text{-SiO}_2\text{-TiO}_2$, *Journal of Materials Science*, 1973, **8**, 192-202.
- [41] **Goel, A., Shaaban, E.R., Melo, F.C.L., Ribeiro, M.J., and Ferreira, J.M.F.** Non-isothermal crystallisation kinetic studies. *Journal of Non-Crystalline Solids*, 2007, **353**, 2383-2391.

- [42] **Hou, Z., Zhang, Y., Zhang, H., Zhang, H., Shao, J. and Chunhui, S.** Study on crystallisation and microstructure of $\text{LiO}_2\text{-Al}_2\text{O}_3\text{-SiO}_2$ glass ceramics, *Journal of University of Science and Technology Beijing*, 2006, **15**[6], 564-569.
- [43] **Montedo, O. R. K, Floriano, F. J. Filho, J. O. and Bernardin, A. M.** Sintering behavior of LZSA glass ceramic, *Materials Research*, 2009, **12**[2], 197-200.
- [44] **Höland, W. and Beall, G.** *Glass ceramic technology*, The American Ceramic Society, Ohio. 2002.
- [45] **Borrell, A., Moreno, O. G., Torrecillas, R., Victoria, G. R., and Fernández.** Lithium aluminosilicate reinforced with carbon nanofibre and alumina for controlled-thermal-expansion materials, *Science and Technology of Advanced Materials*, 2012, **13**, 1-7.
- [46] **Xia, L., Wang, X., Wen, G., Li, X., Qin, C. and Song, L.** Influence of brick pattern interface structure on mechanical properties of continuous carbon fibre reinforced lithium aluminosilicate glass ceramics matrix composites, *Journal of the European Ceramic Society*, 2012, **32**, 409-418.
- [47] **Arun, K.V.** *Fundamentals of inorganic glasses*, Academic Press, San Diego, 1994.
- [48] **West, A.R.** *Solid state chemistry and its applications*, John Wiley&Sons Ltd, New York, 1984.
- [49] **Gupta, P.K.** *Glass Fibres for composite materials*; **Bunsell, A.R.**, *Fibre reinforcements for composite materials*, Elsevier, Amsterdam, 1988.

- [50] **Hu, A. M., Li, M. and Mao, D.L.** Growth behavior, morphology and properties of lithium aluminosilicate glass ceramics with different amount of CaO, MgO and TiO₂ additive, 2008, *Ceramic International*, 2007, **34**, 1393-1397.
- [51] **Michel, M.D., Mikowski, A., Lepienski, C.M., Foerster, and Serbena, F.C.** High temperature microhardness of soda-lime glass, *Journal of Non-Crystalline Solids*, 2004, **348**,131-138.
- [52] **Ziemath, E.C., Saggiaro, B.Z., and Fossa, J.S.** Physical properties of silicate glasses doped with SnO₂, *Journal of Non-Crystalline Solids*, 2005, **351**[52-54], 3870-3878.
- [53] **Johnson, J.A., J. Urquidi, Holland, D., Johnson, C.E., and Appelyard, P.G.** Strontium environment transition in tin silicate glasses by neutron and X-ray diffraction *Journal of Non-Crystalline Solids*, 2007, **353**[44-46],4048-4092.
- [54] **Cowking, A., Attou, A., Siddiqui, A. M. and Sweet, M. A. S.** Testing E-glass fibre bundles using acoustic emission, *Journal of Materials Science*, 1991, **26**, 192-202.
- [55] **Aslanova, M. S.** *Glass fibre, In: Strong fibre, Handbook composites*, Volume 1, Editor, Watt, W and Perov, B. V., Elsevier Science Publisher, North-Holland, 1985.
- [56] **Otto, W. H.** Compaction effects in glass fibres, *Journal of American Ceramic Society*, 1961, **44**[2], 68-72.
- [57] **Wanner, A.** Elastic modulus measurements of extremely porous ceramic materials by ultrasonic phase spectroscopy, *Materials Science and Engineering*, 1998, **A248**, 35-43.

- [58] **Sohn, S. B.** and **Choi, S.Y.** Crystallisation behaviour in the glass system MgO-Al₂O₃-SiO₂: Influence of CeO₂ addition. *Journal of Non-Crystalline Solids*, 2001, **282**, 221-227.
- [59] **Golubkov, V.V., Dymshits, O. S., Zhilin, A. A., Chuvaeva, T.I., and Shashkin, A.V.** On the phase separation and crystallisation of glasses in the MgO-Al₂O₃-SiO₂-TiO₂ system, *Glass Physics and Chemistry*, 2003, **29 (3)**, 254-266.
- [60] **Shao, H., Liang, K., and Peng, F.** Crystallisation kinetic of MgO-Al₂O₃-SiO₂ system glass-ceramics, *Ceramic International*, 2004, **30**, 927-930.
- [61] **Tilley, R. J. D.** *Understanding solids :The science of material*, Wiley, Chicester, 2004
- [62] **Shelby, J. E.** *Introduction to glass science and technology*. The Royal Society of Chemistry, Herts, United Kingdom.1997.
- [63] **Shyu, J.J. and Wu, 1991.** Effect of TiO₂ addition on the nucleation of apatite in an MgO-CaO-SiO₂.P₂O₅ glass. *Journal of Materials Science Letter*, 1991, **10**, 1056-1058.
- [64] **Minsheng, M., Wen, N., Yali, W., Zhongjie, W. and Fengmei, L.** The effect of TiO₂ on phase separation and crystallisation of glass-ceramics in CaO-MgO- Al₂O₃-SiO₂- Na₂O system, *Journal of Non-Crystalline Solids*, 2008, **354**, 5395-5401.
- [65] **Gür, C.H. and Ozturk, A.** Determination of the influence of TiO₂ on the elastic properties of mica based glass-ceramic by ultrasonic velocity measurement, *Journal of Non-Crystalline Solids*, 2005, **351**, 3655-3662.

- [66] **Guo, X.** and **Yang, H.** Effects of fluorine on crystallisation, structure and performances of lithium aluminosilicate glass ceramic, *Materials Research Bulletin*, 2006, **41**, 396-405.
- [67] **Khater, G. A.**, and **Idris, M. H.** Role of TiO₂ and ZrO₂ on crystallisation phases and microstructure in Li, Ba aluminosilicate glass, *Ceramic International*, 2007, **33**, 233-238.
- [68] **Pinckney, L.R.** *Phase-separated glasses and glass ceramics*, In: *Ceramic and glasses, Vol 4, Engineered materials Handbook*, ASM International, United States, 1991.
- [69] **Matthews, F.L.** and **Rawlings, R.D.** *Composite materials; engineering and science*, Chapman & Hall, London, 1994.
- [70] **Prewo, K. M.** and **Brennan, J. J.** High-strength silicon carbide fibre-reinforced glass-matrix composites, *Journal of Materials Science*, 1980, **15**, 463-468.
- [71] **El-Shennawi, A. W. A.**, **Omar, A. A.** and **El-Ghannam, A. R.** Crystallisation of spodumene-lithium magnesium orthosilicate glasses, *Ceramic International*, 1990, **16**, 47- 52.
- [72] **Khazanov V. E.**, **Dorzhev, D. B.** and **Mishura, A. S.** Features of formation of refractory magnesium-aluminosilicate fibre, *Stekloplastik Scientific-Industrial Association*, 1988, **10**, 17-19.
- [73] **Stringer, L. G.** and **Jones, R. W.** Glass ceramic fibre reinforced tin, *International Conference on the Strength of Metals and Alloys*, 1976, 1311-1315.

- [74] **Yuan, B., Chen, Q.Q.** and **Wang, M. Q.** Crystallisation and properties of Li-Al-B-Ti-Zn-silicate sytem glass ceramic fibres, *Journal of Materials Science*, 1989, **24**, 4488-4494.
- [75] **Raju, C.B.** Crystallisation of glass fibres obtained from lepidolite-bearing pegmatites, *Journal of Materials Science Letters*, 1992, **11**, 547-549.
- [76] **Hirose, C., Komatsu, T., Sato, R.** and **Matusita, K.** Microstructure of superconducting $\text{Bi}_2\text{Sr}_2\text{CaCu}_2\text{O}_x$ glass ceramic fibres, *Journal of Materials Science Letters*, 1990, **10**, 1146-1148.
- [77] **Komatsu, T., Hirose, C., Ohki, T., Sato, R.** and **Matusita, K.** Preparation of Ag-coated superconducting $\text{Bi}_2\text{Sr}_2\text{CaCu}_2\text{O}_x$ glass ceramic fibres, *Applied Physics Letters*, 1990, **57**[2], 183-185.
- [78] **Hu, Y., Zheng, H.** and **Mackenzie, J. D.** High- T_c superconducting Bi(Al)-Ca-Sr-Cu-O glass ceramic fibres drawn from glass preforms, *Journal of Materials Science*, 1995, **30**, 3913-3918.
- [79] **Chu, C. W.** Superconductivity up to 114 K in the Bi-Al-Ca-Sr-Cu-O compound system without rare-earth elements, *Physical Review Letters*, 1988, **60**[10], 941-943.
- [80] **Tick , P.A.** Are low-loss glass ceramic optical waveguides possible? *Optic Letters*, 1998, **23**[24], 1904-1905.
- [81] **Tick, P. A., Borelli, N. F.** and **Reaney, I. M.** The relationship between structure and transparency in glass-ceramic materials, *Optical Materials*, 2000, **15**, 81-91.
- [82] **Samson, B. N., Pinckney, L. R., Wang, J., Beall, G. H.** and **Borrelli, F.** Nickel-doped nanocrystalline glass ceramic fibre, *Optical Letters*, 2002, **27**[15], 1309-1311.

- [83] **Liu, J., Gong, C. and Fan, G.** Preparation and properties of barium-ferrite-containing glass ceramic fibres via an electrospinning/sol-gel process, *Journal of Sol-Gel Science Technology*, 2012, **61**, 185-191.
- [84] **Padini, L. C., and Manhani, L. G. B.** Influence of the testing gage length on the strength, Young's modulus and Weibull modulus of carbon fibres and glass fibres, *Materials Research*, 2002, **5[4]**, 411-420.
- [85] **Varner, J.** *Strength and fracture mechanics of glass*, in *Strength of glass: Basics and test procedure*, Editor, Hüttentechnische Vereinigung Der deutschen Glasindustrie, Germany, 2003.
- [86] **Sugarman, B.** A Review : Strength of glass, *Journal of Materials Science*, 1967, **2[3]**, 275-283.
- [87] **Morley, J. G.** *High-performance fibre composite*, Academic Press, London, 1987.
- [88] **Kurkjian, C. R., Gupta, P. K. and Brow, R. K.** The strength of silicate glasses: What do we know what do we need to know?, *International Journal of Applied Glass Science*, 2010, **1[1]**, 27-37.
- [89] **Kurkjian, C. R.** Mechanical strength of glasses-studies then and now, *The Glass Researcher*, 2002, **11[2]**, 2-6.
- [90] **Bartenev, G. M. and Sidorov, A. B.** The effect of length of glass fibers on their strength, *Glass and Ceramics*, 1965, **22[9]**, 597-599.
- [91] **Kotchick, D. M., Hink, R. C. and Tressler R. E.** Gauge length and surface damage effects on the strength distributions of silicon carbide and sapphire filaments, *Journal of Composite Materials*, 1975, **9**, 327-336.

-
- [92] **Griffith, A. A.** The phenomena of rupture and flow in solids, *Philosophical Transaction of Royal Society A*, 1921, **221**, 163-198.
- [93] **Wang, X.** Predicting the strength variation of wool from its diameter variation, *Textile Research Journal*, 2000, **70**[3], 191-194.
- [94] **Zhang, Y., Wang, X., Pan, N. and Postle, R.** Weibull analysis of the tensile behavior of fibres with geometrical irregularities, *Journal of Materials Science*, 2002, **37**, 1401-1406.
- [95] **Zwang, S. V. D.** The concept of filament strength and the weibull modulus, *Journal of Testing and Evaluation*, 1989, **17**[5], 292-298.
- [96] **Weibull, W.** A statistical distribution function of wide applicability, *Journal of Applied Mechanics*, 1951, **18**, 293-297.
- [97] **Thomason, J. L. and Kalinka, G.** A technique for the measurement of reinforcement fibre tensile strength at sub-millimetre gauge lengths, *Composites Part A: Applied Science and Manufacturing*, 2001, **32**[1], 85-90.
- [98] **Yang, L. and Thomason, J. L.** Effect of silane coupling agent on mechanical performance of glass fibre, *Journal of Material Science Technology*, 2012, DOI: 10.1007/s10853-012-6960-7.
- [99] **Naito, K., Yang, J. M., Tanaka, Y. and Kagawa, Y.** The effect of gauge length on tensile strength and Weibull modulus of polyacrylonitrile (PAN)- and pitch-based carbon fibres, *Journal of Material Science Technology*, 2012, **47**, 632-642.
- [100] **Morimoto, T., Nakagawa, S., and Ogihara S.** Bias in the Weibull strength estimation of a SiC fibre for the small gauge length case, *Japan Society mechanical Engineering International Journal*, 2005, **48**, 194-198.

- [101] **Virk, A. S., Hall, W. and Summerscales, J.** Tensile properties of jute fibres, *Material Science Technology*, 2009, **25**, 1289-1295.
- [102] **Naito, K., Tanaka, Y., Yang, J. M. and Kagawa, Y.** Tensile properties of ultrahigh strength PAN-based, ultrahigh modulus pitch-based and high ductility pitch-based carbon fibres, *Carbon*, 2008, **46**, 189-195.
- [103] **Andersons, J., Joffe, R., Hojo, M. and Ochiai, S.** Glass fibre strength distribution determined by common experimental methods, *Composites Science and Technology*, 2002, **62**[1], 131-145.
- [104] **Asloun, M. E, Donnet, J. B., Guilpain, G., Nardin, M., and Schultz, J.** On the estimation of the tensile strength of carbon fibres at short lengths, *Journal of Materials Science*, 1989, **24**[10], 3504-3510.
- [105] **Zafeiropoulos, N. E. and Baillie, C. A.** A study of the effect of surface treatments on the tensile strength of flax fibres: Part II. Application of Weibull statistics, *Composites Part A: Applied Science and Manufacturing*, 2007, **38**[2], 629-638.
- [106] **Thamae, T., Aghedo, C., Baillie, C. and Matovic, D.** *Tensile properties of hemp and Agave American fibres*, In: *Handbook of tensile properties of textile and technical fibres*, Bunsell, A. R., Editor, Woodhead, Cambridge, 2009.
- [107] **Feih, S., Thranner, A. and Lilholt, H.** Tensile strength and fracture surface characterisation of sized and unsized glass fibers, *Journal of Materials Science*, 2005, **40**[7], 1615-1623.
- [108] **Trustrum, K. and Jayatilaka, A. D. S.** On estimating the Weibull modulus for a brittle material, *Journal of Materials Science*, 1979, **14**, 1080-1084.

- [109] **Faucher, B.** and **Tyson, W. R.** On the determination of Weibull parameters, *Journal of Materials Science Letters*, 1988, **7**, 1199-1203.
- [110] **Bansal, N. P.** Chemical vapour deposited SiC (ScS-0) fibre-reinforced strontium aluminosilicate glass ceramic composites, *Journal of Materials Research*, 1997, **12**[3],745-753.
- [111] **Ye, F., Liu, L.** and **Huang, L.** Fabrication and mechanical properties of carbon short fibre reinforced barium aluminosilicate glass ceramic matrix composites, *Composites Science and Technology*, 2008, **68**, 1710-1717.
- [112] **Zhao, Y., Malzbender, J.** and **Gross, S. M.** The effect of room temperature and high temperature exposure on the elastic modulus, hardness and fracture toughness of glass ceramic sealants for solid oxide fuel cells, *Journal of European Ceramic Society*, 2011, **31**, 541-548.
- [113] **Vicens, J., Farizy, G.** and **Chermant, J.L.** Microstructure of ceramic composites with glass ceramic matrices reinforced by SiC-based fibres, *Aerospace Science and Technology*, 2003, **7**, 135-146.
- [114] **Doreau, F., Maupas, H., Kervadec, D., Ruterana, P., Vicens, J.** and **Chermant, J. L.** The complexity of the matrix microstructure in SiC-Fibre-reinforced glass ceramic composites, *Journal of the European Ceramic Society*, 1995, **15**, 1235-1247.
- [115] **Brennan, J. J.** and **Prewo, K. M.** Silicon carbide fibre reinforced glass ceramic matrix composites exhibiting high strength and toughness, *Journal of Materials Science*, 1982, **17**, 2371-2382.
- [116] **Phillips, D. C.** Interfacial bonding and the toughness of carbon fibre reinforced glass and glass ceramics, *Journal of Materials Science*, 1974, **9**, 1847-1854.

- [117] **Ma, J., Liao, K. and Hing, P.** Effect of aluminum nitride on the properties of cordierite, *Journal of Materials Science*, 2000, **35**, 1847-1854.
- [118] **Zhao, C., Lambrinou, K. and Biest, O. V. D.** Hot pressing 'window' for (P₂O₅, B₂O₃)-containing magnesium aluminosilicate reinforced with SiC fibres, *Journal of Materials Science*, 1999, **34**, 1865-1871.
- [119] **Metcalf, B. L., Donald, I. W. and Bradley, D. J.** Development and properties of a SiC fibre-reinforced magnesium aluminosilicate glass-matrix composite, *Journal of Materials Science*, 1992, **27**, 3075-3081.
- [120] **Wallenberger, F. T. and Bingham, P. A.** *Fibreglass and glass technology: energy-friendly compositions and applications*, Springer, London, 2009.
- [121] **Quinn, K.R. and Carreno, C.A.** High temperature thermoplastic composite, *Advanced Materials & Processes*, 1991, **141(8)**, 19-31.
- [122] **Bussu, G. and Lazzeri, A.** On the use of dynamic mechanical thermal analysis (DMTA) for measuring glass transition temperature of polymer matrix fibre reinforced composite, *Journal of Materials Science*, 2006, **41**, 6072-6076.
- [123] **Wallace, M. M. and Bert, C. W.** Experimental determination of dynamic Young's modulus and damping of an aramid-fabric/polyester composite material, In *Proceedings of the Oklahoma Academic Science*, 1979, **59**, 98-101.
- [124] **Almagableh, A., Gupta, S., Mantena, P. R., and Al-Ostaz, A.** Dynamic mechanical analysis of graphite platelet and nanoclay reinforced vinyl ester, and MWCNT reinforced nylon 6, 6 nanocomposites. In *Proceedings of the 2008 SAMPE Fall Technical Conference*, 2008, 8-11.

- [125] **Thomason, J. L.** A note on the investigation of the composite interphase by means of thermal analysis, *Composite Science and Technology*, 1992, **44**, 87-90.
- [126] **Wetton, R. E.** and **Corish, P. J.** DMTA studies of polymer blends and compatibility, *Polymer Testing*, 1989, **8**, 303-312.
- [127] **Scobbo, Jr J. J.** Dynamic mechanical analysis of compatibilized polymer blends, *Polymer Testing*, 1991, **10**, 279-290.
- [128] **Sepe, M. P.** Dynamic mechanical analysis pinpoints plastics temperature limits, *Advanced Materials & Processes*, 1992, **141(4)**, 32-35.
- [129] **Kuzak, S.G.** and **Shanmugam, A.** Dynamic Mechanical Analysis of Fibre-Reinforced Phenolics, *Journal of Applied Polymer Science*. 1999, **73**, 649-658.
- [130] **Ward, I. M.** *Mechanical properties of solid polymer*, 2nd Edt, John Wiley & Son, Chichester, 1983.
- [131] **Kelly, S.S., Rials, T.G.** and **Glasser W.G.** Relaxation behaviour of the amorphous component of wood, *Journal of Materials Science*, 1987, **22**, 617-624.
- [132] **Yee, R. Y.** and **Stephens, T.S.** A TGA technique for determining graphite fibre content in epoxy composites, *Thermochimia Acta*, 1996, **272**, 191-199.
- [133] **Moon, C. R., Bang, B.R., Choi, W.J., Kang, G.H.,** and **Park, S.Y.** A technique for determining fibre content in FRP by thermogravimetric analyser, *Polymer Testing*, 2005, **24**, 376-380.

- [134] ASTM Standard E1131. *Standard test method for compositional analysis by thermogravimetry*, American Society for Testing and Materials (ASTM) International, USA, 1998.
- [135] ASTM D3171-99. *Standard test methods for constituent content of composite materials*, American Society for Testing and Materials (ASTM) International, USA, 1998.
- [136] **Marshall, D. B.** and **Evans, A. G.** Failure mechanisms in ceramic fibre/ceramic matrix composites, *Journal of American Ceramic Society*, 1985, **63**[5], 225-234.
- [137] **Dzral, L.T.** The interphase in epoxy composite, *Advances in Polymer Science*, 1986, **75**, 1-32.
- [138] **Thouless, M. D., Sbaizero, O, Sigl, L. S.,** and **Evans, A. G.** Effect of interface mechanical properties on pullout in a SiC-Fibre-Reinforced Lithium Aluminum Silicate Glass Ceramic, *Journal of American Ceramic Society*, 1989, **72**[4], 525-532.
- [139] **Swain, R. E., Reifsnider, K. L., Jayaraman, K.** and **El-Zein, M.** Interface/interphase concepts in composite material systems, *Journal of Thermoplastic Composite Materials*, 1990, **3**, 13-23.
- [140] **Chawla, N., Chawla, K. K., Koopman, M., Patel, B., Coffin, C.** and **Eldridge, J. I.** Thermal-shock behaviour of a Nicalon-fibre-reinforced hybrid glass ceramic composite, *Composite Science and Technology*, 2001, **61**, 1923-1930.
- [141] **Herrera-Franco, P. J.** and **Dzral, L. T.** Comparison of methods for the measurement of fibre/matrix adhesion in composite, *Composites*, 1992, **23**[1], 2-27.

- [142] **Berg, J.** and **Jones, F. R.** The role of sizing resins, coupling agents and their blends on the formation of the interphase in glass fibre composite, *Composite Part A: Applied Science and Manufacturing*, 1998, **29A**, 1261-1272.
- [143] **Zhao, F. M.** and **Takeda, N.** Effect of interfacial adhesion and statistical fibre strength on tensile strength of unidirectional glass fibre / epoxy composites. Part I: experiment results, *Composites Part A: Applied Science and Manufacturing*, 2000, **31A**, 1203 – 1214.
- [144] **Paul, A.** *Chemistry of glasses*, Chapman and Hull Ltd., New York, 1982.
- [145] **Thomason, J. L.** and **Adzima, L. J.** Sizing up the interphase: an insider's guide to the science of sizing, *Composites Part A: Applied Science and Manufacturing*, 2000, **32A**, 1203 – 1214.
- [146] **Zinck, P., Pays, M. F., Rezakhanlou, R.** and **Gerard, J. F.** Mechanical characterisation of glass fibres as an indirect analysis of the effect of surface treatment, *Journal of Materials Science*, 1999, **34**, 2121-2133.
- [147] **Hull, D.** and **Clyne, T. W.**, *An introduction to composite materials*, 2nd Ed, Cambridge University Press, Cambridge, 1996.
- [148] **Low, B. Y., Gardner, S. D., Pittman, C. U.** and **Hackett, R. M.** A micromechanical characterisation of graphite-fibre/epoxy composites containing a heterogeneous interphase region, *Composites Science and Technology*, 1994, **52**, 589-606.
- [149] **Dzral, L. T.** The role of the fibre-matrix interphase on composite properties, *Vacuum*, 1990, **4[7-9]**, 1615-1618.

-
- [150] **Sun, E. Y., Lin, H. T. and Brennan, J. J.** Intermediate-temperature environmental effects on boron nitride-coated silicon carbide-fibre-reinforced glass ceramic composites, *Journal of American Ceramic Society*, 1997, **80**[3], 609-614.
- [151] **Liu, Z., Zhao, F. and Jones, F. R.** Optimising the interfacial response of glass fibre composites with a functional nanoscale plasma polymer coating, *Composite Science and Technology*, 2008, **68**, 3163-3170.
- [152] **Swait, T. J., Soutis, C. and Jones, F. R.** Optimisation of interfacial properties for tensile strength by plasma polymerisation, *Composite Science and Technology*, 2008, **68**, 2302-2309.
- [153] ASTM Standard D693, *Standard test method for density of glass by buoyancy*, American Society for Testing and Materials (ASTM) International, USA, 1998.
- [154] **Oliver, W. C. and Pharr, G.M.** An improved technique for determining hardness and elastic modulus using load and displacement sensing indentation experiments, *Journal of Materials Research*, 1992, **7**[6], 1564-1583
- [155] ASTM Standard C1157-03, (Reapproved 2008) *Standard test for tensile strength and Young modulus of fibre*, American Society for Testing and Materials (ASTM) International, USA, 2008.
- [156] ASTM C 1239-07, *Standard practice for reporting uniaxial strength data and estimating Weibull distribution parameters for advanced ceramic*, American Society for Testing and Materials (ASTM) International, USA, 1998.

- [157] ASTM C 494-95, *Standard practice for measuring ultrasonic velocity in materials*, American Society for Testing and Materials (ASTM) International, USA, 1995.
- [158] ASTM Standard D792, *Standard test methods for density and specific gravity (relative density) of plastic by displacement*, American Society for Testing and Materials (ASTM) International, USA, 1998.
- [159] **Goswami, M., Mirza, T., Sarkar, A., Manikandan, S., Sangeeta, Verma, S. L., Gurusurthy, K. R., Shrikhande, V. K. and Kothiyal, G. P.** Preparation and characterization of magnesium-aluminium-silicate glass ceramics, *Bulletin Materials Science*, 2000, **23**[5], 377-382.
- [160] **Hunger, A., Carl, G. Andreas, G., and Christian, R.** Young's moduli and microhardness of glass ceramics in the system MgO/Al₂O₃/TiO₂/ ZrO₂/SiO₂ containing quartz nanocrystals, *Materials Chemistry and Physics*, 2010, **122**, 502-506.
- [161] **Bray, C.** *Ceramic and glass: a basic technology*. Society of Glass Technology, Sheffield, United Kingdom, 2000.
- [162] **Arvind, A., Kumar, R., Deo, M. N., Shrikhande, V. K. and Kothiyal, G. P.** Preparation, structural and thermo-mechanical properties of lithium aluminium silicate glass ceramics, *Ceramic International*, 2009, **35**, 1661-1666.
- [163] **Xingzhong, G., Lingjie, Z. and Hui, Y.** Effects of Li replacement on the nucleation, crystallisation and microstructure of Li₂O-Al₂O₃-SiO₂, *Journal of Non-Crystalline Solids*, 2008, **354**, 4031-4036.
- [164] **Hu, A. M., Liang, K. M., Li, M. and Mao, D. L.** Effect of nucleation temperatures and time on crystallisation behavior and properties of Li₂O-Al₂O₃-SiO₂, *Materials Chemistry and Physics*, 2006, **98**, 430-433.

- [165] **Ananthanarayanan, A., Dixit, A. and Lenka, R. K.** Some studies on the phase formation and kinetics in TiO₂ containing lithium aluminum silicate glasses nucleated by P₂O₅, *Journal of Thermal Analysis Calorimetry*, **2011**, 106, 839-844.
- [166] **Tiryakioğlu, M. and Hudak, D.** Guidelines for two parameter Weibull analysis for flaw-containing materials, *Metallurgical and Materials Transaction B*, 2011, **42B**, 1130-1135.
- [167] **Shamsudin, Z., Hodzic, A., Soutis, C., Hand, R. J., Hayes, S. A., and Bond, I. P.** Characterisation of thermo-mechanical properties of MgO-Al₂O₃-SiO₂ glass ceramic with different heat treatment temperatures, *Journal of Materials Science*, 2011, **46(17)**, 5822-5829.
- [168] **Wallenberger, F.T and Brown, S.D.** High – modulus glass fibres for new transportation and infrastructure composites and new infrared uses, *Composite Science and Technology*, 1994, **51**,243-263.
- [169] **Zarzycki, J.** *Glasses and the vitreous state*, Cambridge University Press, Cambridge, 1991.
- [170] **Jumahaat, A.** *Effect of nanofiller on thermo-mechanical properties of polymers and composite laminates*, PhD, The University of Sheffield, 2011.
- [171] **Madsen, B., Thygesen, A. and Lilholt, H.** Plant fibre composites- porosity and volumetric interaction, *Composite Science and Technology*, 2007, **67**, 1584-1600..